SpringerBriefs in the Mathematics of Materials 5

Hisashi Naito

Trivalent Discrete Surfaces and Carbon Structures

Springer

SpringerBriefs in the Mathematics of Materials

Volume 5

SpringerBriefs in Mathematics of Materials introduces in a compact format recent topics in materials science where mathematical ideas are essential.

Materials science has developed in interdisciplinary study and has dealt with complex multiscale systems in multiphysics in an ad hoc manner until recently. Now a new phase of materials science with mathematical and computational tools is emerging in response to developments in the high-performance computing century. This series is intended for mathematicians, physicists, and other scientists, as well as doctoral students in related areas.

Hisashi Naito

Trivalent Discrete Surfaces and Carbon Structures

Springer

Hisashi Naito
Graduate School of Mathematics
Nagoya University
Chikusa-ku, Nagoya, Japan

ISSN 2365-6336 ISSN 2365-6344 (electronic)
SpringerBriefs in the Mathematics of Materials
ISBN 978-981-99-5768-2 ISBN 978-981-99-5769-9 (eBook)
https://doi.org/10.1007/978-981-99-5769-9

This Springer imprint is published by the registered company Springer Nature Singapore Pte Ltd.
The registered company address is: 152 Beach Road, #21-01/04 Gateway East, Singapore 189721, Singapore

In memory of my wife Yumiko.

Preface

Topological crystallography, which was pioneered by Motoko Kotani and Toshikazu Sunada in 2000, describes crystal structures using graph theory and variational principles. One of the conventional tools describing crystal structures is space groups, which denote the symmetry of placements of atoms. But space groups do not consider the atomic bonds of crystals. Since crystal structure includes placements of atoms and chemical bonds between atoms, graph theory is a natural tool to describe them. On the other hand, one of the important notions to describe physical phenomena is the principle of least action, which corresponds to the variational principle in mathematics.

Although the description of crystal structures using space groups is not directly related to the least action principle, topological crystallography provides a relationship between the symmetry of crystal structures and the variational principle. Precisely, for a given graph structure which describes a crystal, we define the energy of realizations of the graph, i.e., placements of vertices of the graph in a Euclidean space of suitable dimension, and obtain a nice structure as a minimizer of the energy. Moreover, such structures give us the most symmetric among all placements of the graph, which is proved by using the random walk theory on graphs.

On the other hand, we can regard some molecular structures, for example, fullerenes and carbon nanotubes, as surfaces, especially as discrete surfaces. Recently, sp^2-carbon structures (including fullerenes and nanotubes) have received much attention in science and technology, since they have rich π-electrons and hence rich physical properties. From a mathematical viewpoint, sp^2-carbon structures can be regarded as trivalent graphs in $\mathbb{R}^3$, and hence trivalent *discrete surfaces*. There are many discrete surface theories in mathematics. For example, the theory of triangular surfaces is useful for computer graphics. But this is based on discretizations or discrete analogues of continuous or smooth objects. In the case of the theory of triangular surfaces, it is a discretization of smooth real objects. In other words, conventional discrete surface theories are "from continuous to discrete". In contrast, discrete surfaces, which describe crystal/molecular structures, are essentially discrete. Even in the case of trivalent discrete surfaces, it is not easy to define the curvatures of them. In this monograph, we also discuss a theory of trivalent discrete surfaces modeled on

crystal/molecule structures in $\mathbb{R}^3$, and subdivisions/convergence of them. The aim of subdivision and convergence theory is to find an underlying continuous object in crystals/molecules. It is difficult to calculate the physical properties of a crystal structure with a huge number of atoms using current computer resources; however, it is possible to treat such systems by calculating underlying continuous objects. By considering the above, our discrete surface theory is "from discrete to continuous".

I would like to thank Prof. Motoko Kotani for encouraging me to write this monograph, and Prof. Toshikazu Sunada for leading me to the study of discrete geometric analysis. I would also like to thank Profs. Tatsuya Tate, Makoto Tagami, Yoshiyuki Kawazoe, and Hiroyuki Isobe, Dr. Toshiaki Omori, Dr. Shintaro Akamine, and members of the research project "Discrete Geometric Analysis for Material Design" for helpful discussions and comments on my research. I am grateful to Dr. Tomoya Naito for his valuable comments and suggestions. Lastly, I would like to thank the members of the Japanese girls group "Nogizaka46" for encouraging my research.

Enjoy a discrete world!

Nagoya, Japan Hisashi Naito
May 2021

Contents

Chapter 1
Overview of This Monograph

Let us start with a question here. Which figure in Fig. 1.1 is the most symmetric?

Obviously, figure (c) in Fig. 1.1 has less symmetry than (a) and (b); however, it is difficult to compare symmetries of (a) and (b).

One of the basic tools for describing symmetries of crystal structures is space groups, which describe symmetry of atoms (vertices/points) in a crystal structure. For example, the symmetry of a regular hexagonal tiling of $\mathbb{R}^2$ is described by the group $P6m$, and the space group of the symmetry of a regular three-colored hexagonal tiling (see Fig. 1.2b) is $P3m1$. Similarly, the group $P6m$ describes the symmetry of a regular hexagonal lattice. The groups describing the symmetry of (a) and (b) of Fig. 1.1 are $P4mm$ and $P6m$, respectively, and one is never included in the other.

Topological crystallography, which was pionnered by Kotani and Sunada [28–30, 54], describes symmetries of both of vertices and of edges (atomic bonds of crystal structure). Why does nature select (b) among (a)–(c) in Fig. 1.3? Note that these lattices are created by the same graph. Topological crystallography answers this question. In mathematics, a structure consisting of vertices and edges (connectivity of vertices) is called a graph, and graph theory is one of the basic tools of topological crystallography (Chap. 2). However, graphs describe only vertices and their connectivities, as in Fig. 2.2; placements of vertices and edges in $\mathbb{R}^n$ are not defined in the notion of graphs. Therefore, we should define placements of a given graph structure, which describes crystal structure, and should consider how to define *nice placement* of the graph. By defining the energy of placements of a graph, we may find a nice placement, which is called a *standard realization*, by using variational principles. A standard realization gives us one of the most symmetric objects among all placements of the graph (Chap. 3). In the first few sections, we discuss topological crystallography including graph theory and geometry. The most important reference of this part is Sunada's lecture note [53]. The author discusses an introduction to topological crystallography along with it.

H. Naito, *Trivalent Discrete Surfaces and Carbon Structures*,
SpringerBriefs in the Mathematics of Materials 5,
https://doi.org/10.1007/978-981-99-5769-9_1

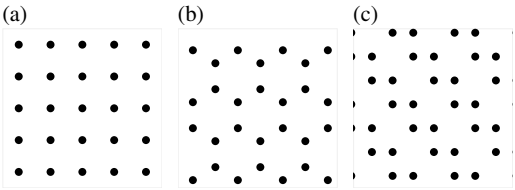

Fig. 1.1 Which figure is the most symmetric?

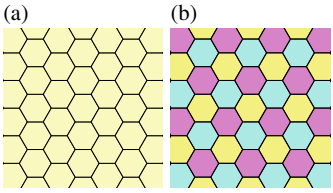

Fig. 1.2 Space groups of **a** and **b** are $P6m$ and $P3m1$. Since $P3m1$ is a subgroup of $P6m$, we can say that figure **a** has higher symmetry than figure **b**

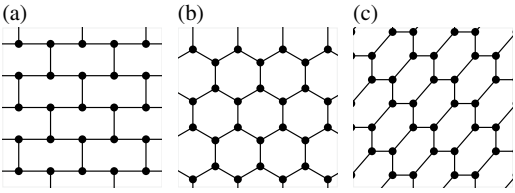

Fig. 1.3 Different realizations of the hexagonal lattice

In the remaining chapters, we consider trivalent discrete surfaces which are mathematical models of types of molecule/crystal structures such as graphenes, carbon nanotubes, and fullerenes (Chap. 4). We define the Gauss curvature and the mean curvature for *trivalent discrete surfaces*, and we also construct negatively-curved fullerenes by using standard realizations (Chap. 5). Moreover, we discuss subdivisions of trivalent discrete surfaces, which are not only of mathematical interest (Chap. 6). Numerical methods in physics are difficult to apply to a huge number of systems. Subdivision of structure may give us a good approximation of a continuous model, and such a continuous model may give faster calculation of physical properties. A spectrum of the Laplacian of graphs is deeply related to the electronic properties of crystal/molecule structures. We will discuss such properties from a mathematical viewpoint, and give several examples.

This monograph is based on the lecture note [39], and the main target of this monograph is students in mathematics; however, the author's intention is that students in physics/chemistry can also find it useful.

Chapter 2
Graph Theory

Graph theory is one of the main tools to describe topological crystals. After a standard definition of graphs, we discuss homology groups and covering spaces of graphs, which are important notions describing symmetry of topological crystals. We also discuss the Laplacian and its spectrum. Definitions and notations follow standard textbooks of graph theory, for example [4, 6] and Sunada's lecture note [54].

2.1 Graph

Definition 2.1 For finite or countable sets V and E, an ordered pair $X = (V, E)$ with $i\colon E \longrightarrow V \times V$ and $\iota\colon E \longrightarrow E$ is called a *graph* if i and ι satisfy

$$\iota^2 = \mathrm{id}_E, \quad \iota(e) \neq e, \quad i(\iota(e)) = \tau(i(e)), \text{ for any } e \in E,$$

where $\tau\colon (u, v) \mapsto (v, u)$ for $(u, v) \in V \times V$. An element $v \in V$ and an element $e \in E$ is called a *vertex* and a *directed edge* of X, respectively. The map i is called the *incident map* and the map ι is called the *inversion map* of X.

Usually, a graph $X = (V, E)$ is defined as $E \subset V \times V$ for an ordered pair (V, E); however, by this definition, multiple edges cannot be described.

For each edge $e \in E$, we write $i(e) = (o(e), t(e))$, we call $o(e)$ and $t(e)$ the *origin* and the *terminus* of e, respectively, and we also call $o(e)$ and $t(e)$ *ends* of e. If a vertex $v \in V$ is an end of e, we say that v is *incident* with e. Moreover, we call $\overline{e} = \iota(e)$ the *inverse edge* of $e \in E$. By identifying e and $\overline{e}$, we obtain an *undirected edge*. An *orientation* of an undirected graph $X = (V, E)$ is a subset $E^o \subset E$ such that (V, E^o) is a directed graph with $E^o \cup \overline{E^o} = E$ and $E^o \cap \overline{E^o} = \emptyset$, where $\overline{E^o} = \{e \in E \mid \overline{e} \in E^o\}$.

H. Naito, *Trivalent Discrete Surfaces and Carbon Structures*,
SpringerBriefs in the Mathematics of Materials 5,
https://doi.org/10.1007/978-981-99-5769-9_2

In general, we also consider *weights* of vertices and/or edges: functions $w_v : V \longrightarrow \mathbb{R}_{>0}$ and $w_e : E \longrightarrow \mathbb{R}_{>0}$ are called weights of vertices and edges, respectively.

Definition 2.2 A graph $X = (V, E)$ is called *finite*, if the number of vertices $|V|$ and the number of edges $|E|$ are finite. For a vertex $v \in V$, write $E_v = \{e \in E \mid o(e) = v\}$, which is the set of edges with $o(e) = v$. The number of edges emanating with $v \in V$ is called the *degree* $\deg(v) = |E_v|$ of v. A graph is called *locally finite* when $\deg(v)$ is finite for any $v \in V$.

Definition 2.3 If a locally finite graph X satisfies $\deg(v) = d$ for all $v \in V$, we call X a *regular graph* of degree d. In particular, if X is a regular graph of degree three, we call it a *trivalent graph*.

Definition 2.4 For a graph $X = (V, E)$, successive edges

$$(u_1, u_2)(u_2, u_3) \cdots (u_{k-2}, u_{k-1})(u_{k-1}, u_k), \quad (u_i, u_j) \in E,$$

is called a *path* between u_1 and u_k, and if $u_1 = u_k$, it is called a *closed path*. If a closed path passes through a vertex only once, we call it a *simple closed path*. A graph is *connected*, if there exists a path between arbitrary two vertices, and a connected graph is called a *tree*, if the graph contains no simple closed path.

Remark 2.1 In this monograph, we assume that graphs are non-weighted (weight functions are constant), connected, locally finite and undirected unless otherwise stated; however, which may contain loops and/or multiple edges.

The following are typical finite graphs that appeared in this monograph (see Fig. 2.1):

1. *n-bouquet graph* B_n: a graph of n self-loops and one vertex;
2. a *cycle graph* C_n: a graph of the n-gon;
3. a *complete graph* K_n: a graph of n-vertices in which any two vertices are adjacent;
4. a *complete bipartite graph* $K_{n,m}$: a graph of $(n + m)$-vertices, the set of vertices V is the disjoint union V_1 and V_2 ($|V_1| = n$, $|V_2| = m$), and any vertices $v_1 \in V_1$ and $v_2 \in V_2$ are adjacent;
5. *polyhedral graphs*: graphs formed from the vertices and the edges of a convex polyhedron, for example, tetrahedral, cubic, octahedral, dodecahedral, icosahedral, and truncated icosahedral graphs.

Example 2.1 All the graphs in Fig. 2.2 are the same.

Definition 2.5 Let $X = (V, E)$ be a finite undirected graph. A tree $T = (V, E_T)$ is called a *spanning tree* of X, if and only if it satisfies $E_T \subset E$ (see Fig. 2.3).

Homology groups of graphs are a special version of common homology groups, since a graph can be considered as a 1-dimensional CW complex. First by choosing an orientation E^o of an undirected graph $X = (V, E)$, we consider a directed graph

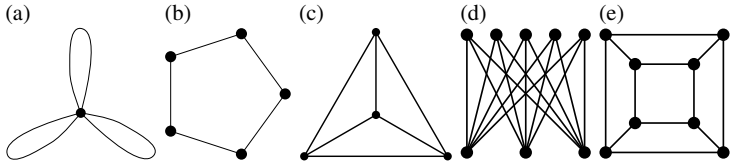

Fig. 2.1 **a** 3-bouquet graph B_3, **b** cycle graph C_5, **c** complete graph K_4 (tetrahedral graph), **d** complete bipartite graph $K_{3,5}$, **e** cubic graph

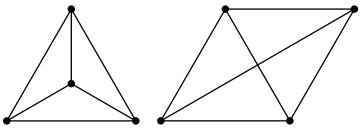

Fig. 2.2 Different figure of a K_4 graph

Fig. 2.3 Examples of spanning trees of a K_4 graph

$X' = (V, E^o)$. Let $C_0(X)$ and $C_1(X)$ be a 0-dimensional and a 1-dimensional chain group of a (directed) graph $X' = (V, E^o)$, namely $C_0(X) = \{\sum_{x\in V} a_x x \mid a_x \in \mathbb{Z}\}$ and $C_1(X) = \{\sum_{e\in E^o} a_e e \mid a_e \in \mathbb{Z}\}$. The boundary operator $\partial\colon C_1(X) \longrightarrow C_0(X)$ is defined by

$$\partial(e) = t(e) - o(e),$$

where $o(e)$ and $t(e)$ are the origin and terminus of the edge e. The homology group $H_0(X, \mathbb{Z})$ and $H_1(X, \mathbb{Z})$ is defined by

$$H_1(X, \mathbb{Z}) = \ker \partial \subset C_1(X), \quad H_0(X, \mathbb{Z}) = C_0(X)/\operatorname{image} \partial.$$

In the following, we write $[e] \in H_1(X, \mathbb{Z})$ for the equivalence class of e.

Proposition 2.1 (Sunada [54]) *For $X = (V, E)$ a locally finite graph, the equivalence class $[c] \in H_1(X, \mathbb{Z})$ of any non-trivial closed path c satisfies $[c] \neq [0]$. Conversely, for each non-zero element $h \in H_1(X, \mathbb{Z})$, there exists a closed path c in X such that $h = [c]$.*

Proof Since $c = e_1 + \cdots + e_k \in C_1(X, \mathbb{Z})$ for a path $c = e_1 \cdots e_k$ $(e_i \in E)$ in X, we obtain $\partial(c) = t(e_1) - o(e_k)$. If e is closed, then $t(e_1) = e(e_k)$, namely $\partial(c) = 0$. Therefore we obtain $[c] \neq [0] \in H_1(X, \mathbb{Z})$.

Next, for any $h \in H_1(X, \mathbb{Z}) = \ker \partial \subset C_1(X, \mathbb{Z})$, there exists $\alpha_i \in \mathbb{Z}$ and $\{e_i\} \subset E$ such that $h = \alpha_1 e_1 + \cdots + \alpha_k e_k$. The equation $\partial h = \sum \alpha_i (t(e_i) - o(e_i)) = 0$ implies that h is the sum of closed paths (see [53]). □

Proposition 2.1 implies that an element of $H_1(X, \mathbb{Z})$ corresponds to a closed path of X. Hence we obtain a method for counting the rank of $H_1(X, \mathbb{Z})$.

Proposition 2.2 *Assume $X = (V, E)$ is a finite graph, then the first homology group $H_1(X, \mathbb{Z})$ of X satisfies* rank $H_1(X, \mathbb{Z}) = (|E| - |E_T|)/2$, *where $T = (V, E_T)$ is a spanning tree of X.*

Proof By the definition of spanning trees, for each edge $e_0 = (u, v) \in E \setminus E_T$, we find unique path $e = e_1 \cdots e_k$ in T with $o(e_1) = v$, $t(e_k) = u$, satisfying $\widetilde{e_0} = e_0 e$ is a closed path in X. Hence by Proposition 2.1, we obtain $[\widetilde{e_0}] \in H_1(X, \mathbb{Z})$. For each $e_i \in E \setminus E_T$, there exists $[\widetilde{e_i}] \in H_1(X, \mathbb{Z})$ by a similar manner, and $\{[\widetilde{e_i}]\}$ are linearly independent.

Example 2.2 The rank of the first homology group of graphs in Fig. 2.6 are (a) 3, (b) 3, (c) 2, and (d) 4, respectively.

Remark 2.2 An algorithm to find a spanning tree of a finite graph is well-known as Kruskal's algorithm. By using the algorithm we find a spanning tree within $O(|E| \log |E|)$ (see Algorithm 7.1).

2.2 Covering Graph

We start with the definition of covering spaces for topological spaces [50], and covering graphs are also a special case of covering spaces for topological spaces.

Definition 2.6 A topological space X is a *covering space* of a topological space X_0 if there exists a surjective continuous map $p\colon X \longrightarrow X_0$, which is called a *covering map*, such that for each $x \in X_0$, there exists an open neighbourhood U of x and open sets $\{V_i\} \subset X$ satisfying $p^{-1}(U) = \sqcup V_i$ with $p|_{V_i}\colon V_i \longrightarrow U$ homeomorphic.

Theorem 2.1 *For any topological space X_0, there exists the unique simply connected covering space $\tilde{X}$, which is called the* universal covering *of X_0.*

For a covering map $p\colon X \longrightarrow X_0$, there exists a transformation group T on X such that for any $\sigma \in T$, $p \circ \sigma = p$. The group T is called the *covering transformation group*. If $\widetilde{X}$ is the universal covering space of X_0, then the covering transformation group of $p\colon \tilde{X} \longrightarrow X$ is the fundamental group $\pi_1(X)$ of X.

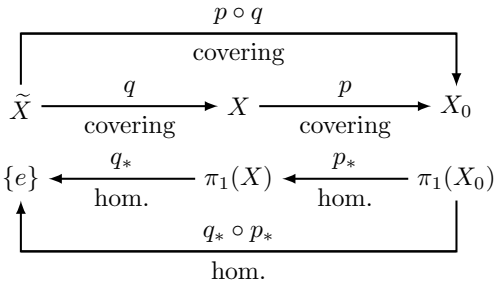

Example 2.3

1. The 1-dimensional Euclidean space (the real line) $\mathbb{R}$ is the universal covering space of S^1, since $p\colon \mathbb{R} \longrightarrow S^1, p(x) = x \pmod{2\pi}$. The covering transformation group of p is $\mathbb{Z}$, hence $\pi_1(S^1) \cong \mathbb{Z}$.
2. The 2-dimensional Euclidean space $\mathbb{R}^2$ is the universal covering space of $T^2 = \mathbb{R}^2/\mathbb{Z}^2$, since $p\colon \mathbb{R}^2 \longrightarrow T^2, p(x, y) = [x \pmod{2\pi}, y \pmod{2\pi}]$. The covering transformation group of p is $\mathbb{Z}^2$. Hence $\pi_1(T^2) \cong \mathbb{Z}^2$.
3. Let $SO(3)$ be a special orthogonal group, and I be an icosahedral group which is a discrete subgroup of $SO(3)$. The quotient space $SO(3)/I$ is called a Poincarè homology sphere and its universal covering space is S^3. The covering transformation group of this covering is I_h, which is called the *binary icosahedral group*.

Definition 2.7 (*Sunada* [54]) A covering $p\colon X \longrightarrow X_0$ with an abelian covering transformation group is called an *abelian covering*.

Definition 2.8 (*Sunada* [54]) Let $X = (V, E)$ and $X_0 = (V_0, E_0)$ be locally finite graphs. The graph X is a *covering graph* over X_0 if there exists a surjective map $p\colon X \longrightarrow X_0$, which is called a *covering map*, such that for each $x \in V, p|_{E_x}\colon E_x \longrightarrow E_{0,p(x)}$ is bijective.

Definition 2.9 (*Sunada* [54]) Let X be a covering graph over a locally finite graph X_0 and $p\colon X \longrightarrow X_0$ be the covering map. The *covering transformation group* $G(p)$ is a group that consists of all automorphisms $\sigma : X \longrightarrow X$ satisfying $p \circ \sigma = p$. A covering map $p\colon X \longrightarrow X_0$ is called *regular* if the action $G(p)$ on $p^{-1}(x)$ is transitive for all $x \in X_0$ i.e., $G(p)x = p^{-x}(x)$ for all $x \in X_0$.

For a regular covering map $p\colon X \longrightarrow X_0$, the graph X_0 is isomorphic to the quotient graph $X/G(p)$, which is the orbit space for the $G(p)$-action. For any topological space X_0, there exists the Hurewicz isomorphism $H_1(X_0, \mathbb{Z}) \cong \pi_1(X_0)/[\pi_1(X_0), \pi_1(X_0)]$, where $[G, G] = \langle aba^{-1}b^{-1} \mid a, b \in G\rangle$ is the commutator subgroup of a group G. Let $\widetilde{X}_0$ be the universal covering graph over a locally finite graph X_0; a covering graph $\overline{X}_0 = \widetilde{X}_0/[\pi_1(X_0), \pi_1(X_0)]$ over X_0 is an abelian one, whose transformation group is $H_1(X_0, \mathbb{Z})$. For each abelian covering map $p\colon X \longrightarrow X_0$, there exists a subcovering map $p_1 : \overline{X}_0 \longrightarrow X$ of $\overline{p}\colon \overline{X}_0 \longrightarrow X_0$. Hence, the covering graph $\overline{X}_0$ is called the *maximal abelian covering graph* of X_0 (cf. Sunada [54, Theorem 6.1]).

Coverings in examples 1 and 2 in Example 2.3 are abelian coverings, but 3 is not abelian since I_h is not abelian. Moreover, I_h has no non-trivial abelian quotients, the maximal abelian covering of a Poincaré homology sphere is itself.

Example 2.4

1. Let $C_n = (V_n, E_n)$ be a cycle graph with n vertices. If there exists $k \in \mathbb{N}$ such that $m = kn$, then $p\colon C_m \longrightarrow C_n, (V_m \ni x_{kj} \mapsto x_j \in V_n)$ is a covering map, whose covering transformation group is the abelian group of order k. The universal

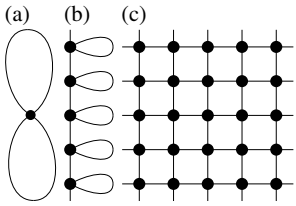

Fig. 2.4 **a** 2-bouquet graph, **b** covering graph of 2-bouquet graph, **c** square lattice, which is a maximal abelian covering graph of **a** and **b**

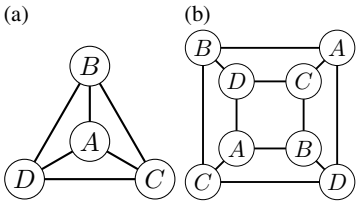

Fig. 2.5 **a** K_4 graph, **b** cubic graph: double covering of K_4 graph (a tetrahedron graph)

covering graph of C_n is the graph $C = (V, E)$, $V = \mathbb{Z}$, $E = \{(n, n+1) \mid n \in \mathbb{Z}\}$. The covering transformation group is $\mathbb{Z}$, hence C is also a maximal abelian covering space of C_n.

2. Let X_0 be a 2-bouquet graph (Fig. 2.4b). The graphs X_1 and X_2 (Fig. 2.4c, d) are covering graphs of X_0, whose covering transformation groups are $\mathbb{Z}$ and $\mathbb{Z}^2$, respectively. Since $H_1(X_0, \mathbb{Z}) \cong \mathbb{Z}^2$, the graph X_2, which is called a square lattice, is a maximal abelian covering. The universal covering graph of X_0 is a regular tree of degree 4. The fundamental group $\pi_1(X)$ is a free group with 3 elements.
3. The graph shown in Fig. 2.5b is a double covering of the K_4 graph.

2.3 Graph Laplacian

In this section, we first recall the assumptions that graphs are undirected and admit multiple and loop edges.

Definition 2.10 Let $X = (V, E)$ be a finite graph with $V = \{v_i\}_{i=1}^n$. The *adjacency matrix* $A = A_X = [a_{ij}]$ of X is an $n \times n$ matrix defined by $a_{ij} = \sharp[\text{edges } (v_i, v_j)]$.

Note that the adjacency matrix A_X of X is symmetric, since X is undirected.

Remark 2.3 Let A be an adjacency matrix of a graph X;

1. an (i, j)-element of A^k expresses the number of paths from v_i to v_j by k-steps;
2. if A^{n-1} $(n = |V|)$ is not block diagonal, then X is connected;
3. if X is simple and undirected, then $(1/6)\,\mathrm{tr}(A^3)$ expresses the number of triangles contained in X.

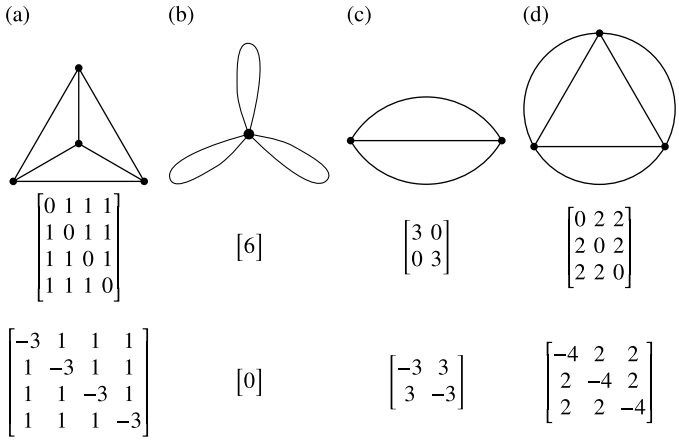

Fig. 2.6 Examples of graphs, their adjacency matrices (the second row), and their Laplacian (the third row)

Definition 2.11 Let $X = (V, E)$ be a finite graph with $V = \{v_i\}_{i=1}^n$. The *Laplacian* $\Delta = \Delta_X$ of X is an $n \times n$ matrix defined by $\Delta_X = A_X - \mathrm{Diag}_X$, where $\mathrm{Diag}_X = \mathrm{diag}(\deg(v_1), \ldots, \deg(v_n))$ is a diagonal matrix with the i-th diagonal elements $\deg(v_i)$.

Since, we assume X is undirected, the Laplacian Δ_X is symmetric. If X is a regular graph of degree d, $\Delta_X = A_X - dI_n$, where $n = |V|$ and I_n is the identity matrix of size n.

Remark 2.4 The Laplacian is also called the *Kirchhoff matrix*, it is sometimes defined by $\mathrm{Diag}_X - A_X$ (inverse sign of our definition). The matrix $\mathrm{Diag}_X + A_X$ is called the *signless Laplacian*.

Definition 2.12 Let $X = (V, E)$ be a finite directed graph with $V = \{v_i\}_{i=1}^n$ and $E = \{e_\alpha\}_{\alpha=1}^m$. The *gradient matrix* $D_X = [d_{i\alpha}]$ and *incidence matrix* $M_X = [m_{i\alpha}]$ of X are $n \times m$ matrices defined by

$$d_{i\alpha} = \begin{cases} 1 & (o(e_\alpha) = v_i), \\ -1 & (t(e_\alpha) = v_i), \\ 0 & (\text{otherwise}), \end{cases} \quad \text{and} \quad m_{i\alpha} = \begin{cases} 1 & (o(e_\alpha) = v_i), \\ 1 & (t(e_\alpha) = v_i), \\ 0 & (\text{otherwise}), \end{cases}$$

respectively.

Example 2.5 Incidence matrices and gradient matrices of graphs (under a suitable orientation) in Fig. 2.6 are

$$M_X = \begin{bmatrix} 1&1&0&0 \\ 1&0&0&0 \\ 1&0&0&1 \\ 0&1&1&0 \\ 0&0&1&1 \\ 0&1&0&1 \end{bmatrix}, \qquad \begin{bmatrix} 3 \\ 3 \\ 3 \end{bmatrix}, \qquad \begin{bmatrix} 1&1 \\ 1&1 \\ 1&1 \end{bmatrix}, \qquad \begin{bmatrix} 1&1&0 \\ 0&1&1 \\ 1&0&1 \\ 1&1&0 \\ 0&1&1 \\ 1&0&1 \end{bmatrix},$$

$$D_X = \begin{bmatrix} 1&-1&0&0 \\ 1&0&0&0 \\ 1&0&0&-1 \\ 0&1&-1&0 \\ 0&0&1&-1 \\ 0&-1&0&1 \end{bmatrix}, \qquad \begin{bmatrix} 0 \\ 0 \\ 0 \end{bmatrix}, \qquad \begin{bmatrix} 1&-1 \\ 1&-1 \\ 1&-1 \end{bmatrix}, \qquad \begin{bmatrix} 1&-1&0 \\ 0&1&-1 \\ -1&0&1 \\ 1&-1&0 \\ 0&1&-1 \\ -1&0&1 \end{bmatrix},$$

respectively.

Proposition 2.3 *For a finite graph X, the Laplacian Δ_X satisfies*

$$\Delta_X = -D_X D_X^T. \tag{2.1}$$

Proof By using the notation $D_X = [d_{i\alpha}]$ and $\Delta_X = [\ell_{ij}]$, we have

$$-d_{i\alpha}d_{\alpha j} = \begin{cases} 1 & i_X(e_\alpha) = (v_i, v_j) \text{ or } (v_j, v_i), \\ 0 & \text{otherwise}, \end{cases}$$

for $i \neq j$, hence we obtain

$$-\sum_{\alpha=1}^{|E|} d_{i\alpha}d_{\alpha j} = \sharp[\text{edges between } v_i \text{ and } v_j] = \ell_{ij}, \quad i \neq j.$$

On the other hand,

$$d_{i\alpha}d_{\alpha i} = \begin{cases} 1 & e_\alpha \text{ is not a loop edge, and } o(e_\alpha) \text{ or } t(e_\alpha) = v_i, \\ 0 & \text{otherwise}, \end{cases}$$

since $d_{i\alpha} = 0$ if e_α is a loop edge. Hence we obtain

$$\begin{aligned} -\sum_{\alpha=1}^{|E|} d_{i\alpha}d_{\alpha j} &= -\deg(v_i) + \sharp[\text{loop edges with which } v_i \text{ is incident}] \\ &= -\ell_{ii}. \end{aligned}$$

This proves the claim. □

For a finite graph $X = (V, E)$, the Laplacian Δ_X is a $|V| \times |V|$ matrix, therefore we may define *eigenvalues* of Δ_X usual way.

Theorem 2.2 *Eigenvalues* $\{\lambda_i\}_{i=0}^{|V|-1}$ *of* $-\Delta_X$ *of a finite graph* $X = (V, E)$ *are non-negative. Moreover, if the graph* X *is connected, then* $\lambda_0 = 0$ *and* $\lambda_1 > 0$ *are satisfied, writing eigenvalues in ascending order* $\lambda_0 \leq \cdots \leq \lambda_{|V|-1}$.

Proof By Proposition 2.3, we may write $-\Delta_X = D_X^T D_X$ and

$$\langle -\Delta_X v, v\rangle = \left\langle D_X D_X^T v, v\right\rangle = |D_X^T v|^2, \tag{2.2}$$

where $v \in \mathbb{R}^n$ and $\langle \bullet, \bullet\rangle$ is the standard inner product of $\mathbb{R}^n$ ($n = |V|$). Since Δ_X is a symmetric matrix and satisfies (2.2), eigenvalues of $-\Delta_X$ are real and non-negative.

By the definition of $\Delta_X = [d_{ij}]$, we have $\sum_{j=1}^n d_{ij} = 0$ for $i = 1, \ldots, n$. Therefore we obtain

$$\Delta_X x_0 = \left[\sum_{j=1}^n d_{1j} \cdots \sum_{j=1}^n d_{nj}\right]^T = 0,$$

where $x_0 = \left[1 \cdots 1\right]^T$. Hence 0 is an eigenvalues of $-\Delta_X$.

By using the Rayleigh principle, we obtain

$$\begin{aligned} \lambda_1 &= \inf_{x\in\mathbb{R}^n, |x|=1, x\perp x_0} \langle -\Delta_X x, x\rangle = \inf_{x\in\mathbb{R}^n, |x|=1, x\perp x_0} |D_X^T x|^2 \\ &= \inf_{x\in\mathbb{R}^n, |x|=1, x\perp x_0} \sum_{(v_i, v_j)\in E} |x_i - x_j|^2. \end{aligned} \tag{2.3}$$

Here, we assume $\lambda_1 = 0$, then there exists $x = \left[x_j\right]^T \perp x_0$ and $x_i = x_j$ for any $(v_i, v_j) \in E$. Here we let $x_{I_0} = 1/\sqrt{n}$, then $x_i = 1/\sqrt{n}$ for all v_i connected to v_{i_0}. Since we assume X is connected, this argument yields that $x = (1/\sqrt{n})x_0$. This contradicts the assumption $x \perp x_0$. Hence we obtain $\lambda_1 > 0$. □

Remark 2.5 The Laplacian Δ_M on a Riemannian manifold is defined as the operator satisfying $\Delta_M = -\nabla^*\nabla$ by using the covariant differentiation ∇ and its L^2-adjoint ∇^* (compare (2.1)). In addition, assume M is compact, then for $u \in C^\infty(M)$, the Laplacian also satisfies $-\langle \Delta_M u, u\rangle_{L^2(M)} = \|\nabla u\|^2_{L^2(M)}$ (compare (2.2)).

In the case that a graph X has special properties, we obtain particular information on eigenvalues of the Laplacian.

Theorem 2.3 *Let* X *be a* d*-regular finite graph, then eigenvalues* $\{\lambda_k\}$ *of* $-\Delta_X$ *satisfy* $\lambda_k \in [0, 2d]$.

There are several proofs of Theorem 2.3; here we prove it using the Gershgorin circle theorem, which is famous in numerical analysis.

Theorem 2.4 (Gershgorin circle theorem) *Let* A *be an* $n \times n$ *complex matrix, and*

$$R_i = \sum_{j \neq i} |a_{ij}|, \quad i = 1, \ldots, n.$$

Then any eigenvalues $\lambda \in \mathbb{C}$ of A are contained in at least one disk $B_{R_i}(a_{ii})$ ($\subset \mathbb{C}$).

Proof Let $\phi = [\phi_j]$ be an eigenvector with eigenvalue λ. Selecting k as the index such that $|\phi_j|$ ($j = 1, \ldots, n$) is a maximum, we have

$$\sum_{j=1}^{n} a_{kj}\phi_j = \lambda\phi_k, \tag{2.4}$$

hence we obtain

$$\sum_{j \neq k}^{n} a_{kj}\phi_j = (\lambda - a_{kk})\phi_k. \tag{2.5}$$

Since $\phi_k \neq 0$ and $|\phi_j/\phi_k| \leq 1$, by (2.5), we obtain

$$|\lambda - a_{kk}| = \left| \sum_{j \neq k}^{n} a_{kj} \frac{\phi_j}{\phi_k} \right| \leq \sum_{j \neq k}^{n} |a_{kj}| \left| \frac{\phi_j}{\phi_k} \right| \leq \sum_{j \neq k}^{n} |a_{kj}| = R_k, \tag{2.6}$$

therefore we obtain the claim. □

Proof (Proof of Theorem 2.3) Since X is d-regular, $-\Delta_X = [a_{ij}]$ satisfy $a_{ii} = d$, $a_{ij} = 0$, or -1 ($i \neq j$), and $\sum_{j \neq i} a_{ij} = -d$. Therefore by Theorem 2.4, eigenvalues $\{\lambda_k\}$ of $-\Delta_X$ satisfies

$$|\lambda_k - d| \leq \sum_{i \neq j} |a_{ij}| = d,$$

namely $\lambda_k \in [0, 2d]$. □

Definition 2.13 A locally finite graph $X = (V, E)$ is called *bipartite*, if and only if there exists V_1, $V_2 \subset V$ such that V is the disjoint union of V_1 and V_2, and each edge $e \in E$ has one end in V_1 and the other end in V_2. The set (V_1, V_2) is called a *bipartition* of V.

Example 2.6 A graph $K_{3,3}$ is bipartite (see Fig. 2.7); however, complete graphs K_n ($n \geq 3$) are not bipartite, since there exists a closed path with odd length, in particular, a close path with length 3. But, a cubic graph (a double covering graph of K_4) is bipartite.

Theorem 2.5 *Assume $X = (V, E)$ is a finite bipartite graph. If λ is an eigenvalue of the* adjacency matrix *A_X of X, then $-\lambda$ is also an eigenvalue of A_X.*

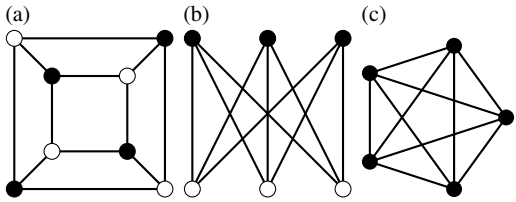

Fig. 2.7 **a** Cubic graph (double cover of K_4 graph), **b** $K_{3,3}$ graph, **c** K_5 graph. The cubic graph and $K_{3,3}$ are bipartite, but K_5 is not bipartite, since it contains a closed path with length 3

Proof Let $V = V_1 \cup V_2$ is a bipartition of V, and let $V_1 = \{v_1, v_3, \ldots, v_{|V|/2-1}\}$, $V_2 = \{v_2, v_4, \ldots, v_{|V|/2}\}$. Now we assume $\phi = [\phi_i]$ is an eigenvector with eigenvalue λ, i.e., $A_X\phi = \lambda\phi$, and we define $\widetilde{\phi} = [(-1)^i\phi_i]$. Then the $2i$-th elements of $A_X\widetilde{\phi}$ satisfies

$$[A_X\widetilde{\phi}]_{2i} = \sum_{j=1}^{n}(-1)^j a_{2ij}\phi_j = -\sum_{j=1}^{n} a_{2ij}\phi_j = -\lambda\widetilde{\phi}, \tag{2.7}$$

since adjacencies of $v_{2i} \in V_2$ are contained in V_1. Similarly, we also obtain

$$[A_X\widetilde{\phi}]_{2i-1} = \sum_{j=1}^{n}(-1)^j a_{2i-1\,j}\phi_j = \sum_{j=1}^{n} a_{2i-1\,j}\phi_j = -\lambda\widetilde{\phi}. \tag{2.8}$$

Therefore by (2.7) and (2.8), we obtain $A_X\widetilde{\phi} = -\lambda\widetilde{\phi}$. □

By using Theorem 2.5, we easily obtain the following:

Corollary 2.1 *Let X be a finite bipartite regular graph, then an eigenvector for the maximum eigenvalue of the adjacency matrix A_X is simple and it is given by $\phi = [(-1)^i]$.*

Definition 2.14 The *line graph* $L(X)$ of a locally finite graph $X = (V, E)$ is the graph whose vertices are the undirected edges of X and two undirected edges e_i and $e_j \in E$ are adjacent in $L(X)$ if undirected edges e_i and e_j are adjacent in X. If a graph X has a loop edge e, we define that e is incident itself.

The following theorem helps us to describe line graphs.

Theorem 2.6 *For a finite graph X,*

$$M_X^T M_X = A_{L(X)} + 2I_{|V(X)|} \tag{2.9}$$

holds, where M_X is the incidence matrix of X, $A_{L(X)}$ is the adjacency matrix of $L(X)$, and $I_{|V(X)|}$ is the identity matrix of size $|V(X)|$. In particular, if X is d-regular, then $L(X)$ is $(2d-2)$-regular and

$$M_X^T M_X = \Delta_{L(X)} + 2dI_{|V(X)|}. \tag{2.10}$$

Proof Components $m_{i\alpha}$ of the incidence matrix $M_X = [m_{i\alpha}]$ of X expressed that $m_{i\alpha} = 1$ if a vertex $v_i \in V(X)$ is incident with a non-loop edge $e_\alpha \in E(X)$, $m_{i\alpha} = 2$ if a vertex $v_i \in V(X)$ is incident with a loop edge $e_\alpha \in E(X)$. In the case of $\alpha \neq \beta$, $m_{\alpha k} m_{k\beta} = 1$ if and only if the vertex $v_k \in V$ is incident with e_α and e_β, and hence we obtain

$$\sum_{k=1}^{|V(X)|} m_{\alpha k} m_{k\beta} \\ = \sharp[\text{edges in } L(X) \text{ which } u_\alpha \text{ and } u_\beta \in V(L(X)) \text{ are incident with}]. \tag{2.11}$$

In the case of $\alpha = \beta$, since each column of M_X has just two non-zero components (each edge has two ends), we obtain

$$\sum_{k=1}^{|V(X)|} m_{\alpha k} m_{k\alpha} \\ = 2 + 2\sharp[\text{loop edges in } L(X) \text{ which } u_\alpha \in V(L(X)) \text{ is incident with}]. \tag{2.12}$$

Therefore by (2.11) and (2.12), we obtain (2.9).

Assume that X is d-regular, and write adjacents of $v_1 \in V(X)$ as $v_2, v_{x_1}, \ldots, v_{x_{d-1}}$ and adjacents of v_{x_1} as $v_1, v_{y_2}, \ldots v_{y_{d-1}}$, then adjacents of $v_{12} \in V(L(X))$ are $v_{1x_2}, \ldots, v_{1x_{d-1}}, v_{2y_2}, \ldots, v_{2y_{d-1}}$. Hence the line graph $L(X)$ is $(2d-2)$-regular if X is d-regular, and (2.10) is easily obtained from $\Delta_{L(X)} = A_{L(X)} - (2d-2)I$. □

Example 2.7

1. Let X be the graph in Fig. 2.8, upper row of (a). Then the line graph $L(X)$ of X is Fig. 2.8, lower row of (a). Incidence matrix and gradient matrix (under a suitable orientation) of X are

$$M_X = \begin{bmatrix} 1&1&0&0&0&0&0&1&0 \\ 1&0&1&0&0&0&0&0&1 \\ 0&1&1&1&0&0&0&0&0 \\ 0&0&0&1&1&1&0&0&0 \\ 0&0&0&0&1&0&1&1&0 \\ 0&0&0&0&0&1&1&0&1 \end{bmatrix}, \quad D_X = \begin{bmatrix} 1&1&0&0&0&0&0&1&0 \\ -1&0&1&0&0&0&0&0&1 \\ 0&-1&-1&1&0&0&0&0&0 \\ 0&0&0&-1&1&1&0&0&0 \\ 0&0&0&0&-1&0&1&-1&0 \\ 0&0&0&0&0&-1&-1&0&-1 \end{bmatrix},$$

$$M_X^T M_X = \begin{bmatrix} 2&1&1&0&0&0&0&1&1 \\ 1&2&1&1&0&0&0&1&0 \\ 1&1&2&1&0&0&0&0&1 \\ 0&1&1&2&1&1&0&0&0 \\ 0&0&0&1&2&1&1&1&0 \\ 0&0&0&1&1&2&1&0&1 \\ 0&0&0&0&1&1&2&1&1 \\ 1&1&0&0&1&0&1&2&0 \\ 1&0&1&0&0&1&1&0&2 \end{bmatrix}, \quad D_X D_X^T = \begin{bmatrix} 3&-1&-1&0&-1&0 \\ -1&3&-1&0&0&-1 \\ -1&-1&3&-1&0&0 \\ 0&0&-1&3&-1&-1 \\ -1&0&0&-1&3&-1 \\ 0&-1&0&-1&-1&3 \end{bmatrix},$$

and they satisfy $D_X D_X^T = -\Delta_X$, $M_X^T M_X = A_{L(X)} + 2I_8$. Moreover, since the graph X is 3-regular, $L(X)$ is 4-regular and M_X and $\Delta_{L(X)}$ satisfy $M_X^T M_X = \Delta_{L(X)} + 6I_8$.

2. Let X be the graph in Fig. 2.8, upper row of (b), which has multiple edges. The line graph $L(X)$ of X is Fig. 2.8, lower row of (b). Incidence matrix and gradient

matrix (under a suitable orientation) of X are

$$M_X = \begin{bmatrix} 1&1&1&0&0 \\ 1&1&0&1&0 \\ 0&0&1&1&1 \\ 0&0&0&0&1 \end{bmatrix}, \qquad D_X = \begin{bmatrix} 1&-1&1&0&0 \\ -1&1&0&-1&0 \\ 0&0&-1&1&-1 \\ 0&0&0&0&1 \end{bmatrix},$$

$$M_X^T M_X = \begin{bmatrix} 2&2&1&1&0 \\ 2&2&1&1&0 \\ 1&1&2&1&1 \\ 1&1&1&2&1 \\ 0&0&1&1&2 \end{bmatrix}, \qquad D_X D_X^T = \begin{bmatrix} 3&-2&-1&0 \\ -2&3&-1&0 \\ -1&-1&3&-1 \\ 0&0&-1&1 \end{bmatrix},$$

and they satisfy $D_X D_X^T = -\Delta_X$, $M_X^T M_X = A_{L(X)} + 2I_6$.

3. Let X be the graph in Fig. 2.8, upper row of (c), which has multiple edges and a loop edge. The line graph $L(X)$ of X is Fig. 2.8, lower row of (c). Incidence matrix and gradient matrix (under a suitable orientation) of X are

$$M_X = \begin{bmatrix} 1&1&1&0&0&0 \\ 1&1&0&1&0&0 \\ 0&0&1&1&1&0 \\ 0&0&0&0&1&2 \end{bmatrix}, \qquad D_X = \begin{bmatrix} 1&1&1&0&0&0 \\ -1&-1&0&1&0&0 \\ 0&0&-1&-1&1&0 \\ 0&0&0&0&-1&0 \end{bmatrix},$$

$$M_X^T M_X = \begin{bmatrix} 2&2&1&1&0&0 \\ 2&2&1&1&0&0 \\ 1&1&2&1&1&0 \\ 1&1&1&2&1&0 \\ 0&0&1&1&2&2 \\ 0&0&0&0&2&4 \end{bmatrix}, \qquad D_X D_X^T = \begin{bmatrix} 3&-2&-1&0 \\ -2&3&-1&0 \\ -1&-1&3&-1 \\ 0&0&-1&1 \end{bmatrix},$$

and they satisfy $D_X D_X^T = -\Delta_X$, $M_X^T M_X = A_{L(X)} + 2I_6$. Moreover, the graph X is 3-regular and the line graph $L(X)$ is 4-regular.

4. Let X be the graph in Fig. 2.6c, which has multiple edges. The line graph $L(X)$ of X is the graph in Fig. 2.6d.
5. For 3-bouquet graph B_3, its incidence matrix and gradient matrix (under a suitable orientation) are

$$M_X = \begin{bmatrix} 2&2&2 \end{bmatrix}, \quad D_X = \begin{bmatrix} 0&0&0 \end{bmatrix},$$

and we obtain

$$M_X^T M_X = \begin{bmatrix} 4&4&4 \\ 4&4&4 \\ 4&4&4 \end{bmatrix} = A_{L(X)} + 2I_3, \quad D_X D_X^T = \begin{bmatrix} 0 \end{bmatrix} = -\Delta_X.$$

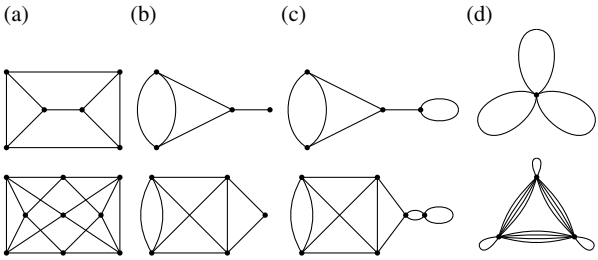

Fig. 2.8 Each graph in the lower row is the line graph of the upper row

Chapter 3
Topological Crystals

Standard realizations of topological crystals describe the most symmetric crystal structure among given graph structures, namely including chemical bonds of atoms in the crystal. In this chapter, we discuss the notion of topological crystals by using abelian covering graphs, and standard realizations by using variational principles. We also explicitly calculate examples of standard realizations.

3.1 Topological Crystals and Their Standard Realizations

Definition 3.1 (*Sunada* [54]) A connected locally finite graph $X = (V, E)$, which may include self-loops and multiple edges, is called a d-dimensional *topological crystal* (or a *crystal lattice*), if and only if there exists a free abelian group G of the rank d, which acts freely on X, such that X/G is finite.

For a topological crystal $X = (V, E)$, there exists a finite graph $X_0 = (V_0, E_0)$ satisfying $X/G = X_0$, where G is an abelian subgroup of $H_1(X_0, \mathbb{Z})$, and X is a covering graph of X_0 whose covering transformation group is G. On the contrary, for a given connected finite graph $X_0 = (V_0, E_0)$ and an abelian subgroup $G \subset H_1(X_0, \mathbb{Z})$, there exists a topological crystal X with $X/G = X_0$.

Definition 3.2 (*Sunada* [54]) A topological crystal X is called *maximal abelian* if and only if $G \cong H_1(X_0, \mathbb{Z})$.

Example 3.1 A *square lattice* X (Fig. 3.1a) is a topological crystal whose base graph X_0 is the 2-bouquet graph (Fig. 3.3a). Since the covering transformation group G is $G = H_1(X_0, \mathbb{Z})$ and rank G = rank $H_1(X_0, \mathbb{Z}) = 2$, a square lattice is 2-dimensional and maximal abelian.

Example 3.2 A *triangular lattice* X (Fig. 3.1b) is a topological crystal whose base graph X_0 is the graph in Fig. 2.6b. Since the covering transformation group G satisfies rank $G = 2$, but $H_1(X_0, \mathbb{Z}) = 3$, a triangular lattice is 2-dimensional and not maximal abelian.

H. Naito, *Trivalent Discrete Surfaces and Carbon Structures*,
SpringerBriefs in the Mathematics of Materials 5,
https://doi.org/10.1007/978-981-99-5769-9_3

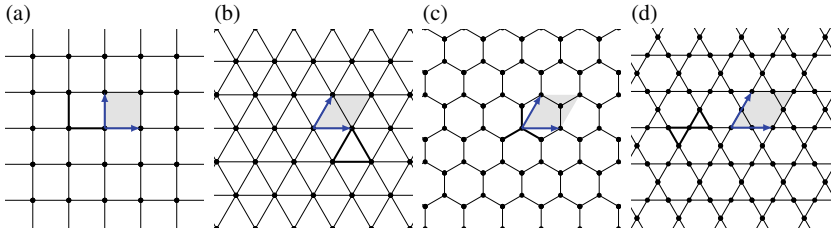

Fig. 3.1 **a** A square lattice, **b** a triangular lattice, **c** a hexagonal lattice, and **d** a kagome lattice, which are standard realizations of representative 2-dimensional topological crystals. Blue vectors in figures are a basis of parallel translations. Thick edges in figures are a fundamental piece of parallel translations

Example 3.3 A *hexagonal lattice* X (Fig. 3.1c) is a topological crystal whose base graph X_0 is the graph in Fig. 2.6c. Since the covering transformation group G is $G = H_1(X_0, \mathbb{Z})$ and rank $G = \text{rank}\, H_1(X_0, \mathbb{Z}) = 2$, a hexagonal lattice is 2-dimensional and maximal abelian.

Example 3.4 A *kagome lattice* X (Fig. 3.1d) is a topological crystal whose base graph X_0 is the graph in Fig. 2.6d. Since the covering transformation group G satisfies rank $G = 2$ but $H_1(X_0, \mathbb{Z}) = 4$, a kagome lattice is 2-dimensional and not maximal abelian.

Example 3.5 A *diamond lattice* X (Fig. 3.24) is a topological crystal whose base graph X_0 is the 3-bouquet graph (Fig. 2.6b). Since the covering transformation group G is $G = H_1(X_0, \mathbb{Z})$ and rank $G = \text{rank}\, H_1(X_0, \mathbb{Z}) = 3$, a diamond lattice is 3-dimensional and maximal abelian.

Definition 3.3 (*Sunada* [54]) A piecewise linear map $\Phi\colon X \longrightarrow \mathbb{R}^d$ is called a *realization* of d-dimensional topological crystal $X = (V, E)$.

A map $\Phi\colon X \longrightarrow \mathbb{R}^d$ is piecewise linear means that first we define $\Phi\colon V \longrightarrow \mathbb{R}^d$ and define $\Phi(e)$ by linear interpolation between $\Phi(o(e))$ and $\Phi(t(e))$.

Definition 3.4 (*Sunada* [54]) A realization Φ of a d-dimensional topological crystal X is called a *periodic realization*, if there exists an injective homomorphism $\rho\colon G \longrightarrow \mathbb{R}^d$ satisfying

$$\Phi(gv) = \Phi(v) + \rho(g), \quad (v \in V,\ g \in G).$$

Example 3.6 Realizations in Fig. 3.2 are different periodic realizations of a hexagonal lattice. It is well-known that the realization (b) is the most symmetric among the three figures in Fig. 3.2. The main problem of this section is to explain the reason why nature selects (b) by mathematics.

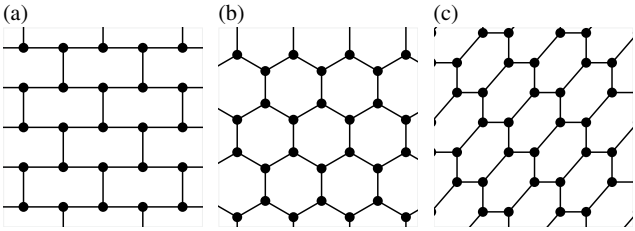

Fig. 3.2 Different periodic realizations of the hexagonal lattice

Definition 3.5 (*Sunada* [54]) Let X be a d-dimensional topological crystal with the base graph $X_0 = (V_0, E_0)$, G be an abelian group acting on X, and Φ or (Φ, ρ) be a periodic realization of X, where $\rho\colon G \longrightarrow GL(d, \mathbb{R})$. The *energy* and the *normalized energy* of Φ are defined by

$$E(\Phi) = \sum_{e \in E_0} |\Phi(t(e)) - \Phi(o(e))|^2, \tag{3.1}$$

and

$$E(\Phi, \rho) = \mathrm{Vol}(\Gamma)^{-2/d} \sum_{e \in E_0} |\Phi(t(e)) - \Phi(o(e))|^2, \tag{3.2}$$

respectively, where $\Gamma = \rho(G)$ and $\mathrm{Vol}(\Gamma)$ is the volume of the fundamental domain of Γ in $\mathbb{R}^d$.

The energy of Φ is a discrete analogue of the Dirichlet energy for smooth maps on a Riemannian manifold.

Definition 3.6 (*Sunada* [54]) For a topological crystal X with *fixed lattice* $\Gamma = \rho(G)$, a critical point Φ of the energy E is called a *harmonic realization* of X.

In the following, we abbreviate $\boldsymbol{v} = \Phi(v)$ and $\boldsymbol{e} = \Phi(e)$ for $v \in V$ and $e \in E$, as long as there are no misunderstandings.

Proposition 3.1 *(Sunada [54]) For a topological crystal X, a realization Φ is harmonic if and only if*

$$\sum_{(u,v) \in (E_0)_v} (\boldsymbol{u} - \boldsymbol{v}) = \boldsymbol{0}, \quad \textit{for all } v \in V_0, \tag{3.3}$$

or equivalently

$$\Delta_{X_0} \boldsymbol{v} = \boldsymbol{0} \quad \textit{for all } v \in V_0. \tag{3.4}$$

That is to say, the sum of vectors creating edges emanating from each v is zero, in other words, each vertex of V satisfies the "balancing condition".

Proof For a fixing Γ with $\mathrm{Vol}(\Gamma) = 1$, we have $E(\Phi) = E(\Phi, \rho)$. By using the gradient matrix D_{X_0} of X_0 under a suitable orientation, we may write

$$E(\Phi) = \frac{1}{2}|D_{X_0}\boldsymbol{e}|^2. \tag{3.5}$$

Let $\Phi_t \colon X \longrightarrow \mathbb{R}^d$ be a variation of Φ with $\Phi_0 = \Phi$. Differentiating $E(\Phi_t)$ by t and using the "integration by parts", we may calculate this as

$$\frac{d}{dt}E(\Phi_t) = \left\langle M_{X_0}\boldsymbol{v}, D_{X_0}\boldsymbol{v}'\right\rangle = \left\langle D_{X_0}^T D_{X_0}\boldsymbol{v}, \boldsymbol{v}'\right\rangle = -\left\langle \Delta_{X_0}\boldsymbol{v}, \boldsymbol{v}'\right\rangle,$$

where $\boldsymbol{v}(t) = \Phi_t(v)$. Therefore, we obtain

$$\left.\frac{d}{dt}E(\Phi_t)\right|_{t=0} = -\left\langle \Delta_{X_0}\boldsymbol{v}, \boldsymbol{v}'\right\rangle = -2\sum_{v\in V_0}\sum_{u\in E_v}\langle \boldsymbol{v}-\boldsymbol{u}, \boldsymbol{x}_u\rangle, \quad \boldsymbol{x}_u = \left.\Phi_t'(u)\right|_{t=0},$$

and get the result. □

Remark 3.1 1. In Definition 3.6, if we do not assume that the lattice Γ is fixed, then critical points admit $\Phi = 0$ and $E(\Phi) = 0$.
2. For a smooth map $u \colon \Omega \longrightarrow \mathbb{R}$ with $u|_{\partial\Omega} = 0$, where Ω is a domain in $\mathbb{R}^N$, the Dirichlet energy E of u is defined by $E(u) = \frac{1}{2}\int_\Omega |\nabla u|^2\, dV$, and its Euler–Lagrange equation is $\Delta u = 0$ (the Laplace equation). This is why the critical points of E for topological crystals are called harmonic.

Example 3.7 Realizations (b) and (c) of Fig. 3.2 are harmonic, since each vertex $v \in V_0$ satisfies the balance condition (3.4), but the realization (a) of Fig. 3.2 is not harmonic. Hence, the harmonic conditions (3.3) or (3.4) are not sufficient to select (b) among this three realizations in Fig. 3.2.

Proposition 3.2 (Sunada [54]) *Harmonic realizations of X are unique up to affine transformations.*

Proof The Eq. (3.3) is invariant under affine transformations. Let $\{e_i\}_{i=1}^d$ be a $\mathbb{Z}$-basis of the abelian group G, which acts on X. Assume $\Phi_1(X)$ and $\Phi_2(X)$ are harmonic realizations of X with respect to lattice $\Gamma_1 = \rho_1(L)$ and $\Gamma_2 = \rho_2(L)$, respectively. Then, there exists an $A \in GL(d, \mathbb{R})$ such that $\rho_1(g) = A\rho_2(g)$ for $g \in G$. Hence, we obtain that there exists $\boldsymbol{b} \in \mathbb{R}^d$ such that $\Phi_1 = A\Phi_2 + \boldsymbol{b}$. □

Definition 3.7 (*Sunada* [54]) For a topological crystal X, *standard realizations* of X are critical points of E among all realizations Φ and Γ with $\mathrm{Vol}(\Gamma) = 1$.

A standard realization is also called an *equilibrium placement*, defined by Delgado-Friedrichs–O'Keeffe [8].

Theorem 3.1 (Kotani–Sunada [29], Sunada [54]) *For any topological crystals X, there exists the unique standard realization up to Euclidean motions.*

Kotani–Sunada proved Theorem 3.1 by using a theory of harmonic maps. Eells–Sampson [11] proved the existence theorem of harmonic maps from a compact Riemannian manifold into a non-positively curved Riemannian manifold. The energy (3.1) is the Dirichlet energy of maps from a 1-dimensional CW complex into a Euclidean space. Hence, by Eells–Sampson's theorem, there exists a standard realization (an energy minimizing harmonic map) in each homotopy class. Sunada also gave another proof of Theorem 3.1 in his lecture note [54]. On the other hand, the existence of standard realizations can be also proved by showing the strong convexity of the energy (3.1).

Since we may consider standard realizations as discrete harmonic maps from a 1-dimensional CW complex into $\mathbb{R}^d$, recently, Kajigaya–Tanaka [20] studied the existence of discrete harmonic maps into Riemann surfaces of genus greater than or equal to two (negatively curved Riemann surfaces).

Theorem 3.2 (Sunada [52–54]) *For a d-dimensional topological crystal X, a realization Φ is standard if and only if*

$$\sum_{e\in E_0} \boldsymbol{e} = \boldsymbol{0}, \tag{3.6}$$

$$\sum_{e\in E_0} \langle \boldsymbol{x}, \boldsymbol{e}\rangle \boldsymbol{e} = c\boldsymbol{x} \quad \textit{for all } \boldsymbol{x} \in \mathbb{R}^d \textit{ and for some } c > 0. \tag{3.7}$$

Proof First, we define $T\colon \mathbb{R}^d \longrightarrow \mathbb{R}^d$ by $T\boldsymbol{x} = \sum_{e\in E_0} \langle \boldsymbol{x}, \boldsymbol{e}\rangle \boldsymbol{e}$. Since

$$\langle T\boldsymbol{x}, \boldsymbol{y}\rangle = \sum_{e\in E_0} \langle \boldsymbol{x}, \boldsymbol{e}\rangle \langle \boldsymbol{y}, \boldsymbol{e}\rangle = \langle \boldsymbol{x}, T\boldsymbol{y}\rangle, \tag{3.8}$$

we obtain that T is symmetric. We can prove that Φ is a standard realization if and only if there exists a positive constant $c > 0$ such that $T = cI$.

On the other hand, for any symmetric matrix T of size d with positive eigenvalues, there exists an orthogonal matrix P such that $P^T TP = \mathrm{diag}(\lambda_1, \ldots, \lambda_d)$, where $\lambda_j > 0$ are eigenvalues of T. The inequality of arithmetic and geometric means implies

$$\mathrm{tr}\, T = \mathrm{tr}\, P^T TP \geq d(\det P^T TP)^{1/d} = d(\det T)^{1/d},$$

and the equality holds if and only if $T = \lambda I_d$.

Here, we write $E_0 = \{e_\alpha\}_{\alpha=1}^{|E_0|}$, and $\boldsymbol{e}_i = [e_{\alpha 1}, \ldots, e_{\alpha d}] \in \mathbb{R}^d$. Since the Eq. (3.7) is equivalent to

$$\langle T\boldsymbol{x}, \boldsymbol{y}\rangle = \sum_{e\in E_0} \langle \boldsymbol{e}, \boldsymbol{x}\rangle \langle \boldsymbol{e}, \boldsymbol{y}\rangle = c\langle \boldsymbol{x}, \boldsymbol{y}\rangle, \tag{3.9}$$

taking an orthogonal basis $\{\boldsymbol{x}_j\}_{j=1}^d$ of $\mathbb{R}^d$, and setting $\boldsymbol{x} = \boldsymbol{x}_j$, and $\boldsymbol{y} = \boldsymbol{x}_k$, we obtain

$$\sum_{\alpha=1}^{|E_0|} e_{\alpha j} e_{\alpha k} = c\delta_{jk}, \tag{3.10}$$

and

$$\mathrm{Vol}(\Gamma)^{2/d} E(\Phi, \rho) = \sum_{e \in E_0} |\boldsymbol{e}|^2 = \sum_{\alpha=1}^{|E_0|} \sum_{j=1}^{d} e_{\alpha j}^2 = cd. \tag{3.11}$$

Now, we assume that (Φ_1, ρ_1) is a standard realization of X and (Φ_2, ρ_2) is a harmonic realization of X. By Proposition 3.2, there exists an $A = [a_{ij}] \in GL(d, \mathbb{R})$ and $\boldsymbol{b} \in \mathbb{R}^d$ such that $\Phi_2 = A\Phi_1 + \boldsymbol{b}$ and $\rho_1 = A\rho_2$. Then, we obtain

$$\mathrm{Vol}(\Gamma_1) = |\det A| \, \mathrm{Vol}(\Gamma_2), \quad f_{\alpha i} = \sum_{j=1}^{d} a_{ij} e_{\alpha j},$$

and

$$\begin{aligned}
\mathrm{Vol}(\Gamma_2)^{2/d} E(\Phi_2, \rho_2) &= \sum_{i=1}^{d} \sum_{\alpha=1}^{|E_0|} f_{\alpha i}^2 = \sum_{i=1}^{d} \sum_{j,k=1}^{d} \sum_{\alpha=1}^{|E_0|} a_{ij} a_{ik} e_{\alpha j} e_{\alpha_k} \\
&= \sum_{i=1}^{d} \sum_{j,k=1}^{d} \sum_{\alpha=1}^{|E_0|} a_{ij} a_{ik} \delta_{jk} = c \sum_{i=1}^{d} \sum_{j=1}^{d} a_{ij} a_{ij} = c \, \mathrm{tr} A^T A \\
&\geq cd (\det A^T A)^{1/d} = cd |\det A|^{2/d} = cd (\mathrm{Vol}(\Gamma_2)/\mathrm{Vol}(\Gamma_1))^{2/d} \\
&= cd \, \mathrm{Vol}(\Gamma_2) E(\Phi_1, \rho_1).
\end{aligned}$$

This implies that $E(\Phi_2, \rho_2) \geq E(\Phi_1, \rho_1)$ if and only if the Eq. (3.7) holds. □

Theorem 3.3 (Sunada [52–54]) *Assume that Φ is a standard realization of a d-dimensional topological crystal. Then, each element $\sigma \in \mathrm{Aut}(X)$ extends as an element of $\mathrm{Aut}(\Phi(X)) \subset O(d) \ltimes \mathbb{R}^d$ (Euclidean motion group of $\mathbb{R}^d$).*

Theorem 3.3 means that standard realizations, which are obtained by a variational principle, have maximal symmetry among all the realizations of a topological crystal.

Example 3.8 The realization (b) of Fig. 3.2 is a standard realization of a hexagonal lattices, whereas, the realization (c) of Fig. 3.2 is not standard.

Example 3.9 Let $\triangle ABC$ be a triangle on a plane and O be the barycenter of the triangle, and consider a graph $X = (V, E)$ consisting of $V = \{O, A, B, C\}$ and $E = \{(O, A), (O, B), (O, C)\}$. By a property of the barycenter of triangles, we obtain $\overrightarrow{OA} + \overrightarrow{OB} + \overrightarrow{OC} = \mathbf{0}$. That is to say, the balancing condition (3.3) holds for $O \in V$; however, the condition (3.7) only holds for the case that $\triangle ABC$ is a regular triangle.

Kotani–Sunada considered topological crystals from probabilistic motivations [26, 27, 30, 52]. A *random walk* on a graph $X = (V, E)$ is a stochastic process associated with $p\colon E \longrightarrow [0, 1]$ satisfying $\sum_{e \in E_x} p(e) = 1$. In the case of $p(e) = 1/(|E_x|)$, the random walk is called *simple random walk*. The function p is considered as *transition probability* from $o(e)$ to $t(e)$. Define $p_X(n, x, y) = \sum p(e_1) \cdots p(e_n)$, where summation over all paths with $e = e_1 \cdots e_n$, $o(e_1) = x$, $t(e_n) = y \in V$, is called n-step probability from x to y.

Kotani–Sunada studied asymptotic behaviors of random walks on topological crystal.

Theorem 3.4 (Kotani–Sunada [27]) *Let $X = (V, E)$ be a d-dimensional topological crystal, and $\Phi\colon X = (V, E) \longrightarrow \mathbb{R}^d$ be a standard realization of X with the lattice Γ, then the transition probability p_X on X satisfies*

$$|\Phi(x) - \Phi(y)| = \lim_{n \to \infty} 2n \left(\frac{p_X(n, x, x)}{p_X(n, y, x)} + \frac{p_X(n, y, y)}{p_X(n, x, y)} - 2 \right). \tag{3.12}$$

The right hand side of (3.12) consists of information only on (abstract) topological crystals, hence distance between the vertices of a standard realization determined by them. Theorem 3.3 is proved by this fact.

3.2 Construction of Standard Realizations

In this section, we demonstrate how to construct a standard realization from a given base graph explicitly.

Let $X_0 = (V_0, E_0)$ be a finite graph with $d = \operatorname{rank} H_1(X_0, \mathbb{Z})$. We consider X_0 as a directed graph by defining directions of edges. Then, we may define a natural inner product on d-dimensional vector space $C_1(X_0, \mathbb{R})$ by

$$\langle e_1, e_2 \rangle = \begin{cases} 1 & \text{if } e_1 = e_2, \\ -1 & \text{if } e_1 = \overline{e_2}, \\ 0 & \text{otherwise,} \end{cases}$$

for $e_1, e_2 \in E_0$. By using the inner product, we may identify $C_1(X_0, \mathbb{R})$ to $\mathbb{R}^{|E_0|}$, hence we may also identify $H_1(X_0, \mathbb{R})$ to $\mathbb{R}^d$.

Let $X = (V, E)$ be the maximum abelian covering of X_0, and $\pi : X \longrightarrow X_0$ be the covering map. Fix a vertex $v_0 \in V_0$, and define $\Phi\colon X \longrightarrow H_1(X_0, \mathbb{R})$ by

$$\Phi(v) = P(\pi(e_1)) + \cdots + P(\pi(e_n)), \tag{3.13}$$

where $e = e_1 \cdots e_n$ is a path in X connecting $v_0 = o(e_1)$ and $v = t(e_n)$, and $P\colon C_1(X_0, \mathbb{R}) \longrightarrow H_1(X_0, \mathbb{R})$ is the orthogonal projection.

Proposition 3.3 (Sunada [54]) *The map* $\Phi\colon X \longrightarrow H_1(X_0, \mathbb{R})$ *defined by* (3.13) *is a harmonic realization of* X*, namely,*

$$\sum_{e\in(E_0)_v} P(e) = 0 \in H_1(X_0, \mathbb{R}). \tag{3.14}$$

Proof First, we prove that

$$\sum_{e\in(E_0)_v} \langle e, c\rangle = 0 \tag{3.15}$$

for an arbitrary closed path $c = e_1 \cdots e_n$ in X_0. If c does not contain an edge whose origin or terminus is v, then the Eq. (3.15) obviously holds. Let e_j and e_{j+1} be edges in c satisfying $t(e_j) = o(e_{j+1}) = v$, then $\langle e, e_j + e_{j+1}\rangle = 1 - 1 = 0$. Hence, we obtain (3.15).

The equality (3.15) implies that

$$\sum_{e\in(E_0)_v} e \in H_1(X_0, \mathbb{R})^{\perp},$$

since $H_1(X_0, \mathbb{R})$ is generated by closed paths in X_0. Therefore, we obtain

$$0 = P\left(\sum_{e\in(E_0)_v} e\right) = \sum_{e\in(E_0)_v} P(e),$$

and hence we get (3.14). □

Proposition 3.4 (Sunada [54]) *The map* $\Phi\colon X \longrightarrow H_1(X_0, \mathbb{R})$ *defined by* (3.13) *is a standard realization of* X*, namely, there exists a constant* $c > 0$ *such that*

$$\sum_{e\in E_0} \langle P(e), x\rangle^2 = c|x|^2, \quad x \in H_1(X_0, \mathbb{R}). \tag{3.16}$$

Proof Since the set of oriented edges $E_0^o := \{e_i\}_{i=1}^n$ is an orthonormal basis of $C_1(X_0, \mathbb{R})$, we obtain

$$\sum_{e\in E_0^o} \langle P(e), x\rangle^2 = \sum_{e\in E_0^o} \langle e, x\rangle^2 = |x|^2,$$

and

$$\sum_{e\in E_0} \langle P(e), x\rangle^2 = \sum_{e\in E_0^o} \langle P(e), x\rangle^2 + \sum_{\overline{e}\in E_0^o} \langle P(e), x\rangle^2 = 2\sum_{e\in E_0^o} \langle P(e), x\rangle^2,$$

hence we get (3.16). □

By the above arguments, the realization Φ of X_0 is into $H_1(X_0, \mathbb{R})/H_1(X_0, \mathbb{Z})$. The torus $H_1(X_0, \mathbb{R})/H_1(X_0, \mathbb{Z})$ is called an *Albanese torus*. Therefore, to calculate explicit coordinates of standard realizations, we should compute correspondences between the Albanese torus and $\mathbb{R}^d/\mathbb{Z}^d$.

3.2.1 Explicit Calculations in Cases of Maximal Abelian Coverings

Now we demonstrate explicit calculations to obtain a standard realization of a d-dimensional topological crystal X, which is a maximum abelian covering of $X_0 = (V_0, E_0)$. This method follows Sunada [54] and Naito [37]. In the following, set $b = \operatorname{rank} H_1(X_0, \mathbb{Z})$, but in this section we consider cases of maximal abelian coverings, and we assume $b = d$.

Step 1

First, compute a spanning tree $T = (V_0, E_T)$ of X_0 by Kruskal's algorithm (Algorithm 7.1), and set $E_0 \setminus E_T = \{e_i\}_{i=1}^{b}$ and $E_T = \{e_i\}_{i=b+1}^{|E|}$. Then, we may select a $\mathbb{Z}$-basis $\{\alpha_i\}_{i=1}^{b}$ of $H_1(X_0, \mathbb{Z})$ as follows. For each edge $e_i \in E_0 \setminus E_T$, we may find a path p_i in E_T such that $o(p_i) = t(e_i)$ and $t(p_i) = o(e_i)$. The path $p_i e_i \in E_0$ is a closed path in E_0, and hence by Propositions 2.1 and 2.2, we may set $\alpha_i = [p_i e_i]$.

Step 2

Since $\{\alpha_i\}_{i=1}^{b}$ is a $\mathbb{Z}$-basis of $H_1(X_0, \mathbb{Z})$, for each edge $e \in E_0$ there exists $a_i(e) \in \mathbb{R}$ such that

$$P(e) = \sum_{i=1}^{b} a_i(e)\alpha_i \in H_1(X_0, \mathbb{R}). \tag{3.17}$$

Since $e \in C_1(X_0, \mathbb{R})$ and P is the orthogonal projection from $C_1(X_0, \mathbb{R})$ onto $H_1(X_0, \mathbb{R})$. Then $P(e)$ satisfies

$$\langle P(e) - e, \alpha_j \rangle = 0, \text{ for any } j. \tag{3.18}$$

Substituting (3.17) into (3.18), we obtain

$$\sum_{i=1}^{b} a_i(e)\langle \alpha_i, \alpha_j \rangle = \langle e, \alpha_j \rangle. \tag{3.19}$$

Set $G = [\langle \alpha_i, \alpha_j \rangle] \in GL(b, \mathbb{R})$, $\boldsymbol{a}(e) = [a_i(e)]^T$, and $\boldsymbol{b}(e) = [\langle e, \alpha_i \rangle]^T \in \mathbb{R}^b$, then (3.19) is written as

$$\boldsymbol{a}(e) = G^{-1}\boldsymbol{b}(e). \tag{3.20}$$

We get $\boldsymbol{a}(e)$ for each $e \in E_0$, then we obtain the realization

$$P(e) = \boldsymbol{e} = \sum_{i=1}^{b} a_i(e)\alpha_i, \text{ in } H_1(X_0, \mathbb{R}). \tag{3.21}$$

On the other hand, we easily calculate $\boldsymbol{b}(e)$ and G, since e and α_i are given by linear combinations of $\{e_i\}_{i=1}^{b}$ and $\{e_i\}_{i=b+1}^{|E|}$. Therefore, by (3.20), we obtain $\boldsymbol{a}(e)$. We remark that the matrix G is the Gram matrix of the basis $\{\alpha_i\}_{i=1}^{b}$ (see Remark 3.3). Taking an orthonormal basis $\{\boldsymbol{x}_i\}_{i=1}^{b}$ of $H_1(X_0, \mathbb{R})$ we write

$$\alpha_i = \sum_{j=1}^{b} \beta_{ij}\boldsymbol{x}_j, \tag{3.22}$$

then we obtain the expression of the realization in the Cartesian coordinates of $H_1(X_0, \mathbb{R}) \cong \mathbb{R}^b$ as

$$\boldsymbol{e} = \sum_{i=1}^{b} a_i(e)\alpha_i = \sum_{i=1}^{b} \left(\sum_{j=1}^{b} a_i(e)\beta_{ij} \right) \boldsymbol{x}_j, \quad \text{for } e \in E_0. \tag{3.23}$$

To obtain the relation (3.22), we may use the Cholesky decomposition. The Cholesky decomposition, which is a famous algorithm in numerical calculations and is a special case of LU decomposition, gives us the decomposition $G = U^T U$ for any positive definite symmetric matrix G by an upper triangular matrix U within $O(n^3)$-times calculations (see for example [14] and Sect. 7.5.2).

Step 3

Fix a vertex $v_0 \in V_0$, and set $\boldsymbol{v_0} = \boldsymbol{0}$ (origin of $\mathbb{R}^b$). For each vertex $v_j \in V_0$, we find the shortest path $e = e_{j1} \cdots e_{jk} \in E_T$ with $o(e_{j1}) = v_0$ and $t(e_{jk}) = v_j$, which is the shortest path in the spanning tree found in Step 1 connecting v_0 and v_j. By using (3.21), we obtain

$$\boldsymbol{v}_j = \sum_{i=1}^{k} \boldsymbol{e}_{ji} = \sum_{i=1}^{k} \sum_{k=1}^{b} a_k(e_{ji})\alpha_k, \quad j = \{1, \ldots, |V|\}. \tag{3.24}$$

In the above, we realize edges in the spanning tree. Hence, to complete calculation, we compute realizations of edges which are not contained in the spanning tree. For each $e_\ell \in E_0 \setminus E_T$, we define $\boldsymbol{v}_{|V|+\ell} \in \mathbb{R}^b$ by

$$\boldsymbol{v}_{|V|+\ell} = \boldsymbol{v}(e_\ell) + \boldsymbol{e}_\ell, \tag{3.25}$$

where $v(e_\ell) = o(e_\ell)$.

Vertices $\{\boldsymbol{v}_j\}_{j=1}^{|V|} \cup \{\boldsymbol{v}_{|V|+\ell}\}_{\ell=1}^{b} \subset \mathbb{R}^b$ (or edges $\{\boldsymbol{e}_i\}_{i=1}^{|E_0|}$) with the period lattice $\{\alpha_i\}_{i=1}^{b}$ give us a standard realization of X with period lattice Γ. The set of realizations of edges $\{\boldsymbol{e}_j\}_{j=1}^{|E|}$ is called the *building block*. In other words, Information of adjacency of the graph and the building block give us a standard realization.

Remark 3.2 Dijkstra's algorithm gives us shortest paths from a vertex to any other vertices within $O(|E| + |V| \log |V|)$ (Algorithm 7.2).

Remark 3.3 For a basis $\{\alpha_i\}_{i=1}^{n}$ of $\mathbb{R}^n$, the matrix

$$G(\{\alpha_i\}) = G = \begin{bmatrix} \langle \alpha_1, \alpha_1 \rangle & \cdots & \langle \alpha_1, \alpha_n \rangle \\ \vdots & \ddots & \vdots \\ \langle \alpha_n, \alpha_1 \rangle & \cdots & \langle \alpha_n, \alpha_n \rangle \end{bmatrix}$$

is called the *Gram matrix* of $\{\alpha_i\}_{i=1}^{n}$. We describe α_i as row vectors, then

$$G = \begin{bmatrix} \alpha_1 & \cdots & \alpha_n \end{bmatrix} \begin{bmatrix} \alpha_1 & \cdots & \alpha_n \end{bmatrix}^T.$$

Example 3.10 (*Square lattices in* $\mathbb{R}^2$*, Fig.* 3.1*a, Sunada* [54]) The base graph $X_0 = (V_0, E_0)$ of square lattices in $\mathbb{R}^2$ is the 2-bouquet graph (Fig. 3.3a), and rank $H_1(X_0, \mathbb{R}) = 2$. Write $V_0 = \{v_0\}$ and $E_0 = \{e_1, e_2\}$, as in Fig. 3.3a, then a spanning tree of X_0 is $T = (V_0, \{\emptyset\})$, namely, $E_T = \{\emptyset\}$. Hence, we may take $\alpha_1 = e_1$ and $\alpha_2 = e_2$ as a $\mathbb{Z}$-basis of $H_1(X_0, \mathbb{Z})$, and obtain

$$G = \begin{bmatrix} \langle \alpha_1, \alpha_1 \rangle & \langle \alpha_1, \alpha_2 \rangle \\ \langle \alpha_2, \alpha_1 \rangle & \langle \alpha_2, \alpha_2 \rangle \end{bmatrix} = \begin{bmatrix} 1 & 0 \\ 0 & 1 \end{bmatrix}, \quad G^{-1} = G,$$

$$\begin{bmatrix} \boldsymbol{b}(e_1) & \boldsymbol{b}(e_2) \end{bmatrix} = \begin{bmatrix} \langle e_1, \alpha_1 \rangle & \langle e_2, \alpha_1 \rangle \\ \langle e_1, \alpha_2 \rangle & \langle e_2, \alpha_2 \rangle \end{bmatrix} = \begin{bmatrix} 1 & 0 \\ 0 & 1 \end{bmatrix},$$

$$\begin{bmatrix} \boldsymbol{a}(e_1) & \boldsymbol{a}(e_2) \end{bmatrix} = G \begin{bmatrix} \boldsymbol{b}(e_1) & \boldsymbol{b}(e_2) \end{bmatrix} = \begin{bmatrix} 1 & 0 \\ 0 & 1 \end{bmatrix}.$$

On the other hand, the shortest paths from $\boldsymbol{v}_0$ to other vertices are

$$\mathrm{spath}(\boldsymbol{v}_0, \boldsymbol{v}_i) = (\boldsymbol{v}_0 \boldsymbol{v}_i), \quad i = 1, 2,$$

where $\mathrm{spath}(\boldsymbol{v}, \boldsymbol{u})$ denotes the shortest path from $\boldsymbol{v}$ to $\boldsymbol{u}$.

Taking a basis $\{\boldsymbol{x}_i\}_{i=1}^{2}$ of $\mathbb{R}^2$ satisfying $G(\{\boldsymbol{x}_i\}) = G$ as $\boldsymbol{x}_i = [1, 0]^T$ and $\boldsymbol{x}_2 = [0, 1]^T$, we obtain

$$\boldsymbol{v}_0 = \begin{bmatrix} 0 \\ 0 \end{bmatrix}, \quad \boldsymbol{v}_1 = \boldsymbol{v}_0 + a(\alpha_1) = \begin{bmatrix} 1 \\ 0 \end{bmatrix}, \quad \boldsymbol{v}_2 = \boldsymbol{v}_0 + a(\alpha_2) = \begin{bmatrix} 0 \\ 1 \end{bmatrix}.$$

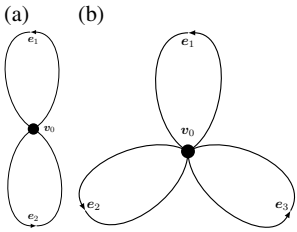

Fig. 3.3 **a** The 2-bouquet graph, which is the base graph of square lattices, **b** the 3-bouquet graph, which is the base graph of cubic lattices

The above data allow us to draw Fig. 3.1a.

Example 3.11 (*Hyper-cubic lattice in* $\mathbb{R}^n$*, Sunada* [54]) A generalization of Example 3.10 is hyper-cubic lattices in $\mathbb{R}^n$. In the case of $n = 3$, these are called cubic lattices. The base graph $X_0 = (V_0, E_0)$ of hyper-cubic lattices is the n-bouquet graph (Fig. 3.3b), namely $V_0 = \{v\}$, $E_0 = \{e_i\}_{i=1}^n$, as in Fig. 3.3b. Since a spanning tree of X_0 is $T = (V_0, \{\emptyset\})$, we may take an orthonormal $\mathbb{Z}$-basis of $H_1(X_0, \mathbb{Z})$ by $\{\alpha_i\}_{i=1}^n$, where $\alpha_i = e_i$. By similar calculations, we obtain

$$G = G^{-1} = \big[a(e_i)\big] = \big[b(e_i)\big] = I_n \quad \text{(the identity matrix of size } n\text{)}.$$

Hence, we obtain

$$\boldsymbol{v}_0 = \boldsymbol{0}, \quad \boldsymbol{v}_i = \boldsymbol{e}_i \quad \text{(standard } i\text{-th unit vector of } \mathbb{R}^n\text{)}, \quad i = 1, \ldots, n.$$

A standard realization of hyper-cubic lattices is an orthonormal cubic lattice in $\mathbb{R}^n$.

Example 3.12 (*Hexagonal lattices, Fig. 3.1c, Sunada* [54]) The base graph $X_0 = (V_0, E_0)$ of hexagonal lattices in $\mathbb{R}^2$ is the graph with two vertices and three edges connecting both vertices (Fig. 3.4a), and rank $H_1(X_0, \mathbb{R}) = 2$. Write $V_0 = \{v_0, v_1\}$ and $E_0 = \{e_1, e_2, e_3\}$ as in Fig. 3.4, then a spanning tree of X_0 is $T = (V_0, \{e_3\})$. Hence, we may take $\alpha_1 = e_1 - e_3$ and $\alpha_2 = e_2 - e_3$ as a $\mathbb{Z}$-basis of $H_1(X_0, \mathbb{Z})$, and obtain

$$G = \begin{bmatrix} 2 & 1 \\ 1 & 2 \end{bmatrix}, \quad G^{-1} = \frac{1}{3}\begin{bmatrix} 2 & -1 \\ -1 & 2 \end{bmatrix}$$

$$\big[\boldsymbol{b}(e_1)\ \boldsymbol{b}(e_2)\ \boldsymbol{b}(e_3)\big] = \begin{bmatrix} 1 & 0 & -1 \\ 0 & 1 & -1 \end{bmatrix},$$

$$\big[\boldsymbol{a}(e_1)\ \boldsymbol{a}(e_2)\ \boldsymbol{a}(e_3)\big] = \frac{1}{3}\begin{bmatrix} 2 & -1 & -1 \\ -1 & 2 & -1 \end{bmatrix}.$$

The shortest paths from $\boldsymbol{v}_0$ to other vertices are

$$\mathrm{spath}(\boldsymbol{v}_0, \boldsymbol{v}_i) = (\boldsymbol{v}_0 \boldsymbol{v}_i), \quad i = 1,\ 2,$$

then we obtain

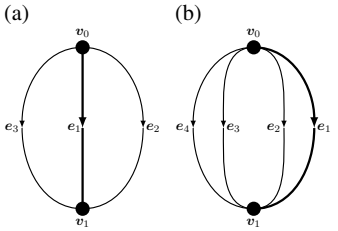

Fig. 3.4 **a** The base graph of hexagonal lattices, **b** the base graph of diamond lattices. Thick edges represent a spanning tree

$$\boldsymbol{v}_1 = \boldsymbol{v}_0 + \frac{2}{3}\alpha_1 - \frac{1}{3}\alpha_2, \quad \boldsymbol{v}_2 = \boldsymbol{v}_0 - \frac{1}{3}\alpha_1 + \frac{2}{3}\alpha_2, \quad \boldsymbol{v}_3 = \boldsymbol{v}_0 - \frac{1}{3}\alpha_1 - \frac{1}{3}\alpha_2.$$

Choosing a basis $\{\boldsymbol{x}_i\}_{i=1}^2$ satisfying $G(\{\boldsymbol{x}_i\}) = G$ as

$$U^T = \begin{bmatrix} \boldsymbol{x}_1 \\ \boldsymbol{x}_2 \end{bmatrix} = \begin{bmatrix} \sqrt{2} & 0 \\ 1/\sqrt{2} & \sqrt{3/2} \end{bmatrix},$$

which satisfies $G = U^T U$, we obtain

$$\boldsymbol{v}_0 = \begin{bmatrix} 0 \\ 0 \end{bmatrix}, \qquad \boldsymbol{v}_1 = \begin{bmatrix} 1/\sqrt{2} \\ -1/\sqrt{6} \end{bmatrix},$$
$$\boldsymbol{v}_2 = \begin{bmatrix} 0 \\ \sqrt{2/3} \end{bmatrix}, \qquad \boldsymbol{v}_3 = \begin{bmatrix} -1/\sqrt{2} \\ -1/\sqrt{6} \end{bmatrix}.$$

Since $\langle \boldsymbol{v}_i, \boldsymbol{v}_j \rangle = (-1/2)|\boldsymbol{v}_i|\,|\boldsymbol{v}_j|$, $(i \neq j)$, angles between edges are $2\pi/3$, and

$$G = 2\begin{bmatrix} 1 & 1/2 \\ 1/2 & 1 \end{bmatrix}$$

are satisfied. The above data allow us to draw Fig. 3.1c.

Example 3.13 (*Diamond lattices, Sunada* [54]) The base graph $X_0 = (V_0, E_0)$ of a diamond lattice in $\mathbb{R}^3$ is the graph with two vertices and four edges connecting both vertices, and rank $H_1(X_0, \mathbb{R}) = 3$ (see Fig. 3.23). Write $V_0 = \{v_0, v_1\}$ and $E_0 = \{e_1, e_2, e_3, e_4\}$, where $e_i = (v_0, v_1)$, then a spanning tree of X_0 is $T = (V_0, \{e_4\})$. Hence, we may take $\alpha_i = e_i - e_4$ $(i = 1,\ 2,\ 3)$ as a $\mathbb{Z}$-basis of $H_1(X_0, \mathbb{Z})$, and obtain

$$G = \begin{bmatrix} 2 & 1 & 1 \\ 1 & 2 & 1 \\ 1 & 1 & 2 \end{bmatrix} = 2 \begin{bmatrix} 1 & 1/2 & 1/2 \\ 1/2 & 1 & 1/2 \\ 1/2 & 1/2 & 1 \end{bmatrix}, \quad G^{-1} = \frac{1}{4} \begin{bmatrix} 3 & -1 & -1 \\ -1 & 3 & -1 \\ -1 & -1 & 3 \end{bmatrix},$$

$$\big[\boldsymbol{b}(e_1)\ \boldsymbol{b}(e_2)\ \boldsymbol{b}(e_3)\ \boldsymbol{b}(e_4)\big] = \begin{bmatrix} 1 & 0 & 0 & -1 \\ 0 & 1 & 0 & -1 \\ 0 & 0 & 1 & -1 \end{bmatrix},$$

$$\big[\boldsymbol{a}(e_1)\ \boldsymbol{a}(e_2)\ \boldsymbol{a}(e_3)\ \boldsymbol{a}(e_4)\big] = \frac{1}{4} \begin{bmatrix} 3 & -1 & -1 & -1 \\ -1 & 3 & -1 & -1 \\ -1 & -1 & 3 & -1 \end{bmatrix},$$

The shortest paths from $\boldsymbol{v}_0$ to other vertices are

$$\mathrm{spath}(\boldsymbol{v}_0, \boldsymbol{v}_i) = (\boldsymbol{v}_0 \boldsymbol{v}_i), \quad i = 1,\ 2,\ 3.$$

Hence, we obtain

$$\boldsymbol{v}_1 = \frac{3}{4}\alpha_1 - \frac{1}{4}\alpha_2 - \frac{1}{4}\alpha_3, \quad \boldsymbol{v}_2 = -\frac{1}{4}\alpha_1 + \frac{3}{4}\alpha_2 - \frac{1}{4}\alpha_3,$$
$$\boldsymbol{v}_3 = -\frac{1}{4}\alpha_1 - \frac{1}{4}\alpha_2 + \frac{3}{4}\alpha_3, \quad \boldsymbol{v}_4 = -\frac{1}{4}\alpha_1 - \frac{1}{4}\alpha_2 - \frac{1}{4}\alpha_3.$$

Choosing a basis $\{\boldsymbol{x}_i\}_{i=1}^3$ satisfying $G(\{\boldsymbol{x}_i\}) = G$ as

$$U^T = \begin{bmatrix} \boldsymbol{x}_1 \\ \boldsymbol{x}_2 \\ \boldsymbol{x}_3 \end{bmatrix} = \begin{bmatrix} \sqrt{2} & 0 & 0 \\ 1/\sqrt{2} & \sqrt{3/2} & 0 \\ 1/\sqrt{2} & 1/\sqrt{6} & 2/\sqrt{3} \end{bmatrix},$$

which satisfies $G = U^T U$, we obtain

$$\boldsymbol{v}_0 = \begin{bmatrix} 0 \\ 0 \\ 0 \end{bmatrix}, \quad \boldsymbol{v}_1 = \begin{bmatrix} 1/\sqrt{2} \\ -1/\sqrt{6} \\ -1/(2\sqrt{3}) \end{bmatrix}, \quad \boldsymbol{v}_2 = \begin{bmatrix} 0 \\ \sqrt{2/3} \\ -1/(2\sqrt{3}) \end{bmatrix},$$
$$\boldsymbol{v}_3 = \begin{bmatrix} 0 \\ 0 \\ 2/\sqrt{3} \end{bmatrix}, \quad \boldsymbol{v}_4 = \begin{bmatrix} -1/\sqrt{2} \\ -1/\sqrt{6} \\ -1/(2\sqrt{3}) \end{bmatrix}.$$

Since $\langle \boldsymbol{v}_i, \boldsymbol{v}_j \rangle = (-1/3)|\boldsymbol{v}_i|\,|\boldsymbol{v}_j|$ $(i \neq j)$, angles between edges are $\arccos(-1/3)$.

Example 3.14 (*Gyroid lattices (K_4 lattices), Sunada* [54]) The base graph $X_0 = (V_0, E_0)$ of a gyroid lattices in $\mathbb{R}^3$ is the K_4 graph, which is the complete graph of four vertices, and rank $H_1(X_0, \mathbb{R}) = 3$. Write $V_0 = \{v_i\}_{i=1}^4$ and $E_0 = \{e_i\}_{i=1}^4$ as in Fig. 3.5a, and take a spanning tree T of X_0 as in Fig. 3.5b. Hence, we may take

$$\alpha_1 = e_1 + e_4 - e_2, \quad \alpha_2 = e_2 + e_5 - e_3, \quad \alpha_3 = e_3 + e_6 - e_1$$

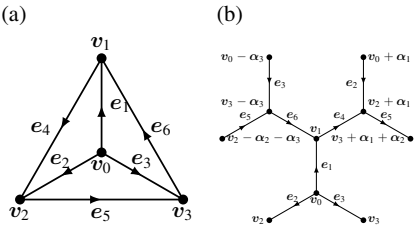

Fig. 3.5 **a** The base graph of gyroid lattices (K_4 lattices), thick edges represent a spanning tree. **b** schematic figure of building block of gyroid lattices

as a $\mathbb{Z}$-basis of $H_1(X_0, \mathbb{Z})$, and obtain

$$A = \begin{bmatrix} 3 & -1 & -1 \\ -1 & 3 & -1 \\ -1 & -1 & 3 \end{bmatrix} = 3 \begin{bmatrix} 1 & -1/3 & -1/3 \\ -1/3 & 1 & -1/3 \\ -1/3 & -1/3 & 1 \end{bmatrix}, \quad A^{-1} = \frac{1}{4} \begin{bmatrix} 2 & 1 & 1 \\ 1 & 2 & 1 \\ 1 & 1 & 2 \end{bmatrix},$$
$$\boldsymbol{b} = \begin{bmatrix} 1 & -1 & 0 & 1 & 0 & 0 \\ 0 & 1 & -1 & 0 & 1 & 0 \\ -1 & 0 & 1 & 0 & 0 & 1 \end{bmatrix}, \quad \boldsymbol{a} = \frac{1}{4} \begin{bmatrix} 1 & -1 & 0 & 2 & 1 & 1 \\ 0 & 1 & -1 & 1 & 2 & 1 \\ -1 & 0 & 1 & 1 & 1 & 2 \end{bmatrix}.$$

Let $\{v_i\}_{i=1}^6$ be as in Fig. 3.5b, then the shortest paths from $\boldsymbol{v}_0$ to other vertices are

$$\mathrm{spath}(\boldsymbol{v}_0, \boldsymbol{v}_i) = (\boldsymbol{v}_0 \boldsymbol{v}_i), \quad \mathrm{spath}(\boldsymbol{v}_0, \boldsymbol{v}_{i+3}) = (\boldsymbol{v}_0 \boldsymbol{v}_i)(\boldsymbol{v}_i \boldsymbol{v}_{i+3}), \quad i = 1,\ 2,\ 3.$$

Hence, we obtain

$$\begin{aligned} \boldsymbol{v}_1 &= \frac{1}{4}\alpha_1 - \frac{1}{4}\alpha_3, & \boldsymbol{v}_4 &= \boldsymbol{v}_1 + \frac{1}{2}\alpha_1 + \frac{1}{4}\alpha_2 + \frac{1}{4}\alpha_3, \\ \boldsymbol{v}_2 &= \frac{1}{4}\alpha_2 - \frac{1}{4}\alpha_1, & \boldsymbol{v}_5 &= \boldsymbol{v}_2 + \frac{1}{4}\alpha_1 + \frac{1}{2}\alpha_2 + \frac{1}{4}\alpha_3 \\ \boldsymbol{v}_3 &= \frac{1}{4}\alpha_3 - \frac{1}{4}\alpha_2 & \boldsymbol{v}_6 &= \boldsymbol{v}_3 + \frac{1}{4}\alpha_1 + \frac{1}{4}\alpha_2 + \frac{1}{2}\alpha_3. \end{aligned}$$

Choosing a basis $\{\boldsymbol{x}_i\}_{i=1}^3$ satisfying $G(\{\boldsymbol{x}_i\}) = G$ as

$$U^T = \begin{bmatrix} \boldsymbol{x}_1 \\ \boldsymbol{x}_2 \\ \boldsymbol{x}_3 \end{bmatrix} = \begin{bmatrix} \sqrt{3} & 0 & 0 \\ -1/\sqrt{3} & 2\sqrt{2/3} & 0 \\ -1/\sqrt{3} & -\sqrt{2/3} & \sqrt{2} \end{bmatrix},$$

which satisfies $G = U^T U$, we obtain

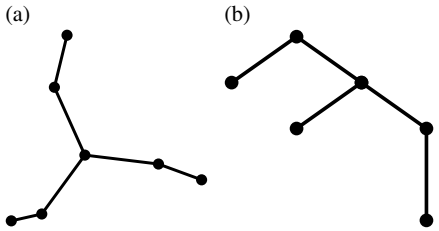

Fig. 3.6 **a** A building block of a gyroid lattice (K_4 lattice) viewed from a perpendicular direction of the plane consisting of $\boldsymbol{v}_1$, $\boldsymbol{v}_2$, and $\boldsymbol{v}_3$, **b** one viewed from a direction parallel to it

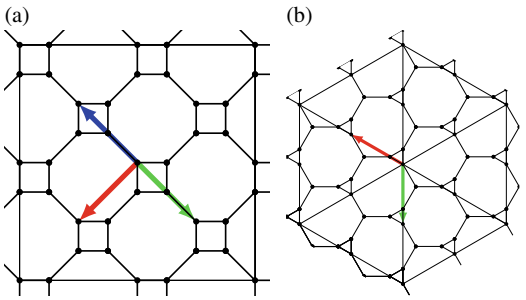

Fig. 3.7 A gyroid lattice (K_4 lattice) from **a** (0, 0, 1)-direction and **b** (1, 1, 1)-direction drawn using coordinates in Remark 3.4. The blue, red, and green vectors are $\boldsymbol{\alpha}_1$, $\boldsymbol{\alpha}_2$, and $\boldsymbol{\alpha}_3$, respectively. In **b**, $\boldsymbol{\alpha}_1$ is the vector perpendicular to the paper from the back to the front

$$\boldsymbol{v}_0 = \begin{bmatrix} 0 \\ 0 \\ 0 \end{bmatrix} \quad \boldsymbol{v}_1 = \begin{bmatrix} 1/\sqrt{3} \\ 1/(2\sqrt{6}) \\ -1/(2\sqrt{2}) \end{bmatrix}, \quad \boldsymbol{v}_2 = \begin{bmatrix} -1/\sqrt{3} \\ 1/\sqrt{6} \\ 0 \end{bmatrix}, \quad \boldsymbol{v}_3 = \begin{bmatrix} 0 \\ -(\sqrt{3/2})/2 \\ 1/(2\sqrt{2}) \end{bmatrix},$$

$$\boldsymbol{v}_4 = \begin{bmatrix} 2/\sqrt{3} \\ 1/\sqrt{6} \\ 0 \end{bmatrix}, \quad \boldsymbol{v}_5 = \begin{bmatrix} -1/\sqrt{3} \\ 5/(2\sqrt{6}) \\ 1/(2\sqrt{2}) \end{bmatrix}, \quad \boldsymbol{v}_6 = \begin{bmatrix} 0 \\ -(\sqrt{3/2})/2 \\ 3/(2\sqrt{2}) \end{bmatrix}.$$

Angles between the lattice vectors $\boldsymbol{x}_i$ and $\boldsymbol{x}_j$ are $\arccos(-1/3)$. Three vertices around a vertex in a gyroid lattice are co-planar, since the lattice is a standard realization. The dihedral angle for two adjacent vertices is $\arccos(-1/3)$ (see Fig. 3.8).

A gyroid lattice is called a K_4 lattice since its base graph is K_4. It is also called a Laves' graph of girth ten, a $(10, 3)$-*a* network, and a diamond twin. The minimum length of closed paths (without backtracking paths) is called the *girth* of the graph. The girth of a gyroid lattice is 10 (see Fig. 3.9), and hence it is called a $(10, 3)$-*a* network.

Remark 3.4 We can also take coordinates where all vertices have rational numbers. Taking

$$\begin{bmatrix} \boldsymbol{x}_1 \\ \boldsymbol{x}_2 \\ \boldsymbol{x}_3 \end{bmatrix} = \begin{bmatrix} -1 & 1 & -1 \\ -1 & -1 & 1 \\ 1 & -1 & -1 \end{bmatrix},$$

then

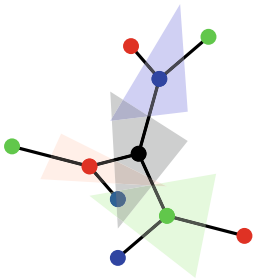

Fig. 3.8 Three vertices around a vertex are co-planar (black, red, green and blue planes). The dihedral angle between the black plane and other planes are $\arccos(-1/3)$

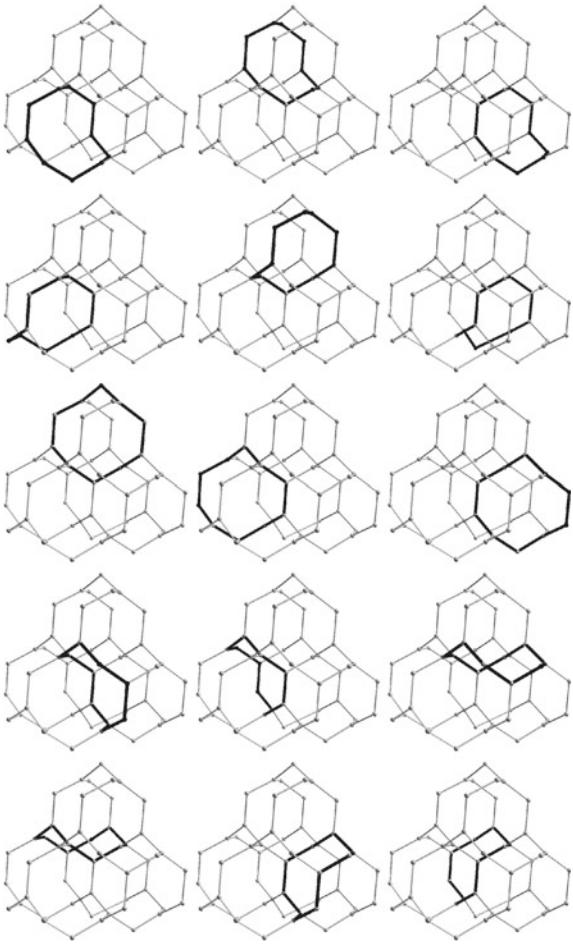

Fig. 3.9 Fifteen 10-membered rings pass through a vertex in a gyroid lattice. Each ring is mutually congruent

$$\boldsymbol{v}_1 = \frac{1}{2}\begin{bmatrix}-1\\1\\0\end{bmatrix}, \quad \boldsymbol{v}_2 = \frac{1}{2}\begin{bmatrix}0\\-1\\1\end{bmatrix}, \quad \boldsymbol{v}_3 = \frac{1}{2}\begin{bmatrix}1\\0\\-1\end{bmatrix},$$
$$\boldsymbol{v}_4 = \frac{1}{2}\begin{bmatrix}-2\\1\\-1\end{bmatrix}, \quad \boldsymbol{v}_5 = \frac{1}{2}\begin{bmatrix}-1\\-2\\1\end{bmatrix}, \quad \boldsymbol{v}_6 = \frac{1}{2}\begin{bmatrix}1\\-1\\-2\end{bmatrix}.$$

Remark 3.5 Let $\Phi(X)$ be a standard realization of diamond or cubic lattices, and $C \in O(3) \setminus SO(3)$. Then, $C(\Phi(X))$ and $\Phi(X)$ are mutually congruent, namely, $\Phi(X)$ and its mirror image are mutually congruent in $\mathbb{R}^3$. This property is called *chiral symmetry*. On the other hand, a standard realization of K_4 lattices is not chiral symmetric. Taking $C \in O(3) \setminus SO(3)$, $X' = XC$ and constructing the realization as in Example 3.14, we obtain a chiral image of $\Phi(X)$.

3.2.2 Explicit Calculations for Generic Cases

In general, a standard realization of a d-dimensional topological crystal X is not a maximal abelian covering of a base graph X_0. In this section, we assume that $d < b = \operatorname{rank} H_1(X_0, \mathbb{Z})$, and explain the explicit algorithm to obtain a standard realization of X. This method followed Sunada [54] (Fig. 3.6).

By choosing a suitable subgroup $H \subset H_1(X_0, \mathbb{R})$ such that $H_1(X_0, \mathbb{R})/X_0$ is a free abelian group with rank $H = d - b$, we may obtain a topological crystal X over the base graph X_0. Such a subgroup H is called the *vanishing subgroup*. Moreover, there exists a d-dimensional subspace V of $H_1(X_0, \mathbb{R})$ such that $H_1(X_0, \mathbb{R}) = V \oplus H$ and $\dim H = b - d$ is a linear space over $\mathbb{R}$. Hence a topological crystal X over X_0 is realized on V ($\dim V = d$).

Step 1

Taking a basis $\{\alpha_i\}_{i=d+1}^{b}$ of H, we find a $\mathbb{Z}$-basis $\{\alpha_i\}_{i=1}^{b}$ of $H_1(X_0, \mathbb{Z})$ (Fig. 3.7).

Step 2

Compute $G = G(\{\alpha_i\})$, $\boldsymbol{b}(e)$, and $\boldsymbol{a}(e)$ as in Step 2 of Sect. 3.2.1, then we obtain a standard realization of a topological crystal $\widetilde{X}$, which is a maximal abelian covering of the base graph X_0. This realization $\Phi^{\max}$ is in $H_1(X_0, \mathbb{R}) \cong \mathbb{R}^b$.

Step 3

Let $p\colon H_1(X_0, \mathbb{R}) \longrightarrow H$ be the orthogonal projection, then $\{\beta_i\}_{i=1}^{d}$ is a $\mathbb{Z}$-basis of the period lattice, where $\beta_i = p(\alpha_i)$. We should obtain $G = [\langle \beta_i, \beta_j \rangle] \in GL(d, \mathbb{R})$, which is the Gram matrix of $\{\beta_i\}_{i=1}^{d}$, to calculate standard realizations of X. Since $\gamma_i - \alpha_i = p(\alpha_i) - \alpha_i \in H$, we may write

$$p(\alpha_i) = \alpha_i + \sum_{j=b+1}^{d} d_{ij}\alpha_j$$

and $\langle p(\alpha_i), \alpha_k \rangle = 0$ for $k = b+1, \ldots, d$, and hence we obtain

$$\langle \alpha_i, \alpha_k \rangle = -\sum_{j=b+1}^{d} d_{ij}\langle \alpha_j, \alpha_k \rangle, \quad k = b+1, \ldots, d, \quad i = 1, \ldots, b. \tag{3.26}$$

Write $G(\{\alpha_i\}) = \begin{bmatrix} G_{11} & G_{12} \\ G_{21} & G_{22} \end{bmatrix}$, where G_{11} isa $d \times d$ matrix, G_{22} is $(b-d) \times (b-d)$ matrix, $G_{12}^T = G_{21}$, and $D = [d_{ij}]$, then (3.26) implies

$$G_{12} = -DG_{22}. \tag{3.27}$$

Therefore, we obtain

$$\begin{aligned} \langle \beta_i, \beta_j \rangle &= \langle p(\alpha_i), p(\alpha_j) \rangle = \langle p^T p(\alpha_i), \alpha_j \rangle = \langle p(\alpha_i), \alpha_j \rangle \\ &= \left\langle \alpha_i + \sum_{k=b+1}^{d} d_{ik}\alpha_k, \alpha_j \right\rangle = \langle \alpha_i, \alpha_j \rangle + \sum_{k=b+1}^{d} d_{ik}\langle \alpha_k, \alpha_j \rangle, \end{aligned} \tag{3.28}$$

and thus, by (3.28), we obtain

$$G = G(\{\beta_i\}) = G_{11} + DG_{21} = G_{11} - G_{12}G_{22}^{-1}G_{21}. \tag{3.29}$$

Since the realization of an edge $e \in E_0$ of the maximal abelian covering of X_0 is written as $\boldsymbol{e}^{\max} = \sum_{i=1}^{b} a(e)\alpha_i$, combining $P\colon C_1(X_0, \mathbb{R}) \longrightarrow H_1(X_0, \mathbb{R})$ and $p\colon H_1(X_0, \mathbb{R}) \longrightarrow H$, we obtain

$$p(P(e)) = p(\boldsymbol{e}^{\max}) = \boldsymbol{e} = \sum_{i=1}^{d} a(e)\beta_i. \tag{3.30}$$

Example 3.15 (*Triangular lattice, Fig. 3.1b, Sunada* [54]) A triangular lattice is the projection of a cubic lattice in $\mathbb{R}^3$ onto a suitable 2-dimensional plane. Hence, $d = 2$ and $b = \operatorname{rank} H_1(X_0, \mathbb{R}) = 3$, and the base graph $X_0 = (V_0, E_0)$ of triangular lattices is that of cubic lattices, i.e., X_0 is the 3-bouquet graph Fig. 3.3b. A fundamental piece of a triangular lattice is a triangle and their edges consist of e_1, e_2 and e_3 using the notation of a cubic lattice in Example 3.11 (see Fig. 3.1b). In other words, by looking at a cubic lattice whose edges are parallel to axes from the (1, 1, 1) direction, we find a triangular lattice. Hence constructing a triangular lattice, we take $H = \mathbb{Z}\alpha_3$, where $\alpha_3 = e_1 - e_2 + e_3$, and $V = \mathbb{Z}\alpha_1 + \mathbb{Z}\alpha_2$, where $\alpha_1 = e_1$, $\alpha_2 = e_2$. Then we obtain

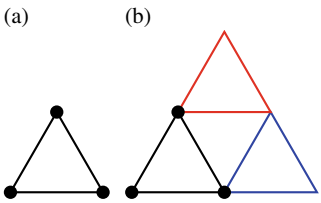

Fig. 3.10 Building block of the triangular lattice, and its translations by $B = \{\boldsymbol{\beta}_1, \boldsymbol{\beta}_2\}$. **a** building block $\{\boldsymbol{b}\}$ of the triangular lattice, **b** the blue and red blocks are the blocks translated by $\boldsymbol{\beta}_1$ and $\boldsymbol{\beta}_2$

$$G(\{\alpha_i\}) = \begin{bmatrix} 1 & 0 & 1 \\ 0 & 1 & -1 \\ 1 & -1 & 3 \end{bmatrix}, \quad \boldsymbol{b}(e) = \begin{bmatrix} 1 & 0 & 0 \\ 0 & 1 & 0 \\ 1 & -1 & 1 \end{bmatrix}, \quad \boldsymbol{a}(e) = \begin{bmatrix} 1 & 0 & -1 \\ 0 & 1 & 1 \\ 0 & 0 & 1 \end{bmatrix}, \tag{3.31}$$

and

$$\boldsymbol{e}_1^{\max} = \alpha_1, \quad \boldsymbol{e}_2^{\max} = \alpha_2, \quad \boldsymbol{e}_3^{\max} = -\alpha_1 + \alpha_2 + \alpha_3. \tag{3.32}$$

By (3.30) and (3.32), we obtain

$$\boldsymbol{e}_1 = \beta_1, \quad \boldsymbol{e}_2 = \beta_2, \quad \boldsymbol{e}_3 = -\beta_1 + \beta_2, \tag{3.33}$$

and by (3.29) and (3.31), we also obtain

$$G = [\langle \beta_i, \beta_j \rangle] = \begin{bmatrix} 1 & 0 \\ 0 & 1 \end{bmatrix} - \frac{1}{3} \begin{bmatrix} 1 \\ -1 \end{bmatrix} [1 \ -1] = \begin{bmatrix} 1 & 0 \\ 0 & 1 \end{bmatrix} - \frac{1}{3} \begin{bmatrix} 1 & -1 \\ -1 & 1 \end{bmatrix} = \frac{2}{3} \begin{bmatrix} 1 & 1/2 \\ 1/2 & 1 \end{bmatrix}.$$

On the other hand, the shortest paths from $\boldsymbol{v}_0$ to other vertices are

$$\mathrm{spath}(\boldsymbol{v}_0, \boldsymbol{v}_i) = (\boldsymbol{v}_0 \boldsymbol{v}_i) = \boldsymbol{e}_i, \quad i = 1, \ 2, \ 3.$$

By using the Cholesky decomposition $G = U^T U$, we may write

$$\begin{bmatrix} \boldsymbol{x}_1 \\ \boldsymbol{x}_2 \end{bmatrix} = \begin{bmatrix} \sqrt{2/3} & 1/\sqrt{6} \\ 0 & 1/\sqrt{2} \end{bmatrix},$$

and hence by (3.33), we obtain

$$\boldsymbol{v}_0 = \begin{bmatrix} 0 \\ 0 \end{bmatrix}, \qquad \boldsymbol{v}_1 = \boldsymbol{v}_0 + \boldsymbol{x}_1 = \begin{bmatrix} \sqrt{2/3} \\ 0 \end{bmatrix}, \qquad \boldsymbol{v}_2 = \boldsymbol{v}_0 + \boldsymbol{x}_2 = \begin{bmatrix} 1/\sqrt{6} \\ 1/\sqrt{2} \end{bmatrix}.$$

The above data allow us to draw Fig. 3.1b (see also Fig. 3.10).

Example 3.16 (*Kagome lattice, Fig. 3.1d, Sunada* [54]) A kagome lattice is a standard realization in $\mathbb{R}^2$ whose base graph X_0 is shown in Fig. 3.13a with $b = \mathrm{rank}\, H_1(X_0, \mathbb{R}) = 4$. A fundamental piece of a kagome lattice is two triangles sharing a vertex (see Fig. 3.1d). Hence we select

$$\alpha_1 = e_4 - e_1, \quad \alpha_2 = e_2 - e_5, \quad \alpha_3 = e_1 + e_2 + e_3, \quad \alpha_4 = e_4 + e_5 + e_6,$$

and $H = \mathbb{Z}\alpha_3 \oplus \mathbb{Z}\alpha_4$. Then, we obtain

$$G(\{\alpha_i\}) = \begin{bmatrix} 2 & 0 & 1 & -1 \\ 0 & 2 & -1 & 1 \\ -1 & 1 & 3 & 0 \\ 1 & -1 & 0 & 3 \end{bmatrix}, \quad \boldsymbol{b}(e) = \begin{bmatrix} -1 & 0 & 0 & 1 & 0 & 0 \\ 0 & 1 & 0 & 0 & -1 & 0 \\ 1 & 1 & 1 & 0 & 0 & 0 \\ 0 & 0 & 0 & 1 & 1 & 1 \end{bmatrix}, \quad \boldsymbol{a}(e) = \frac{1}{6}\begin{bmatrix} 3 & 0 & 3 & 3 & 0 & -3 \\ 0 & 3 & -3 & 0 & -3 & 3 \\ 1 & 1 & 4 & 1 & 1 & -2 \\ 1 & 1 & -2 & 1 & 1 & 4 \end{bmatrix}, \tag{3.34}$$

$$\begin{aligned} \boldsymbol{e}_1^{\max} &= (1/6)(3\alpha_1 + \alpha_3 + \alpha_4), \\ \boldsymbol{e}_2^{\max} &= (1/6)(3\alpha_2 + \alpha_3 + \alpha_4), \\ \boldsymbol{e}_3^{\max} &= (1/6)(3\alpha_1 - 3\alpha_2 + 4\alpha_3 - 2\alpha_4), \\ \boldsymbol{e}_4^{\max} &= (1/6)(3\alpha_1 + \alpha_3 + \alpha_4), \\ \boldsymbol{e}_5^{\max} &= (1/6)(-3\alpha_2 + \alpha_3 + \alpha_4), \\ \boldsymbol{e}_6^{\max} &= (1/6)(-3\alpha_1 + 3\alpha_2 - 2\alpha_3 + 4\alpha_4). \end{aligned} \tag{3.35}$$

By (3.30) and (3.35), we obtain

$$\begin{aligned} &\boldsymbol{e}_1 = -(1/2)\beta_1, \quad &&\boldsymbol{e}_2 = (1/2)\beta_2, \quad &&\boldsymbol{e}_3 = (1/2)(\beta_1 - \beta_2), \\ &\boldsymbol{e}_4 = (1/2)\beta_1, \quad &&\boldsymbol{e}_5 = -(1/2)\beta_2, \quad &&\boldsymbol{e}_6 = -(1/2)(\beta_1 - \beta_2), \end{aligned} \tag{3.36}$$

and by (3.29) and (3.36), we also obtain

$$G = \left[\langle \beta_i, \beta_j \rangle\right] = \begin{bmatrix} 2 & 0 \\ 0 & 2 \end{bmatrix} - \begin{bmatrix} -1 & 1 \\ 1 & -1 \end{bmatrix}\begin{bmatrix} 1/3 & 0 \\ 0 & 1/3 \end{bmatrix}\begin{bmatrix} -1 & 1 \\ 1 & -1 \end{bmatrix} = \frac{4}{3}\begin{bmatrix} 1 & 1/2 \\ 1/2 & 1 \end{bmatrix}.$$

On the other hand, the shortest paths from $\boldsymbol{v}_0$ to other vertices are

$$\mathrm{spath}(\boldsymbol{v}_0, \boldsymbol{v}_i) = (\boldsymbol{v}_0\boldsymbol{v}_i) = \boldsymbol{e}_i, \quad \mathrm{spath}(\boldsymbol{v}_0, \boldsymbol{v}_{i+3}) = (\boldsymbol{v}_0\boldsymbol{v}_{i+3}) = \boldsymbol{e}_{i+3}, \quad i = 1,\ 2,\ 3.$$

By using the Cholesky decomposition, we may write

$$\begin{bmatrix} \boldsymbol{x}_1 \\ \boldsymbol{x}_2 \end{bmatrix} = \begin{bmatrix} 2/\sqrt{3} & 1/\sqrt{3} \\ 0 & 1 \end{bmatrix},$$

and hence by (3.36), we obtain

$$\boldsymbol{e}_1 = -\boldsymbol{e}_4 = \begin{bmatrix} -1/\sqrt{3} \\ 0 \end{bmatrix}, \quad \boldsymbol{e}_2 = -\boldsymbol{e}_5 = \begin{bmatrix} 1/(2\sqrt{3}) \\ 1/2 \end{bmatrix}, \quad \boldsymbol{e}_3 = -\boldsymbol{e}_6 = \begin{bmatrix} 1/(2\sqrt{3}) \\ -1/2 \end{bmatrix},$$

and

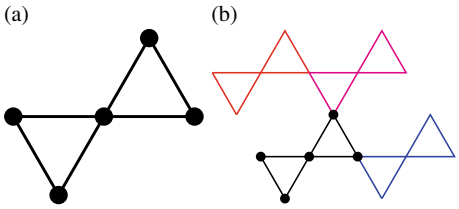

Fig. 3.11 Building block of the triangular lattice, and its translations by $B = \{\boldsymbol{\beta}_1, \boldsymbol{\beta}_2\}$. **a** Building block $\{\boldsymbol{b}\}$ of the triangular lattice, **b** the blue and red blocks are blocks translated by $\boldsymbol{\beta}_1$ and $\boldsymbol{\beta}_2$

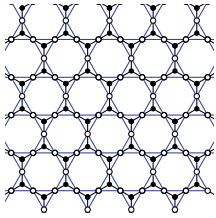

Fig. 3.12 A hexagonal lattice (black vertices and black edges) and a kagome lattice (white vertices and blue edges), using constructions described in Examples 3.12 and 3.16

$$\boldsymbol{v}_0 = \begin{bmatrix} 0 \\ 0 \end{bmatrix}, \quad \boldsymbol{v}_1 = \boldsymbol{v}_0 + \boldsymbol{e}_1 = \begin{bmatrix} -1/\sqrt{3} \\ 0 \end{bmatrix}, \quad \boldsymbol{v}_2 = \boldsymbol{v}_0 + \boldsymbol{e}_2 = \begin{bmatrix} 1/(2\sqrt{3}) \\ 1/2 \end{bmatrix},$$
$$\boldsymbol{v}_3 = \boldsymbol{v}_0 + \boldsymbol{e}_4 = \begin{bmatrix} 1/\sqrt{3} \\ 0 \end{bmatrix}, \quad \boldsymbol{v}_4 = \boldsymbol{v}_0 + \boldsymbol{e}_5 = \begin{bmatrix} -1/(2\sqrt{3}) \\ -1/2 \end{bmatrix}.$$

The above data allow us to draw Fig. 3.1d (see also Fig. 3.11). Since $\triangle \boldsymbol{v}_0\boldsymbol{v}_1\boldsymbol{v}_4$ and $\triangle \boldsymbol{v}_0\boldsymbol{v}_3\boldsymbol{v}_2$ consist of regular triangles, a standard realization of kagome lattices consists of regular triangles that share vertices.

Since the base graph of a kagome lattice is the line graph of the base graph of a hexagonal lattice, a kagome lattice is also the line graph of a hexagonal lattice. Since the Gram matrix G of a kagome lattice is the same as the Gram matrix of a hexagonal lattice, we may choose the common basis $\{\boldsymbol{\alpha}_1, \boldsymbol{\alpha}_2\}$ to construct a kagome and a hexagonal lattice. Taking the base point $\boldsymbol{v}_0$ of a kagome lattice to the midpoint of $\boldsymbol{v}_0$ and $\boldsymbol{v}_1$ of a hexagonal lattice, we obtain Fig. 3.12. Generators α_3 and α_4 of H correspond to edges which have common incidents in the base graph of a hexagonal lattice.

Next, we consider higher-dimensional analogues of kagome lattices. As mentioned in Example 3.16, a standard realization of a kagome lattice consists of regular triangles that share vertices. One of the 3-dimensional analogues of kagome lattices is a hyper-kagome lattice of type II, whose standard realization consists of quadrilaterals that share vertices. Since a triangle in $\mathbb{R}^2$ is a 1-simplex, the other is a hyper-kagome lattice of type I, whose standard realization consists of a 1-skeleton of 2-simplices that sharie vertices.

Example 3.17 (*3D kagome lattice of type I, Sunada* [54]) One of the 3-dimensional analogues of kagome lattices is defined as follows. Let X_0 be a graph in Fig. 3.13b, and $\widetilde{X}$ be its maximal abelian covering. Since $b = \operatorname{rank} H_1(X_0, \mathbb{R}) = 9$, $\widetilde{X}$ is a 9-dimensional topological crystal. Take a $\mathbb{Z}$-basis of $H_1(X_0, \mathbb{R})$ as

$$\alpha_1 = e_1 - e_4, \qquad \alpha_2 = e_2 - e_5, \qquad \alpha_3 = e_3 - e_6,$$
$$\alpha_4 = e_7 - e_2 + e_1, \qquad \alpha_5 = e_8 - e_3 + e_2, \qquad \alpha_6 = e_9 - e_1 + e_3,$$
$$\alpha_7 = e_{10} + e_5 - e_4, \qquad \alpha_8 = e_{11} + e_6 - e_5, \qquad \alpha_9 = e_{12} + e_4 - e_6,$$

and

$$H = \mathbb{Z}\alpha_4 \oplus \mathbb{Z}\alpha_5 \oplus \mathbb{Z}\alpha_6 \oplus \mathbb{Z}\alpha_7 \oplus \mathbb{Z}\alpha_8 \oplus \mathbb{Z}\alpha_9.$$

The number of vertices in a building block in $H_1(X_0, \mathbb{R})$ is 7, and the shortest paths from v_0 are

$$\mathrm{spath}(\boldsymbol{v}_0, \boldsymbol{v}_1) = \boldsymbol{e}_1, \qquad \mathrm{spath}(\boldsymbol{v}_0, \boldsymbol{v}_2) = \boldsymbol{e}_2, \qquad \mathrm{spath}(\boldsymbol{v}_0, \boldsymbol{v}_3) = \boldsymbol{e}_3,$$
$$\mathrm{spath}(\boldsymbol{v}_0, \boldsymbol{v}_4) = -\boldsymbol{e}_4, \qquad \mathrm{spath}(\boldsymbol{v}_0, \boldsymbol{v}_5) = -\boldsymbol{e}_5, \qquad \mathrm{spath}(\boldsymbol{v}_0, \boldsymbol{v}_6) = -\boldsymbol{e}_6.$$

The building blocks are

$$\boldsymbol{e}_1 = \begin{bmatrix} 1/2 \\ 0 \\ 0 \end{bmatrix}, \quad \boldsymbol{e}_2 = \begin{bmatrix} 1/4 \\ \sqrt{3}/4 \\ 0 \end{bmatrix}, \quad \boldsymbol{e}_3 = \begin{bmatrix} 1/4 \\ 1/(4\sqrt{3}) \\ 1/\sqrt{6} \end{bmatrix},$$
$$\boldsymbol{e}_4 = \begin{bmatrix} -1/2 \\ 0 \\ 0 \end{bmatrix}, \quad \boldsymbol{e}_5 = \begin{bmatrix} -1/4 \\ -\sqrt{3}/4 \\ 0 \end{bmatrix}, \quad \boldsymbol{e}_6 = \begin{bmatrix} -1/4 \\ -1/(4\sqrt{3}) \\ -1/\sqrt{6} \end{bmatrix},$$
$$\boldsymbol{e}_7 = \begin{bmatrix} -1/4 \\ \sqrt{3}/4 \\ 0 \end{bmatrix}, \quad \boldsymbol{e}_8 = \begin{bmatrix} 0 \\ -1/(2\sqrt{3}) \\ 1/\sqrt{6} \end{bmatrix}, \quad \boldsymbol{e}_9 = \begin{bmatrix} 1/4 \\ -1/(4\sqrt{3}) \\ -1/\sqrt{6} \end{bmatrix},$$
$$\boldsymbol{e}_{10} = \begin{bmatrix} -1/4 \\ \sqrt{3}/4 \\ 0 \end{bmatrix}, \quad \boldsymbol{e}_{11} = \begin{bmatrix} 0 \\ -1/(2\sqrt{3}) \\ 1/\sqrt{6} \end{bmatrix}, \quad \boldsymbol{e}_{12} = \begin{bmatrix} 1/4 \\ -1/(4\sqrt{3}) \\ -1/\sqrt{6} \end{bmatrix},$$

and

$$\begin{bmatrix} \boldsymbol{x}_1 \\ \boldsymbol{x}_2 \\ \boldsymbol{x}_3 \end{bmatrix} = \begin{bmatrix} 1 & 0 & 0 \\ 1/2 & \sqrt{3}/2 & 0 \\ 1/2 & 1/(2\sqrt{3}) & \sqrt{2/3} \end{bmatrix},$$

then we obtain 3D kagome lattice of type I (Fig. 3.14). This lattice is sometimes called a *Pyrochlore lattice*.

The base graph of a 3D kagome lattice of type I is the line graph of the base lattice of a diamond lattice. As similar as a relationship between a kagome and a hexagonal lattice, a 3D kagome lattice of type I is the line graph of a diamond lattice (see Fig. 3.15).

Example 3.18 (*3D kagome lattice of type II, Sunada* [54]) The other 3-dimensional analogue of kagome lattices is defined as follows. Let X_0 be a graph in Fig. 3.13c, and $\tilde{X}$ be its maximal abelian covering. Since $b = \mathrm{rank}\, H_1(X_0, \mathbb{R}) = 5$, $\tilde{X}$ is a 5-dimensional topological crystal. Take a $\mathbb{Z}$-basis of $H_1(X_0, \mathbb{R})$ as

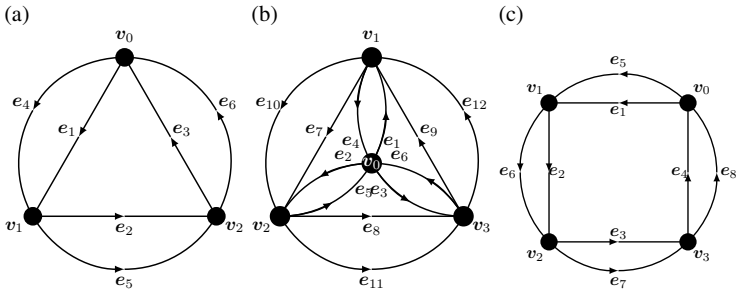

Fig. 3.13 **a** The base graph of kagome lattices, **b** the base graph of 3D kagome lattices of type I, **c** the base graph of 3D kagome lattices of type II

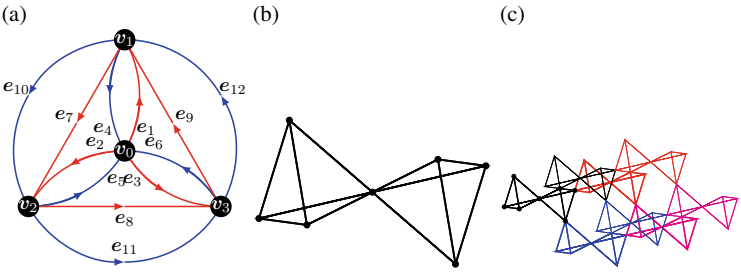

Fig. 3.14 **a** Each graph consisting of blue edges with vertices and red edges with vertices is a tetrahedral graph. **b** Building block $\{\boldsymbol{b}\}$; **c** The blue, red, and magenta blocks are translated by $\boldsymbol{\beta}_1$, $\boldsymbol{\beta}_2$, and $\boldsymbol{\beta}_1 + \boldsymbol{\beta}_2$. Thin layers are translated by $\boldsymbol{\beta}_3$ above them

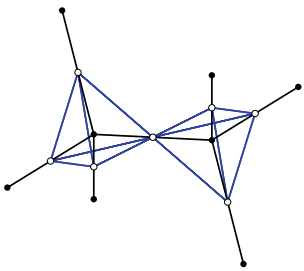

Fig. 3.15 A diamond lattice (black) and a 3D kagome lattice of type I (white vertices and blue edges). Since the 3D kagome lattice of type I is a line graph of a diamond lattice, the vertices of the 3D kagome lattice of type I are located at the midpoints of the edges of the diamond lattice

$$\alpha_1 = e_1 - e_4, \quad \alpha_2 = e_2 - e_5, \quad \alpha_3 = e_3 - e_6,$$
$$\alpha_4 = e_1 + e_2 + e_3 + e_4, \quad \alpha_5 = e_5 + e_6 + e_7 + e_8,$$

and

$$H = \mathbb{Z}\alpha_4 \oplus \mathbb{Z}\alpha_5.$$

The number of vertices in a building block in $H_1(X_0, \mathbb{R})$ is 7, and the shortest paths from v_0 are

$$\mathrm{spath}(v_0, v_1) = e_1, \quad \mathrm{spath}(v_0, v_2) = e_1 + e_2, \quad \mathrm{spath}(v_0, v_3) = e_1 + e_2 + e_3,$$
$$\mathrm{spath}(v_0, v_4) = e_5, \quad \mathrm{spath}(v_0, v_5) = e_5 + e_6, \quad \mathrm{spath}(v_0, v_6) = e_5 + e_6 + e_7.$$

The building blocks are

$$e_1 = \begin{bmatrix} (1/2)\sqrt{3/2} \\ 0 \\ 0 \end{bmatrix}, \quad e_2 = \begin{bmatrix} -1/(2\sqrt{6}) \\ 1/\sqrt{3} \\ 0 \end{bmatrix}, \quad e_3 = \begin{bmatrix} -1/(2\sqrt{6}) \\ -1/(2\sqrt{3}) \\ 1/2 \end{bmatrix}, \quad e_4 = \begin{bmatrix} -1/(2\sqrt{6}) \\ -1/(2\sqrt{3}) \\ -1/2 \end{bmatrix},$$
$$e_5 = \begin{bmatrix} -(1/2)\sqrt{3/2} \\ 0 \\ 0 \end{bmatrix}, \quad e_6 = \begin{bmatrix} 1/(2\sqrt{6}) \\ -1/\sqrt{3} \\ 0 \end{bmatrix}, \quad e_7 = \begin{bmatrix} 1/(2\sqrt{6}) \\ 1/(2\sqrt{3}) \\ -1/2 \end{bmatrix}, \quad e_8 = \begin{bmatrix} 1/(2\sqrt{6}) \\ 1/(2\sqrt{3}) \\ 1/2 \end{bmatrix},$$

and

$$\begin{bmatrix} x_1 \\ x_2 \\ x_3 \end{bmatrix} = \begin{bmatrix} \sqrt{3/2} & -1/\sqrt{6} & -1/\sqrt{6} \\ 0 & 2/\sqrt{3} & -1/\sqrt{3} \\ 0 & 0 & 1 \end{bmatrix},$$

then we obtain a 3D kagome lattice of type II (Fig. 3.16).

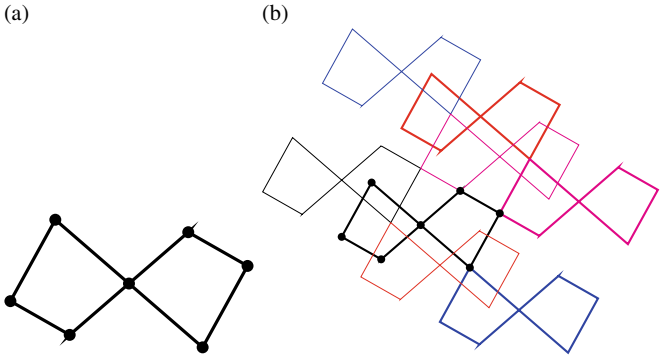

Fig. 3.16 Building block of the 3D kagome lattice of type II, and its translations by $B = \{\beta_1, \beta_2, \beta_3\}$. **a** building block $\{b\}$; **b** The blue, red, and magenta blocks are translated by β_1, β_2, and $\beta_1 + \beta_2$. The thin layer is translated by β_3 of above them

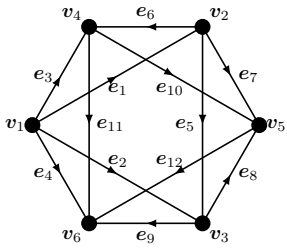

Fig. 3.17 An octahedral graph, which is the line graph of a K_4 graph

Example 3.19 (*3D kagome lattice of type III*) The line graph of a gyroid lattice is also a type of 3D kagome lattice. The line graph X_0 of a K_4 graph is an octahedral graph, shown in Fig. 3.17. Since $b = \operatorname{rank} H_1(X_0, \mathbb{R}) = 7$, $\widetilde{X}$ is a 7-dimensional topological crystal. Take a $\mathbb{Z}$-basis of $H_1(X_0, \mathbb{R})$ as

$$\begin{aligned}
&\alpha_1 = -\boldsymbol{e}_1 - \boldsymbol{e}_6 + \boldsymbol{e}_3, \quad && \alpha_2 = -\boldsymbol{e}_5 - \boldsymbol{e}_8 + \boldsymbol{e}_7, \quad && \alpha_3 = -\boldsymbol{e}_4 + \boldsymbol{e}_2 + \boldsymbol{e}_9,\\
&\alpha_4 = \boldsymbol{e}_1 + \boldsymbol{e}_5 - \boldsymbol{e}_2, && \alpha_5 = \boldsymbol{e}_6 + \boldsymbol{e}_{10} - \boldsymbol{e}_7,\\
&\alpha_6 = \boldsymbol{e}_8 + \boldsymbol{e}_{12} - \boldsymbol{e}_9, && \alpha_7 = \boldsymbol{e}_3 + \boldsymbol{e}_{11} - \boldsymbol{e}_4,
\end{aligned}$$

and

$$H = \mathbb{Z}\alpha_4 \oplus \mathbb{Z}\alpha_5 \oplus \mathbb{Z}\alpha_6 \oplus \mathbb{Z}\alpha_7,$$

then we obtain a 3-dimensional crystal lattice and its Gram matrix is

$$G = 2\begin{bmatrix} 1 & -1/3 & -1/3 \\ -1/3 & 1 & -1/3 \\ -1/3 & -1/3 & 1 \end{bmatrix},$$

which is similar to the Gram matrix of a gyroid lattice. By a similar calculation, we obtain

$$\begin{aligned}
\boldsymbol{e}_1 &= -\frac{1}{4}\beta_1 + \frac{1}{8}\beta_2 + \frac{1}{8}\beta_3, & \boldsymbol{e}_2 &= -\frac{1}{8}\beta_1 - \frac{1}{8}\beta_2 + \frac{1}{4}\beta_3, & \boldsymbol{e}_3 &= \frac{3}{8}\beta_1 - \frac{1}{8}\beta_2,\\
\boldsymbol{e}_4 &= -\frac{1}{8}\beta_2 - \frac{3}{8}\beta_3, & \boldsymbol{e}_5 &= \frac{1}{8}\beta_1 - \frac{1}{4}\beta_2 + \frac{1}{8}\beta_3, & \boldsymbol{e}_6 &= -\frac{3}{8}\beta_1 - \frac{1}{8}\beta_3,\\
\boldsymbol{e}_7 &= \frac{3}{8}\beta_2 - \frac{1}{8}\beta_3, & \boldsymbol{e}_8 &= -\frac{1}{8}\beta_1 - \frac{3}{8}\beta_2, & \boldsymbol{e}_9 &= \frac{1}{8}\beta_1 + \frac{3}{8}\beta_3,\\
\boldsymbol{e}_{10} &= \frac{3}{8}\beta_1 + \frac{3}{8}\beta_2 + \frac{1}{4}\beta_3, & \boldsymbol{e}_{11} &= -\frac{3}{8}\beta_1 - \frac{1}{4}\beta_2 - \frac{3}{8}\beta_3, & \boldsymbol{e}_{12} &= \frac{1}{4}\beta_1 + \frac{3}{8}\beta_2 + \frac{3}{8}\beta_3.
\end{aligned}$$

Then we obtain a 3D kagome lattice of type III (Fig. 3.18a). This lattice is sometimes called a *hyper-kagome lattice*. By taking the base point $\boldsymbol{v}_1 = (1/2)(\boldsymbol{v}_0^{(g)} + \boldsymbol{v}_1^{(g)}) = [1/8, 0, -1/8]$, where $\boldsymbol{v}_i^{(g)}$ are vertices of a gyroid lattice, we obtain a schematic figure expressing a relationship between this and a gyroid lattice (Fig. 3.18b).

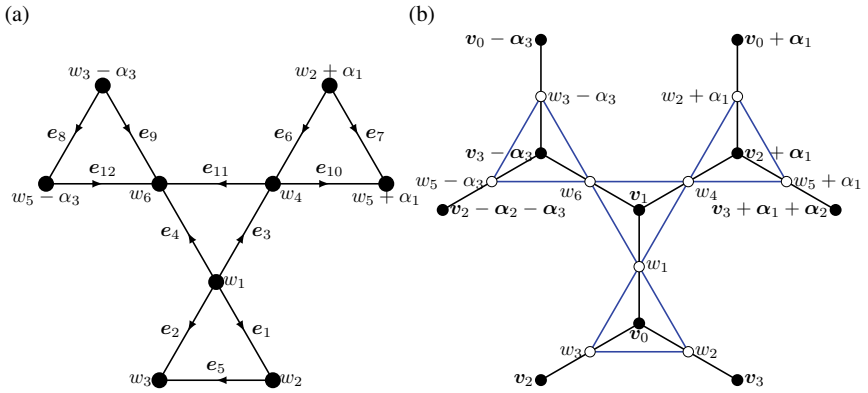

Fig. 3.18 **a** Building block of the 3D kagome lattice of type III. **b** A relationship between the 3D kagome lattice of type III and a gyroid lattice (see also Fig. 3.5b)

Example 3.20 (*Cairo pentagonal tiling, Sunada* [54]) A periodic tessellations is also considered as a topological crystal. A Cairo pentagonal tiling (Fig. 3.19b) is a tessellation by congruent pentagons, and it is topologically equivalent to the basketweave tiling (Fig. 3.19a). It is also called MacMahon's net [40]. Here, we compute a standard realization of the Cairo pentagonal tiling.

We number vertices and edges of the graph of a fundamental region of the basketweave tiling as in Fig. 3.19a. Taking a basis $\{\boldsymbol{p}_1, \boldsymbol{p}_2\}$ of the period lattice, then we obtain the equation of harmonic realizations (the equation of the balancing condition) as

$$
\begin{aligned}
4\boldsymbol{v}_0 &= \boldsymbol{v}_2 + (\boldsymbol{v}_9 - \boldsymbol{p}_2) + (\boldsymbol{v}_4 - \boldsymbol{p}_1) + (\boldsymbol{v}_{11} - \boldsymbol{p}_1 - \boldsymbol{p}_2), & 4\boldsymbol{v}_1 &= \boldsymbol{v}_3 + \boldsymbol{v}_4 + (\boldsymbol{v}_9 - \boldsymbol{p}_2) + (\boldsymbol{v}_{10} - \boldsymbol{p}_2),\\
3\boldsymbol{v}_2 &= \boldsymbol{v}_0 + \boldsymbol{v}_3 + \boldsymbol{v}_6, & 3\boldsymbol{v}_3 &= \boldsymbol{v}_1 + \boldsymbol{v}_2 + \boldsymbol{v}_7,\\
3\boldsymbol{v}_4 &= \boldsymbol{v}_1 + \boldsymbol{v}_5 + (\boldsymbol{v}_0 + \boldsymbol{p}_1), & 3\boldsymbol{v}_5 &= \boldsymbol{v}_7 + \boldsymbol{v}_4 + (\boldsymbol{v}_6 + \boldsymbol{p}_1),\\
4\boldsymbol{v}_6 &= \boldsymbol{v}_2 + \boldsymbol{v}_8 + (\boldsymbol{v}_5 - \boldsymbol{p}_1) + (\boldsymbol{v}_{11} - \boldsymbol{p}_1), & 4\boldsymbol{v}_7 &= \boldsymbol{v}_3 + \boldsymbol{v}_5 + \boldsymbol{v}_8 + \boldsymbol{v}_{10},\\
3\boldsymbol{v}_8 &= \boldsymbol{v}_6 + \boldsymbol{v}_7 + \boldsymbol{v}_9, & 3\boldsymbol{v}_9 &= \boldsymbol{v}_8 + \boldsymbol{v}_0 + \boldsymbol{p}_2 + \boldsymbol{v}_1 + \boldsymbol{p}_2,\\
3\boldsymbol{v}_{10} &= \boldsymbol{v}_7 + \boldsymbol{v}_1 + \boldsymbol{p}_2 + \boldsymbol{v}_{11}, & 3\boldsymbol{v}_{11} &= \boldsymbol{v}_{10} + \boldsymbol{v}_6 + \boldsymbol{p}_1 + \boldsymbol{v}_0 + \boldsymbol{p}_1 + \boldsymbol{p}_2.
\end{aligned}
\tag{3.37}
$$

For a given basis $\{\boldsymbol{p}_1, \boldsymbol{p}_2\}$, we obtain a solution of (3.37) (a harmonic realization of the Cairo pentagonal tiling) as

$$
\begin{aligned}
&\boldsymbol{v}_0 = \boldsymbol{0}, && \boldsymbol{v}_1 = (1/2)\boldsymbol{p}_1, && \boldsymbol{v}_2 = (1/8)(\boldsymbol{p}_1 + 2\boldsymbol{p}_2),\\
&\boldsymbol{v}_3 = (1/8)(3\boldsymbol{p}_1 + 2\boldsymbol{p}_2), && \boldsymbol{v}_4 = (1/8)(6\boldsymbol{p}_1 + \boldsymbol{p}_2), && \boldsymbol{v}_5 = (1/8)(6\boldsymbol{p}_1 + 3\boldsymbol{p}_2),\\
&\boldsymbol{v}_6 = (1/2)\boldsymbol{p}_2, && \boldsymbol{v}_7 = (1/8)(4\boldsymbol{p}_1 + 4\boldsymbol{p}_2), && \boldsymbol{v}_8 = (1/8)(2\boldsymbol{p}_1 + 5\boldsymbol{p}_2),\\
&\boldsymbol{v}_9 = (1/8)(2\boldsymbol{p}_1 + 7\boldsymbol{p}_2), && \boldsymbol{v}_{10} = (1/8)(5\boldsymbol{p}_1 + 6\boldsymbol{p}_2), && \boldsymbol{v}_{11} = (1/8)(7\boldsymbol{p}_1 + 6\boldsymbol{p}_2).
\end{aligned}
\tag{3.38}
$$

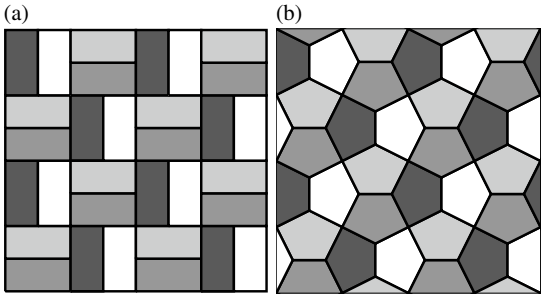

Fig. 3.19 **a** A basketweave tiling, **b** A Cairo tiling. Both 1-skeletons of the tiling are topologically equivalent

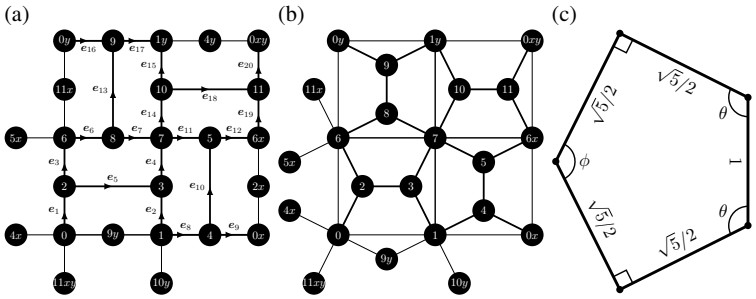

Fig. 3.20 **a** Numbering of vertices and edges of a fundamental region of the basketweave tiling, **b** a fundamental region of a standard realization of the Cairo tiling, **c** the congruent-pentagon of the standard realization. The ratio of length of edges is $1 : (\sqrt{5}/2)$, and angles are $\cos(\theta) = -1/\sqrt{5}$ and $\cos(\phi) = -3/5$ ($\theta \sim 116.57°$ and $\phi \sim 126.87°$)

A harmonic realization (3.38) is standard if and only if $\{\boldsymbol{e}_i\}_{i=1}^{20}$ satisfies (3.7). Taking $\boldsymbol{f}_1 = [1, 0]^T$ and $\boldsymbol{f}_2 = [0, 1]^T$, and solving

$$\sum_{i=1}^{20} \langle \boldsymbol{e}_i, \boldsymbol{f}_j \rangle \boldsymbol{e}_i = c\boldsymbol{f}_j, \quad j = 1, 2, \tag{3.39}$$

we obtain

$$|\boldsymbol{p}_1| = |\boldsymbol{p}_2|, \quad \langle \boldsymbol{p}_1, \boldsymbol{p}_2 \rangle = 0. \tag{3.40}$$

Substituting (3.40) into (3.38), we obtain a standard realization of a Cairo pentagonal tiling (Figs. 3.19b and 3.20c).

Remark 3.6 A carbon structure with a regular hexagonal shape is called a graphene (see Sect. 3.3), and a carbon structure with a Cairo pentagonal-shaped is called a penta-graphene [59].

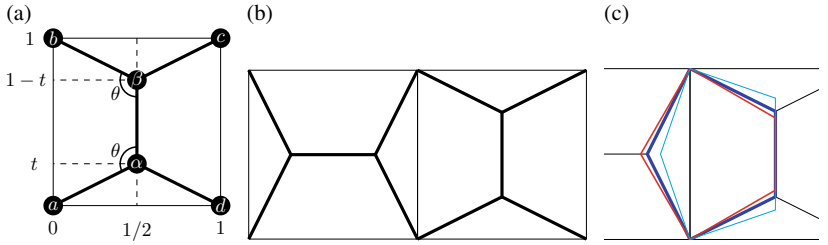

Fig. 3.21 **a** Move α and β on the line $x = 1/2$, and calculate minima of $L(t)$ and $E(t)$. **b** A building block of the pentagonal tiling. **c** The red, blue, and cyan pentagons are minimizers of L, E and C, respectively

Remark 3.7 A Cairo pentagonal tiling is constructed by line segments joining four vertices of a square as in Fig. 3.21a, b. Define three kinds of energy L, E and C by

$$L(t) = |\boldsymbol{a}-\boldsymbol{\alpha}| + |\boldsymbol{b}-\boldsymbol{\alpha}| + |\boldsymbol{c}-\boldsymbol{\beta}| + |\boldsymbol{d}-\boldsymbol{\beta}| + |\boldsymbol{\alpha}-\boldsymbol{\beta}| = 1 - 2t + 2\sqrt{1+4t^2},$$
$$E(t) = |\boldsymbol{a}-\boldsymbol{\alpha}|^2 + |\boldsymbol{b}-\boldsymbol{\alpha}|^2 + |\boldsymbol{c}-\boldsymbol{\beta}|^2 + |\boldsymbol{d}-\boldsymbol{\beta}|^2 + |\boldsymbol{\alpha}-\boldsymbol{\beta}|^2 = 8t^2 - 4t + 2,$$
$$C(t) = |\boldsymbol{a}-\boldsymbol{\alpha}|^{-1} + |\boldsymbol{b}-\boldsymbol{\alpha}|^{-1} + |\boldsymbol{c}-\boldsymbol{\beta}|^{-1} + |\boldsymbol{d}-\boldsymbol{\beta}|^{-1} + |\boldsymbol{\alpha}-\boldsymbol{\beta}|^{-1}.$$

For each $t \in (-1/2, 1/2)$, the configuration in Fig. 3.21b yields a monohedral pentagon tiling. The energy L attains its minimum at $t = 1/(2\sqrt{3})$, and then the angle $\theta = \theta(t)$ in Fig. 3.21a satisfies $\cos(\theta) = -1/2$, $(\theta = 2\pi/3)$. The minimum of L gives us the configuration of the minimum length of line segments, On the other hand, the energy E attains its minimum at $t = 1/4$, and then the angle θ satisfies $\cos(\theta) = -1/\sqrt{5}$. The minimum of E gives us a standard realization of the Cairo pentagonal tiling (see also Fig. 3.20c). The energy C is based on the Coulomb repulsive force, and attains its local minimum at $t \sim 0.17264$; the angle θ satisfies $\cos(\theta) \sim -0.326374$.

Remark 3.8 This algorithm is easily programmable by using Kruskal's and Dijkstra's algorithms, and the Cholesky decomposition. To calculate the Gram matrix G and vectors $a(e)$, $b(e)$, it is easy to set $e_i = [0, \ldots, 1, \ldots, 0] \in \mathbb{R}^{|E|}$.

Example 3.21 Using the software suite Mathematica, coordinates of vertices of standard realizations of topological crystals are easy to compute, if we obtain a $\mathbb{Z}$-basis of $H_1(X_0, \mathbb{Z})$ and a $\mathbb{Z}$-basis of H (and a spanning tree of X_0). The following is a sample code of Mathematica to compute vertices of a kagome lattice (lines 1 and 3 are specific data of a kagome lattice).

```
numberOfEdges = 6; b = 4; d = 2;
e = IdentityMatrix[numberOfEdges];
alpha = {e[[4]] - e[[1]], e[[2]] - e[[5]],
  e[[1]] + e[[2]] + e[[3]], e[[4]] + e[[5]] + e[[6]]};
matrixG0 = alpha.Transpose[alpha];
matrixb = Table[e[[j]].alpha[[i]],
  >{i, 1, b}, {j, 1, numberOfEdges}];
matrixa = Inverse[matrixG0].matrixb;
matrixG11 = matrixG0[[1 ;; d, 1 ;; d]];
matrixG22 = matrixG0[[d + 1 ;; b, d + 1 ;; b]];
matrixG12 = matrixG0[[1 ;; d, d + 1 ;; b]];
matrixG21 = matrixG0[[d + 1 ;; b, 1 ;; d]];
matrixG = matrixG11 - matrixG12.Inverse[matrixG22]. matrixG21;
matrixPa = matrixa[[1 ;; d]];
beta = CholeskyDecomposition[matrixG];
beta.matrixPa
```

The output of this code is

$$\begin{bmatrix} -1/\sqrt{3} & 1/(2\sqrt{3}) & 1/(2\sqrt{3}) & 1/\sqrt{3} & -1/(2\sqrt{3}) & -1/(2\sqrt{3}) \\ 0 & 1/2 & -1/2 & 0 & -1/2 & 1/2 \end{bmatrix},$$

which expresses coordinates of vertices of a kagome lattice. To obtain complete data of standard realizations, we should obtain data of building blocks by using data of the shortest paths from an origin.

Remark 3.9 Crystallographers often call the periodic realizations in $\mathbb{R}^2$ and $\mathbb{R}^3$ of graphs 2-*nets* and 3-*nets*, respectively. The names of 2-nets of each lattice are

sq1	regular square lattice,
hcb	regular hexagonal lattice (honeycomb lattice),
hx1	regular triangular lattice,
kgm	regular kagome lattice,
mcm	1-skeleton of Cairo pentagonal tiling,

and names of 3-nets of each lattice are

pcu	regular cubic lattice,
dia	diamond lattice,
src	gyroid lattice,
crs	3D kagome lattice of type I,
lvt	3D kagome lattice of type II.

Lists of 2-nets and 3-nets are available in EPINET [2].

3.3 Carbon Structures and Standard Realizations

A *graphene* is an allotrope of carbon and is a 2-dimensional crystal structure. Each carbon atom binds chemically with three other carbon atoms by sp^2-orbitals (see Fig. 3.22). From a mathematical viewpoint, a graphene is a standard realization of a hexagonal lattice. A fundamental piece (Fig. 3.22) is a graph with four points, where each points located at the vertices of a regular triangle and its barycenter. Translating the fundamental piece by $\boldsymbol{x}_1$ and $\boldsymbol{x}_2$ with $|\boldsymbol{x}_i| = 1$ and $\langle \boldsymbol{x}_1, \boldsymbol{x}_2 \rangle = (1/2)|\boldsymbol{x}_1|\,|\boldsymbol{x}_2|$, we obtain the structure of graphenes.

A *diamond* is also an allotrope of carbon and is a 3-dimensional crystal structure. Each carbon atom binds chemically with four other carbon atoms by sp^3-orbitals (see Fig. 3.23). From a mathematical viewpoint, a diamond is a standard realization of a graph, which can be called a regular tetrahedral graph. A fundamental piece

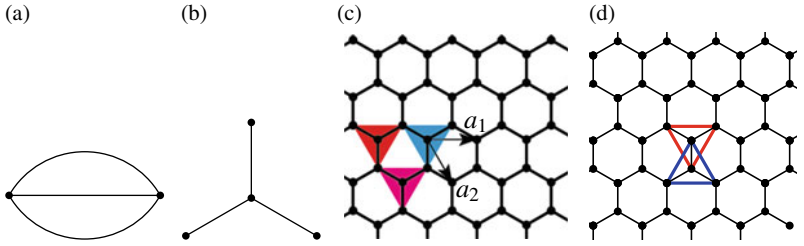

Fig. 3.22 **a** The base graph of a regular hexagonal lattice, **b** a fundamental piece of a regular hexagonal lattice, **c** a graphene structure, which is constructed by **b** and its translations, **d** the barycenter of the blue regular triangle is a vertex of the red regular triangle. The blue triangle is consisted by $\boldsymbol{v}_1$, $\boldsymbol{v}_2$, and $\boldsymbol{v}_3$ (by using notations in Example 3.12), then the red is consisted by $\boldsymbol{v}_0$, $\boldsymbol{v}_0 + \boldsymbol{x}_1$, and $\boldsymbol{v}_0 + \boldsymbol{x}_1 - \boldsymbol{x}_2$. The barycenters of blue and red are $\boldsymbol{v}_0$ and $\boldsymbol{v}_1$, respectively

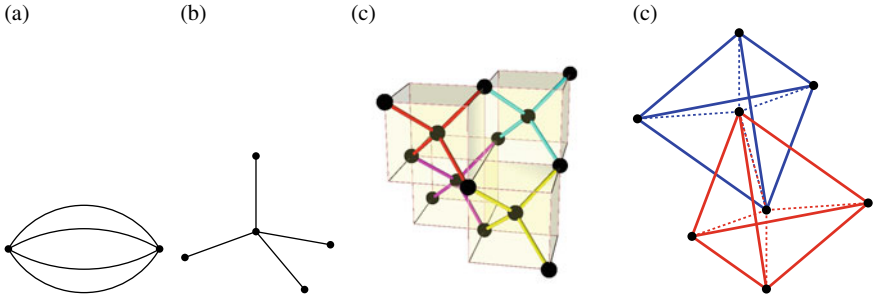

Fig. 3.23 **a** The base graph of a diamond structure, **b** a fundamental piece of a diamond structure, whose vertices are located at the vertices of a regular tetrahedron and its barycenter, **c** a diamond structure. A diamond structure is constructed by **b** and its translations, **d** the barycenter of the blue regular tetrahedron is a vertex of the red regular tetrahedron. The blue tetrahedron consists of $\boldsymbol{v}_1$, $\boldsymbol{v}_2$, $\boldsymbol{v}_3$, and $\boldsymbol{v}_4$ (using notations in Example 3.13), adn the red consists of $\boldsymbol{v}_0$, $\boldsymbol{w}_1 - \boldsymbol{w}_2 = \boldsymbol{v}_0 + \boldsymbol{x}_1 - \boldsymbol{x}_2$, $\boldsymbol{w}_1 - \boldsymbol{w}_3 = \boldsymbol{v}_0 + \boldsymbol{x}_1 - \boldsymbol{x}_3$, and $\boldsymbol{v}_0 + \boldsymbol{w}_1 - \boldsymbol{w}_4 = \boldsymbol{v}_0 + \boldsymbol{x}_1$. The barycenters of blue and red are $\boldsymbol{v}_0$ and $\boldsymbol{w}_1$, respectively

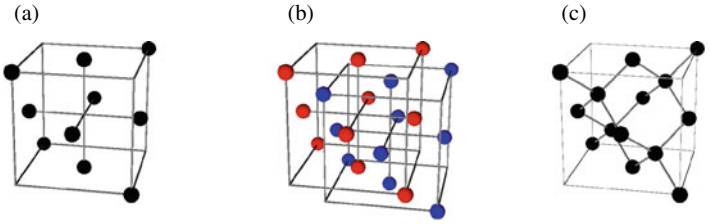

Fig. 3.24 How to construct a diamond structure: **a** Γ: a face centric structure, whose center of the cube is the origin, and the length of edge of the cube is one; each vertex is located at odd point. **b** $\Gamma \cup (\Gamma + w)$: duplicate it and translate to a diagonal direction. **c** We then obtain a diamond structure. Note that **c** is the same as Fig. 3.23c, that is, the usual picture of a diamond structure consists of four units of fundamental pieces constructed by a standard realization

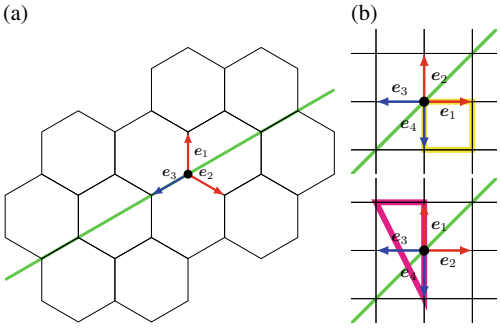

Fig. 3.25 **a** A regular hexagonal lattice is strongly isotropic. For example, exchange $\boldsymbol{e}_1$ and $\boldsymbol{e}_2$, then there exists an element of Euclidean motion such that it preserves the structure. **b** A square lattice does not have a strongly isotropic property. For example, exchanging $\boldsymbol{e}_1$ and $\boldsymbol{e}_4$, the shortest closed path containing $\boldsymbol{e}_1$ and $\boldsymbol{e}_4$ does not maps to a closed path

(Fig. 3.23) is a graph with five points, each point located at the vertices of a regular tetrahedron and its barycenter. Translating the fundamental piece by $\boldsymbol{x}_1$, $\boldsymbol{x}_2$, and $\boldsymbol{x}_3$ with $|\boldsymbol{x}_i| = 1$ and $\langle \boldsymbol{x}_i, \boldsymbol{x}_j \rangle = (1/3)|\boldsymbol{x}_i|\,|\boldsymbol{x}_j|$ if $i \neq j$, we obtain the structure of diamonds.

From textbooks of physical chemistry, the space group of the diamond structure is $Fd\bar{3}m$, which expresses a face-centric structure with a glide reflection, three improper rotations, and certain reflections. Diamond structures are constructed as shown in Fig. 3.24, whose mathematical definition is as follows: Define $\Gamma = \{[x_1, x_2, x_3] \in \mathbb{Z}^3 \mid x_1 + x_2 + x_3 \text{ is odd}\}$ and $w = [1/2, 1/2, 1/2]$. The set $\Gamma_2 = \Gamma \cup (\Gamma + w)$ expresses the set of vertices of a diamond lattice (see Fig. 3.24). On the other hand, the construction of diamond structures by standard realizations is easy (Fig. 3.25).

K_4 *structures* are obtained by standard realizations of the K_4 graph. The K_4 graph is a complete graph with four vertices (each vertex connects to all other vertices). Each carbon atom of K_4 structures binds chemically with three other atoms by sp^2-orbitals (see Fig. 3.26). A fundamental piece is a graph with seven points. Translation vectors

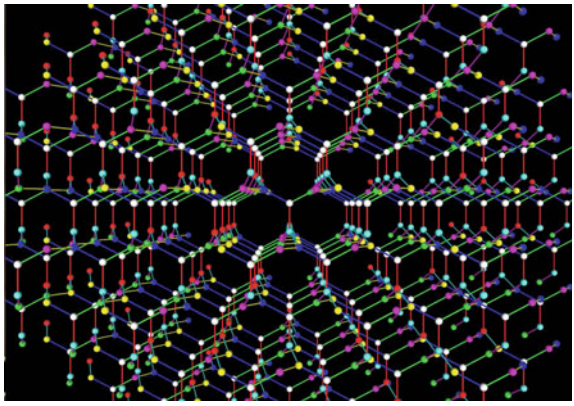

Fig. 3.26 A K_4 structure. This figure is the image of the cover page of *Notices Amer. Math. Soc.*, **55**, drawn by the author

$\{\boldsymbol{x}_i\}_{i=1}^3$ satisfy $|\boldsymbol{x}_i| = 1$ and $\langle \boldsymbol{x}_i, \boldsymbol{x}_j \rangle = -(1/3)|\boldsymbol{x}_i|\,|\boldsymbol{x}_j|$ $(i \neq j)$. Moreover, K_4 structures have chirality, that is, a K_4 structure and its mirror image are not the same.

Definition 3.8 A realization of a topological crystal $X = (V, E)$ is called *strongly isotropic* if and only if for each $x \in V$ and $e_1,\ e_2 \in E_x$, there exists a $\sigma \in \mathrm{Aut}(X)$ such that $\sigma(e_1) = e_2$, $\sigma(e_2) = e_1$, and $\sigma(e_j) = e_j$ for all $e_j \in E_x$.

Theorem 3.5 (Sunada [52]) *A strongly isotropic d-dimensional topological crystal is d- or $(d+1)$-regular. 2-dimensional strongly isotropic topological crystals are hexagonal lattices only. 3-dimensional strongly isotropic topological crystals are diamond lattices and K_4 lattices (and their mirror image) only.*

A standard realization of a strongly isotropic crystal has "maximal symmetry". Graphenes have nice physical properties (see Sect. 3.3), and it is a carbon structure of a standard realization of hexagonal lattices, which is strongly isotropic. Hence, we may expect that K_4-carbons are also have nice physical properties.

Physical properties of the K_4-carbon have been computed by Itoh–Kotani–Naito–Sunada–Kawazoe–Adschiri [19]. It is physically meta-stable and metallic; however, it has not been synthesiz yet. Recently, Mizuno–Shuku–Matsushita–Tsuchiizu–Hara–Wada–Shimizu–Awaga composed a K_4 structure other than carbon [35]. Their structure is a molecular-K_4, a radical molecule NDI-$\triangle(-)$ consists of a K_4 crystal (see Fig. 3.27). There exists an electron between each NDI-$\triangle(-)$, and such electrons are located on a 3D kagome lattice of type III, which is the line graph of K_4 lattice. Hence, such electrons yield flat bands (see also Sect. 7.3). Moreover, they experimentally confirmed that the structure behaves as a spin-liquid.

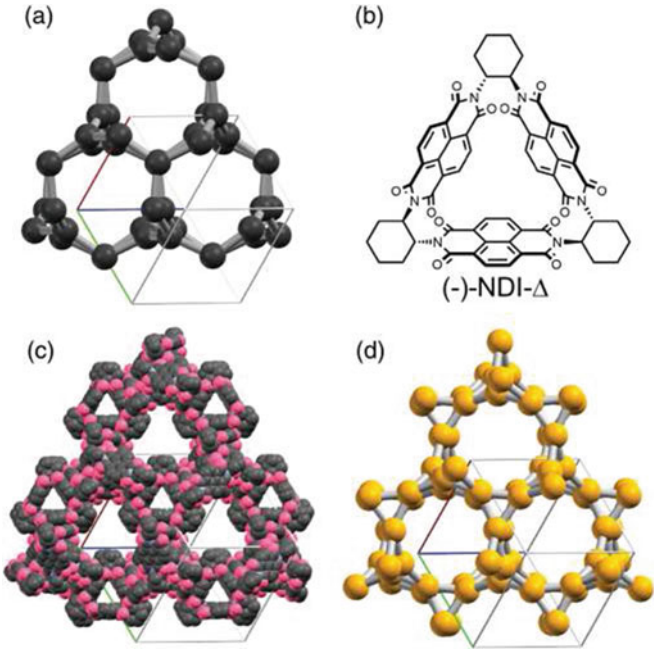

Fig. 3.27 A molecular K_4 structure synthesized by Mizuno–Shuku–Matsushita–Tsuchiizu–Hara–Wada–Shimizu–Awaga, *Phys. Rev. Lett.*, **102**, 055703, (2009)

The electronic properties of graphene are well-known and there exists a Dirac point on the Fermi-level in the electronic band structure (see Sect. 7.3). Similarly, a diamond and a K_4-carbon also have Dirac points in their electronic band structures; however, such Dirac points are not on the Fermi-level (see Tsuchiizu [57]).

Chapter 4
Negatively Curved Carbon Structures

In the 1990s, several new sp^2-carbon structures, fullerenes (including C_{60}), graphene, and carbon nanotubes were found (see Fig. 4.1). These structures look like surfaces in $\mathbb{R}^3$ (atoms of the structures lie on a surface in $\mathbb{R}^3$). Atoms of a graphene, C_{60}, and a nanotube lie on a plane, a sphere, and a cylinder, respectively. Each continuous surface in the above is non-negatively curved, i.e., the Gauss curvature of a sphere is positive, and that of a cylinder and plane are zero. Hence, it is a natural question if an sp^2-carbon structure which looks like a negatively curved surface exists or not.

4.1 Carbon Structures as Discrete Surfaces

In the following, we consider sp^2-carbon structures as "trivalent discrete surfaces" (realizations of 3-regular graphs in $\mathbb{R}^3$, see Chap. 5). Moreover, we assume that graphs are *surface graphs*, that is, each graph is embedded into an oriented surface in $\mathbb{R}^3$ without self-intersections and the embedding defines a decomposition of the surface as a CW complex. By the property of surface graphs, we can define the notion of "faces" (simple closed paths) for trivalent discrete surfaces.

Definition 4.1 For an oriented surface graph $X = (V, E)$, the *Euler number* $\chi(X)$ of X is defined by

$$\chi(X) = |F| - |E| + |V|, \tag{4.1}$$

where $|F|$ is the number of faces of X.

Note that the *Euler number* $\chi(X)$ of a surface graph X is the same as the Euler number of the underlying surface.

H. Naito, *Trivalent Discrete Surfaces and Carbon Structures*,
SpringerBriefs in the Mathematics of Materials 5,
https://doi.org/10.1007/978-981-99-5769-9_4

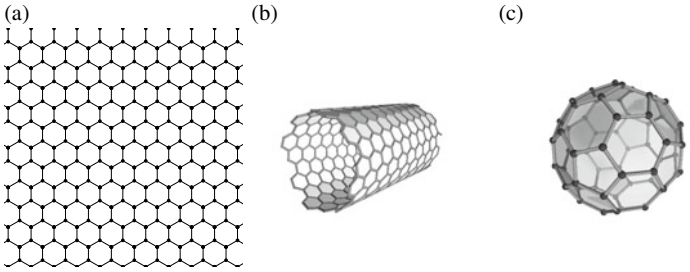

Fig. 4.1 **a** A graphene, **b** (single wall) carbon nanotube, **c** C_{60} (an example of fullerenes)

Proposition 4.1 *Assume that a surface graph $X = (V, E)$ is a trivalent* (3*-regular*) *graph, then we obtain $F = \sum N_k$, $E = (1/2)\sum kN_k$, $V = (1/3)\sum kN_k$, where N_k is the number of k-gons in X. We also obtain*

$$\chi(X) = \sum (1 - k/6)N_k. \tag{4.2}$$

Proof Since X is a surface graph, each edge is shared by two faces, and hence we obtain $|E| = (1/2)\sum kN_k$. Since X is trivalent, each vertex shared by three faces, and hence, we obtain $|V| = (1/3)\sum kN_k$. Substituting them into (4.1), we obtain (4.2). □

Now, we recall classical surface theory in $\mathbb{R}^3$ (see [58]). The Gauss–Bonnet theorem says that for a closed surface Σ, the total curvature $\boldsymbol{K}$ is equal to 2π times the Euler number of Σ, i.e.,

$$\boldsymbol{K} = \int_{\Sigma} K(x)\, dV(x) = 2\pi\chi(\Sigma). \tag{4.3}$$

Here the Euler number $\chi(\Sigma)$ of a smooth surface is defined by

$$\chi(\Sigma) = \operatorname{rank} H_2(\Sigma, \mathbb{Z}) - \operatorname{rank} H_1(\Sigma, \mathbb{Z}) + \operatorname{rank} H_0(\Sigma, \mathbb{Z}),$$

and $\chi(\Sigma)$ is a topological invariant, hence the total curvature $\boldsymbol{K}$ is also a topological invariant.

Therefore, the total curvature $\boldsymbol{K}$ of a trivalent discrete surface X can be defined by

$$\boldsymbol{K} = 2\pi\chi(X), \tag{4.4}$$

similar to (4.3). By the above arguments, we may admit that a trivalent discrete surface X is positively, negatively curved if and only if $\chi(X) > 0$, $\chi(X) < 0$, respectively.

Table 4.1 Number of polygons of C_{60}, a single-wall nanotube (or fundamental region of it), where $\boldsymbol{c}$ is the chiral index of SWNT (see Sect. 7.1), and Mackay–Terrones structure (see Fig. 4.2b)

	N_5	N_6	N_7	N_8	$\lvert V\rvert$	$\lvert E\rvert$	$\lvert F\rvert$	χ
C_{60}	12	20	0	0	60	90	32	2
SWNT $\boldsymbol{c} = (6, 6)$	0	12	0	0	24	36	12	0
Mackay–Terrones	0	90	0	12	192	288	102	−4

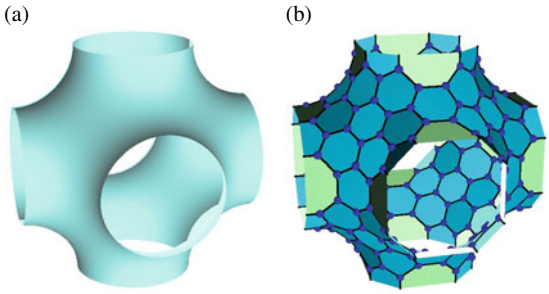

Fig. 4.2 **a** Schwarz P surface, which is a triply periodic minimal surface (the Gauss curvature $K < 0$, the Euler number $\chi = -4$, and the genus $g = -3$), whose period lattice $\{\boldsymbol{e}_i\}_{i=1}^3$ satisfies $\langle \boldsymbol{e}_i, \boldsymbol{e}_j \rangle = \delta_{ij}$. **b** The Mackay–Terrones structure, the period lattice is the same as **a**. Green faces in **b** are octagons (see also Table 4.1 and Fig. 4.3). Note that the structure is constructed by the method described in Chap. 5 as a trivalent discrete surface

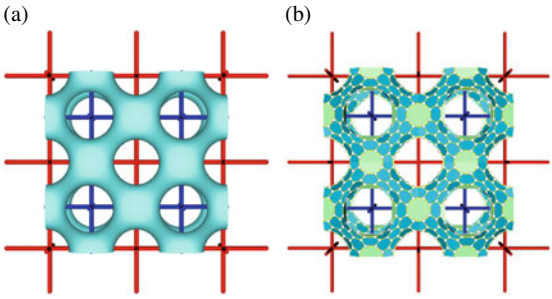

Fig. 4.3 Relationships between a Schwarz surface and two 3-nets. A red-colored 3-net is moved from the blue-colored 3-net to a Wyckoff point of the network. Such a pair of **pcu** is called **2pcu**. A Schwarz P surface appeares as an "interface" of **2pcu**. **a** A Schwarz P surface and **2pcu** network. **b** The Mackay–Terrones structure and **2pcu** network

Remark 4.1 By Proposition 4.1, the number of hexagons does not affect the Euler number. If X is positively curved, then at least one n-gon ($n \leq 5$) should be contained in X. If X is negatively curved, then at least one n-gon ($n \geq 7$) should be contained in X.

By Proposition 4.1, if there exists an sp^2-carbon structure with $\chi(X) < 0$ (negatively curved), then at least one n-gon ($n \geq 7$) exists in X. In 1991, Mackay–Terrones [33] calculated an sp^2-carbon structure which looks like a minimal surface (Schwarz P surface, $\chi(X) = -4$), which contains 12 octagons (see Fig. 4.2b, and also Lenosky–Gonze–Teter–Elser [32]). We call it the *Mackay–Terrones structure*.

4.2 Constructions of Negatively Curved Carbon Structures via Standard Realizations

Tagami–Liang–Naito–Kawazoe–Kotani [55] constructed negatively curved carbon crystals, which are different from the Mackay–Terrones structure, by using standard realizations of topological crystals.

The fundamental region of the Mackay–Terrones structure has octahedral symmetry, which is the same symmetry as that of truncated octahedrons. Truncated octahedrons consist of eight hexagons, which have D_6-symmetry (see Fig. 4.4).

Our method is:

1. we classify and construct a graph in a fundamental region of D_6-action ("kite region") on a hexagon, which is a trivalent graph when we extend it to the hexagonal region by D_6-action (Fig. 4.4c),
2. we extend the graph obtained in 1 to the trivalent graph on a hexagon (Fig. 4.4b),
3. we extend the graph obtained in 2 to the graph on a truncated octahedron (Fig. 4.4a),
4. we calculate a standard realization of the graph obtained in 3.

The structure obtained in 4 is a candidate for sp^2-carbon structure with $\boldsymbol{K} < 0$ ($\chi = -4$).

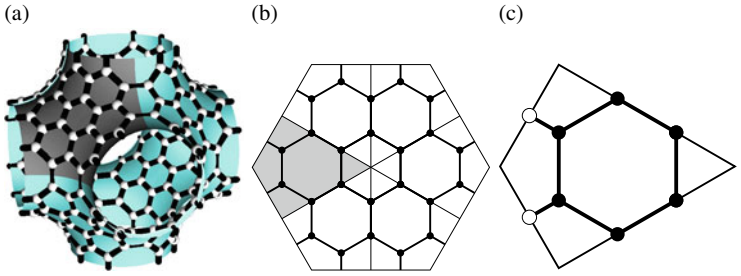

Fig. 4.4 Symmetry of the Mackay–Terrones structure. **a** A fundamental unit of the Mackay–Terrones structure. **b** A fundamental unit of octahedoral symmetry. **c** A fundamental region of D_6-action on **b**. See also Fig. 7.20 (Tagami–Liang–Naito–Kawazoe–Kotani [55] (CC BY-NC-ND 3.0))

Constructing networks in the kite region, we assume the following natural conditions: (a) any inner vertices are of degree 3, (b) any vertices on the boundary are joined with the two adjacent vertices on the boundary, or with an inner vertex and not with both adjacent vertices on the boundary, (c) the network is planar and connected, and there are at least four vertices on the boundary, (d) the network does not have a consecutive sequence of odd vertices on the boundary, and (e) the network is triangle-free.

Proposition 4.2 (Tagami–Liang–Naito–Kawazoe–Kotani [55]) *There is no network with an odd number of vertices that satisfies the conditions given above.*

After constructing a network in the kite region, and extending it to the graph on a truncated octahedron, we may prove the claim:

Theorem 4.1 (Tagami–Liang–Naito–Kawazoe–Kotani [55]) *The equation to obtain standard realization is linear:* $\Delta \boldsymbol{x} = \boldsymbol{b}$*, where* $b_i = \pm \boldsymbol{e}_\alpha$*, if a vertex* v_i *is adjacent to a vertex in neighbouring cell. The linear equation is solvable if and only if* $\sum b_i = 0$*. The period lattice* $\{\boldsymbol{e}_i\}$ *which gives a standard realization is cubic, i.e.,* $\boldsymbol{e} = [\boldsymbol{e}_1, \boldsymbol{e}_2, \boldsymbol{e}_3]$ *is a period lattice of a standard realization, then* $\boldsymbol{e}^T \boldsymbol{e} = \boldsymbol{E}$*. If* Φ *is a standard realization, then* $\mathrm{Aut}(X) \subset \mathrm{Aut}(\Phi(X))$*, and hence* X *has the same symmetries as the Mackay–Terrones structure.*

In our method, we do not solve the Eq. (3.7). Instead, we only solve the harmonic Eq. (3.3) using cubic periodicity. Hence, we should prove that the realization is standard. To prove it, we use the Lagrange multiplier, and the result of the Lagrange multiplier is $\boldsymbol{e}^T \boldsymbol{e} = \boldsymbol{E}$. This shows that the harmonic realizations with the cubic lattice are standard. To find the standard realization in this case specifically, for a given finite graph X and periodic condition $\boldsymbol{f}$, we solve the equation $\Delta_X \boldsymbol{u} = \boldsymbol{f}$. However, since Δ_X is singular, it cannot be solved as $\boldsymbol{u} = \Delta_X^{-1} \boldsymbol{f}$. A numerical method to solve the equation in this case is described in Sect. 7.5.2.

After calculating a standard realization of the network, we calculate physical stability by numerical calculations based on density functional theory (DFT). We construct several networks in the kite region satisfying the above conditions with 6 or 8 vertices, and we obtain four physically stable carbon structures shown in Fig. 4.5. We also obtain the Mackay–Terrones structure in this way and confirm the physical stability of it.

Remark 4.2 No negatively curved sp^2-carbon structure has been synthesized so far. However, a piece of negatively curved carbon structure has been chemically synthesized by Kawasumi–Zhang–Segawa–Scott–Itami [22, Fig. 2].

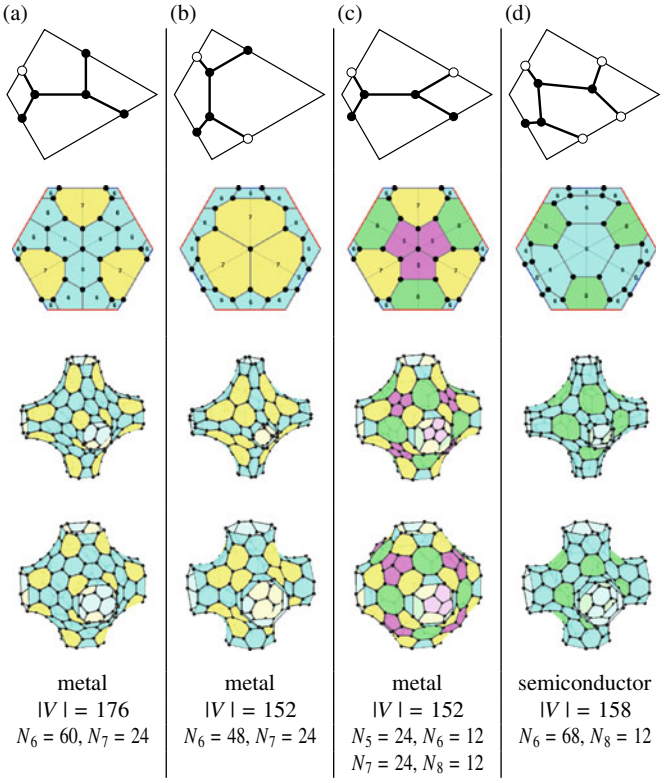

Fig. 4.5 Mackay–Terrones-like structures, which are physically stable and $\chi(X) = -4$ ($\boldsymbol{K} < 0$). For the notion of "metal"/"semiconductor", see Sect. 7.3 (Tagami–Liang–Naito–Kawazoe–Kotani [55] (CC BY-NC-ND 3.0))

Chapter 5
Trivalent Discrete Surfaces

In the previous chapter, we explained "negatively" curved carbon structure; however, the definition of negativity is that the total curvature or the Euler number is negative. Since the Gauss curvature of smooth surfaces is a function defined on each point of the surface, it is not sufficient to say that the discrete surface is negatively curved.

In this chapter, we consider the Gauss curvature and the mean curvature for trivalent discrete surfaces.

5.1 Curvatures of Trivalent Discrete Surfaces

Definition 5.1 (*Kotani–Naito–Omori* [24]) Let $X = (V, E)$ be a trivalent graph, and $\Phi\colon X \longrightarrow \mathbb{R}^3$ be a realization of X. The realization Φ is called a *trivalent discrete surface* if and only if for each $x \in V$, at least two vectors of $\{\Phi(e) \mid e \in E_x\}$ are linearly independent.

The last condition means that a normal vector can be defined on each vertex of $\Phi(X)$, in other words, a plane is defined through adjacent three vertices of each vertex (Definition 5.2).

We remark that this definition of trivalent discrete surfaces is not limited to topological crystals, and thus we can treat C_{60} and single-wall nanotubes (SWNTs) for example. But the definition also contains K_4 structure as a trivalent discrete surface, although it does not look like a discrete surface.

Definition 5.2 (*Kotani–Naito–Omori* [24]) Let $\Phi\colon X \longrightarrow \mathbb{R}^3$ be a trivalent discrete surface. We define the unit normal vector at $\boldsymbol{x} \in \Phi(x)$ as the normal vector of the plane through $\boldsymbol{e}_1$, $\boldsymbol{e}_2$, and $\boldsymbol{e}_3$ (see Fig. 5.1), that is,

H. Naito, *Trivalent Discrete Surfaces and Carbon Structures*,
SpringerBriefs in the Mathematics of Materials 5,
https://doi.org/10.1007/978-981-99-5769-9_5

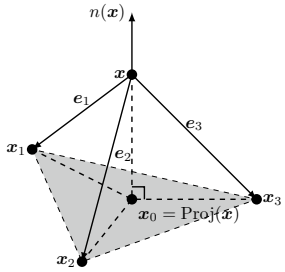

Fig. 5.1 The unit normal vector for trivalent discrete surfaces. The area of the triangle filled in gray is the local area at $\boldsymbol{x}$

$$n(\boldsymbol{x}) = \frac{(\boldsymbol{e}_2 - \boldsymbol{e}_1) \times (\boldsymbol{e}_3 - \boldsymbol{e}_1)}{|(\boldsymbol{e}_2 - \boldsymbol{e}_1) \times (\boldsymbol{e}_3 - \boldsymbol{e}_1)|} = \frac{\boldsymbol{e}_1 \times \boldsymbol{e}_2 + \boldsymbol{e}_2 \times \boldsymbol{e}_3 + \boldsymbol{e}_3 \times \boldsymbol{e}_1}{|\boldsymbol{e}_1 \times \boldsymbol{e}_2 + \boldsymbol{e}_2 \times \boldsymbol{e}_3 + \boldsymbol{e}_3 \times \boldsymbol{e}_1|},$$

and the covariant differentiation is

$$\nabla_{\boldsymbol{e}} \boldsymbol{x} = \mathrm{Proj}(\boldsymbol{e}) = \boldsymbol{e} - \langle \boldsymbol{e}, n(\boldsymbol{x}) \rangle n(\boldsymbol{x}), \quad e \in E_x, \ \ \boldsymbol{e}_i = \boldsymbol{x}_i - \boldsymbol{x}.$$

Before defining curvatures for trivalent discrete surfaces, we recall properties of curvature for smooth surfaces in $\mathbb{R}^3$.

Definition 5.3 (*Curvatures for smooth surfaces*) Let $p\colon \Omega \subset \mathbb{R}^2 \longrightarrow \mathbb{R}^3$ be a smooth surface, and $n(x)$ be a unit normal vector at $x \in \Omega$. We define the first and the second fundamental forms by $\mathrm{I} = \langle dp, dp \rangle$, and $\mathrm{II} = -\langle dn, dp \rangle$, respectively. By using them, the Gauss curvature and the mean curvature are defined by $K(x) = \det(\mathrm{I}^{-1}\,\mathrm{II})$ and $H(x) = \frac{1}{2}\,\mathrm{tr}(\mathrm{I}^{-1}\,\mathrm{II})$, respectively.

The Gauss and the mean curvatures for smooth surfaces can be defined if we define a unit normal vector field $\boldsymbol{n}$. We have already defined a unit normal vector fields $\boldsymbol{n}$ for trivalent discrete surfaces, and we may define the Gauss and the mean curvatures for them similarly.

Definition 5.4 (*Kotani–Naito–Omori* [24]) Let X be a trivalent discrete surface and $\boldsymbol{x}$ be a vertex of X. We define the first and the second fundamental forms by

$$\mathrm{I}(\boldsymbol{x}) = \begin{bmatrix} \langle \boldsymbol{e}_2 - \boldsymbol{e}_1, \boldsymbol{e}_2 - \boldsymbol{e}_1 \rangle & \langle \boldsymbol{e}_2 - \boldsymbol{e}_1, \boldsymbol{e}_3 - \boldsymbol{e}_1 \rangle \\ \langle \boldsymbol{e}_3 - \boldsymbol{e}_1, \boldsymbol{e}_2 - \boldsymbol{e}_1 \rangle & \langle \boldsymbol{e}_3 - \boldsymbol{e}_1, \boldsymbol{e}_3 - \boldsymbol{e}_1 \rangle \end{bmatrix},$$
$$\mathrm{II}(\boldsymbol{x}) = -\begin{bmatrix} \langle \boldsymbol{e}_2 - \boldsymbol{e}_1, n_2 - n_1 \rangle & \langle \boldsymbol{e}_2 - \boldsymbol{e}_1, n_3 - n_1 \rangle \\ \langle \boldsymbol{e}_3 - \boldsymbol{e}_1, n_2 - n_1 \rangle & \langle \boldsymbol{e}_e - \boldsymbol{e}_1, n_3 - n_1 \rangle \end{bmatrix},$$

and we define the *Gauss curvature* $K(\boldsymbol{x})$ and the *mean curvature* $H(\boldsymbol{x})$ at $\boldsymbol{x}$ by

$$K(\boldsymbol{x}) = \det(\mathrm{I}(\boldsymbol{x})^{-1}\,\mathrm{II}(\boldsymbol{x})),$$
$$H(\boldsymbol{x}) = \frac{1}{2}\operatorname{tr}(\mathrm{I}(\boldsymbol{x})^{-1}\,\mathrm{II}(\boldsymbol{x})).$$

The next proposition is one of important properties of the Gauss curvature and the mean curvature for smooth surfaces.

Proposition 5.1 *For a smooth surface $p\colon \Omega \longrightarrow \mathbb{R}^3$ with a unit normal vector field n, the Gauss curvature K satisfies $\nabla_1 n(x) \times \nabla_2 n(x) = K(x)(\nabla_1 p(x) \times \nabla_2 p(x))$, and the mean curvature H satisfies $\frac{d}{dt}A(x,t)\big|_{t=0} = -H(x)A(x)$, where $A(x)$ is the area element of p and $A(x,t)$ is the one of the parallel transformations p_t ($p_t(x) = p(x) + tn(x)$) of the surface along the normal direction. Moreover, Steiner's formula $A(x,t) = (1 + 2tH(x) + t^2K(x))A(x)$ holds.*

The Gauss and the mean curvatures for trivalent discrete surfaces satisfy similar properties to Proposition 5.1.

Theorem 5.1 (Kotani–Naito–Omori [24]) *For a trivalent discrete surface Φ, the Gauss curvature K satisfies $\nabla_i n(\boldsymbol{x}) \times \nabla_j n(\boldsymbol{x}) = K(\boldsymbol{x})(\boldsymbol{e}_i \times \boldsymbol{e}_j)$, where $\nabla_i = \nabla_{e_i}$, and the mean curvature H satisfies $\frac{d}{dt}\big|_{t=0}\mathcal{A}(\Phi + t\boldsymbol{n}) = -2\sum_{x\in V} H(\boldsymbol{x})A(\boldsymbol{x})$, where $A(\boldsymbol{x}) = \boldsymbol{e}_1 \times \boldsymbol{e}_2 + \boldsymbol{e}_2 \times \boldsymbol{e}_3 + \boldsymbol{e}_3 \times \boldsymbol{e}_1$ is the local area at $\boldsymbol{x}$ and $\mathcal{A}(\Phi) = \sum_{x\in V} A(\boldsymbol{x})$ is the total area. Moreover, Steiner type formula $\mathcal{A}(\Phi + t\boldsymbol{n}) = \sum_{x\in V}(1 + 2tH(\boldsymbol{x}) + t^2K(\boldsymbol{x}))A(\boldsymbol{x})$ also holds.*

Remark 5.1 It is well-known that the first and the second fundamental form for smooth surfaces are symmetric. As a result, principal curvatures (eigenvalues of $\mathrm{I}(\boldsymbol{x})^{-1}\,\mathrm{II}(\boldsymbol{x})$) are real; however, the second fundamental form $\mathrm{II}(\boldsymbol{x})$ for trivalent discrete surfaces is not always symmetric. Hence, principal curvatures are not always real (see Remark 5.4).

Remark 5.2 There are many kinds of discrete surfaces, and there are many definitions of the Gauss curvature and the mean curvature for discrete surfaces. The most famous kind of discrete surface is polygons in $\mathbb{R}^3$, which consist of planer polygons as faces. The Gauss curvature for polygons is called the *angle defects* (5.1), and the mean curvature is called the *cotangent formula* (5.2) defined by Pinkall–Polthier [46]. The angle defects and the cotangent formula are defined as

$$K(x) = 2\pi - \sum \theta_i, \tag{5.1}$$
$$H(x) = \frac{1}{2}\sum(\cot\alpha_j + \cot\beta_j)(x - p_j), \tag{5.2}$$

where θ_i are angles surrounding the vertex x, and α_i and β_i are angles shown in Fig. 5.2.

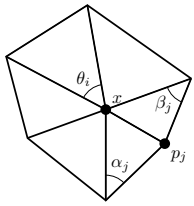

Fig. 5.2 Definitions of angles θ_i, α_j, and β_j

We note that the angle defects cannot be applied to trivalent discrete surfaces. The Mackay–Terrones structure and structures in Sect. 4.2 satisfy the balanced condition (3.6), hence a vertex and adjacent three vertices are co-planar, and $K(x) \equiv 0$ by the angle defects. This means that the angle defects cannot apply to trivalent discrete surfaces as the definition of the Gauss curvature. This observation is one of motivations for defining trivalent discrete surfaces and their curvatures.

5.2 Examples of Trivalent Discrete Surfaces and Their Curvatures

Proposition 5.2 *If a trivalent discrete surface is planar, then $K \equiv 0$, $H \equiv 0$. Here, a trivalent discrete surface is planar if and only if there exists a plane $L \subset \mathbb{R}^3$ such that $\boldsymbol{x} \in L$ for all vertices $\boldsymbol{x}$.*

Proposition 5.3 (Kotani–Naito–Omori [24]) *If a trivalent discrete surface satisfies $\boldsymbol{x} = rn(\boldsymbol{x})$ for any $x \in V$, then $K \equiv 1/r^2$, $H \equiv -1/r$.*

We call a surface satisfying $\boldsymbol{x} = rn(\boldsymbol{x})$ for all $\boldsymbol{x}$ *sphere-shaped*. Regular polyhedra and semi-regular polyhedra (including C_{60}) are sphere-shaped.

Proposition 5.4 (Kotani–Naito–Omori [24]) *Let* $\mathrm{CNT}(\lambda, \boldsymbol{c})$ *be an SWNT with the chiral index $\boldsymbol{c} = (c_1, c_2)$ and the scale factor λ, that is,*

$$(x, y) \mapsto (r(\lambda, \boldsymbol{c}) \cos(x/r(\lambda, \boldsymbol{c})), r(\lambda, \boldsymbol{c}) \sin(x/r(\lambda, \boldsymbol{c})), y).$$

Then the Gauss curvature and the mean curvature of $\mathrm{CNT}(\lambda, \boldsymbol{c})$ *are*

$$K(\lambda, \boldsymbol{c}) = \frac{4m_z(\boldsymbol{c})^2(m_x(\boldsymbol{c})^2 + m_y(\boldsymbol{c})^2)}{3r(\lambda, \boldsymbol{c})^2(m_x(\boldsymbol{c})^2 + m_y^2(\boldsymbol{c}) + (4/3)m_z(\boldsymbol{c})^2)^2},$$
$$H(\lambda, \boldsymbol{c}) = -\frac{m_x(\boldsymbol{c})}{2r(\lambda, \boldsymbol{c})} \cdot \frac{m_x(\boldsymbol{c})^2 + m_y(\boldsymbol{c})^2 + (8/3)m_z(\boldsymbol{c})^2}{(m_x(\boldsymbol{c})^2 + m_y(\boldsymbol{c})^2 + (4/3)m_z(\boldsymbol{c})^2)^{3/2}},$$

which are constants. Here

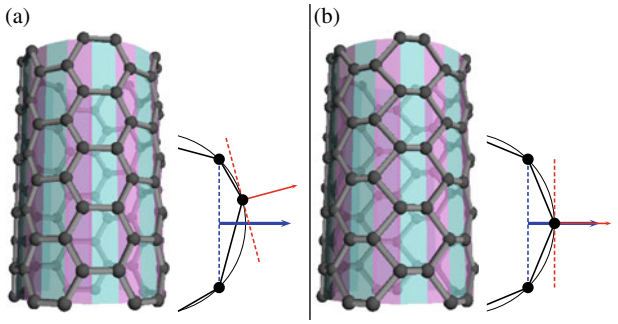

Fig. 5.3 **a** CNT$(\lambda, \boldsymbol{c})$ satisfies $H \not\equiv -1/(2r)$, whose normal vectors are not parallel to normal vectors of the underlying cylinder. **b** A small change of CNT$(\lambda, \boldsymbol{c})$ satisfies $H \equiv -1/(2r)$, whose normal vectors are parallel to normal vectors of the underlying cylinder (Kotani–Naito–Omori [24] (CC BY-NC-ND 4.0))

$$
\begin{aligned}
m_x(c) &= C_1 \cos(C_2/2) \sin(T_2/2) - C_2 \cos(C_1/2) \sin(T_1/2), \\
m_y(c) &= -C_1 \sin(C_2/2) \sin(T_2/2) + C_2 \sin(C_1/2) \sin(T_1/2), \\
m_z(c) &= \sin(T_1/2) \sin(T_2/2) \sin((T_1 + T_2)/2), \\
(C_1, C_2) &= \left(\frac{\pi t_1 d(c)}{c_1^2 + c_1 c_2 + c_2^2}, \frac{\pi t_2 d(c)}{c_1^2 + c_1 c_2 + c_2^2}, \right), \\
d(c) &= \gcd(c_1 + 2c_2, 2c_1 + c_2),
\end{aligned}
$$

and $r(\lambda, c) = \lambda\sqrt{c_1^2 + c_1 c_2 + c_2^2}/(2\pi)$ *is the radius of circular cylinder on which* CNT(λ, c) *winds. In particular,* $c_1 = c_2$*, then* $m_z(\boldsymbol{c}) = 0$*, and*

$$
K(\lambda, \boldsymbol{c}) = 0, \quad H(\lambda, \boldsymbol{c}) = -\frac{1}{2r(\lambda, \boldsymbol{c})} \cos \frac{C_1}{2}.
$$

Remark 5.3 Vertices of CNT(λ, c) are located on a cylinder with radius r whose Gauss curvature and the mean curvature are 0 and $-1/(2r)$, respectively. But the mean curvature of CNT(λ, c) is not $-1/(2r)$ even if $c_1 = c_2$. As shown in Fig. 5.3a, the normal vector of the SWNT at each vertex is out of the normal vector of the underlying cylinder. By a little modification of the SWNT shown in Fig. 5.3b, we can align normal vectors of the SWNT and the underlying cylinder, then the Gauss and the mean curvatures of such trivalent discrete surfaces are 0 and $-1/(2r)$, respectively.

One of the motivations for defining Gauss and mean curvatures for trivalent discrete surfaces is to make sure that the Mackay–Terrones structure and the structure of Sect. 4.2, which are considered to be on negatively curved surfaces, are negatively curved. Curvatures of trivalent discrete surfaces defined so far are calculated numerically for these structures, as shown in Figs. 5.4 and 5.5; we can confirm that these structures are negatively curved. In addition, since all vertices of the Mackay–

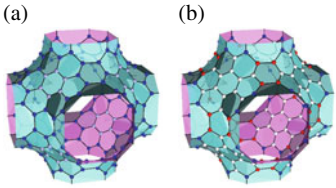

Fig. 5.4 **a** The Gauss curvatures of the Mackay–Terrones structure, **b** the mean curvatures of the Mackay–Terrones structure. By our definition of curvatures, The Mackay–Terrones structure is *pointwise* negatively curved. Blue (red) vertices are negatively (positively) curved, and color densities express relative absolute values of curvatures (Kotani–Naito–Omori [24] (CC BY-NC-ND 4.0))

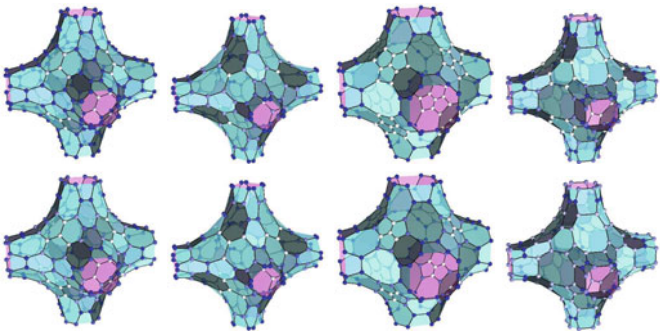

Fig. 5.5 Curvatures of structures in Fig. 4.5. Upper row: the Gauss curvature, lower row: the mean curvature. These structures are *pointwise* negatively curved. Blue (red) vertices are negatively (positively) curved, and color densities express relative absolute values of curvatures (Kotani–Naito–Omori [24] (CC BY-NC-ND 4.0))

Terrones structure with the standard realization are considered to lie on the Schwarz P surface, we expect the mean curvature to be zero, i.e., a discrete minimal surface. However, this is not the case according to the numerical calculation (see Fig. 5.4). In the following, we briefly explain how to construct a trivalent discrete minimal surface.

Remark 5.4 Curvatures of K_4 structures satisfy $K > 0$ and $H \equiv 0$. In the case of smooth surfaces, the mean curvature $H \equiv 0$, then the Gauss curvature $K \leq 0$, since the second fundamental form II is symmetric. On the other hand, in our discrete case, II is not symmetric, and thus $H \equiv 0$ does not imply $K \leq 0$,

5.3 Construction of Trivalent Minimal Discrete Surfaces

The Mackay–Terrones structure is not minimal ($H \not\equiv 0$), contrary to expectations. But we may construct the minimal configuration by deforming the structure.

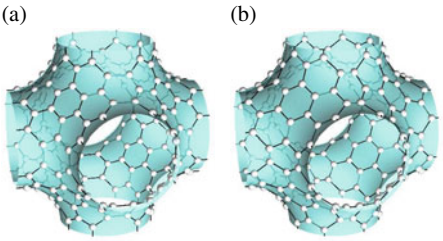

Fig. 5.6 **a** The Mackay–Terrones structure (standard realization), **b** minimal realization of the same structure (Kotani–Naito–Omori [24] (CC BY-NC-ND 4.0))

Theorem 5.2 (Kotani–Naito–Omori [24]) *Let* $\Phi\colon X = (V, E) \longrightarrow \mathbb{R}^3$ *be a trivalent discrete surface. Then the mean curvature* $H\colon V \longrightarrow \mathbb{R}$ *is written as*

$$\nabla_{e_2-e_3}\boldsymbol{n} \times \nabla_1\Phi + \nabla_{e_3-e_1}\boldsymbol{n} \times \nabla_2\Phi + \nabla_{e_1-e_2}\boldsymbol{n} \times \nabla_3\Phi = 4H(x)A(x)\boldsymbol{n}(x). \quad (5.3)$$

If a function $H\colon V \longrightarrow \mathbb{R}$ is given, then a trivalent discrete surface, which solves (5.3), has H as the mean curvature, i.e., the Eq. (5.3) is the "prescribed mean curvature equation". A trivalent discrete surface is called *minimal*, if $H(\boldsymbol{x}) \equiv 0$.

Theorem 5.3 (Kotani–Naito–Omori [24]) *The trivalent discrete surface* Φ *is minimal if and only if it satisfies the the system of equations*

$$\nabla_{\boldsymbol{e}_2-\boldsymbol{e}_3}n \times \nabla_{\boldsymbol{e}_1}\Phi + \nabla_{\boldsymbol{e}_3-\boldsymbol{e}_1}n \times \nabla_{\boldsymbol{e}_2}\Phi + \nabla_{\boldsymbol{e}_1-\boldsymbol{e}_2}n \times \nabla_{\boldsymbol{e}_3}\Phi = 0. \quad (5.4)$$

By using Theorem 5.3, we may construct a minimal configuration as follows: (1) let Φ_0 be a trivalent discrete surface and $\boldsymbol{n}_j$ is its normal vector fields, (2) solve (5.4) for given $\boldsymbol{n}_j$, and iterate this procedure until $|H| < \varepsilon$. This procedure may be corrupted to a degenerate surface (e.g., one point, in general); however, in the case of the Mackay–Terrones structure, the procedure can be iterated successfully and we obtain a minimal configuration (see Fig. 5.6).

Another method to construct minimal configuration of trivalent discrete surfaces is to use the mean curvature flow. The classical mean curvature flow equation is

$$\frac{\partial \Sigma_t}{\partial t}(x) = -H_t(x)\boldsymbol{n}_t(x), \quad (5.5)$$

where $\Sigma = \Sigma_t$ is a family of smooth surfaces and H_t, $\boldsymbol{n}_t$ are its mean curvatures and unit normal vector fields. Huisken [17] shows that if the initial surface Σ_0 is a convex closed embedded surface, then there exists a solution of (5.5) on $[0, T)$, and Σ_t converges to a round point within finite time.

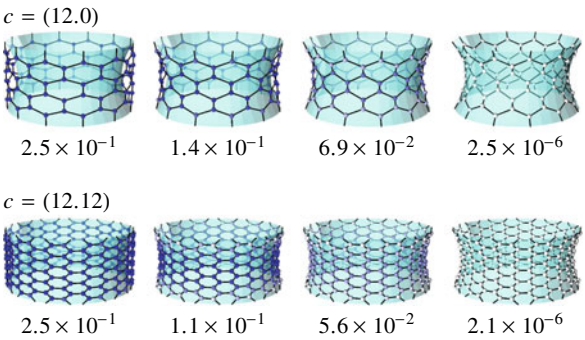

Fig. 5.7 Numerical calculation of (5.6) with the Dirichlet boundary condition (vertices on boundaries are fixed). Blue surfaces are catenoids and the values in below them are the maximum value of H in each figure

If we select a suitable initial value with small mean curvatures, then we expect the existence and convergence of solutions of the mean curvature flow for trivalent discrete surfaces. Namely, for an initial trivalent discrete surface Φ_0, we solve the mean curvature flow for trivalent discrete surfaces Φ_t:

$$\frac{\partial \Phi_t}{\partial t}(x) = -H_t(x)\boldsymbol{n}_t(x). \tag{5.6}$$

The Schwarz P surface is stable with respect to the area functional subject to constant volume, but unfortunately is unstable without the volume constraint cf. [48]. Therefore, the solution of (5.6) with the initial value as the Mackay–Terrones structure will be corrupted to a point. But, we may numerically construct a "trivalent catenoid" by using (5.6) with the initial value as SWNTs (see Fig. 5.7).

Chapter 6
Subdivisions of Trivalent Discrete Surfaces

In this chapter, we consider "subdivisions" of trivalent discrete surfaces. In our context, there are no underlying continuous objects, and trivalent discrete surfaces are essentially discrete objects. For example, the Mackay–Terrones structure is constructed using the Schwarz P surface as a model, but there are no relations between the structure and the surface itself. We can find a "limit" of a sequence of trivalent discrete surfaces, and make a relationship between a trivalent discrete surface and a continuous surface.

To discuss the convergence theory of trivalent discrete surfaces, we should consider how to subdivide a trivalent graph, and how to realize the subdivided graph. The Goldberg–Coxeter subdivision for trivalent graphs defined by Dutour–Deza [9, 10] is the nice definition to subdivide a trivalent graph (see also Goldberg [13] and Omori–Naito–Tate [41]). Kotani–Naito–Omori [24], Tao [56], and Kotani–Naito–Tao [25] discuss convergences of sequences of trivalent discrete surfaces.

6.1 Goldberg–Coxeter Constructions

A subdivision of a trivalent discrete surface should can be of the same topological type as the original one, hence the requisite conditions that subdivisions should satisfy are:

1. A subdivision $\boldsymbol{X}_1$ of a trivalent discrete surface $\boldsymbol{X}_0$ is also a trivalent discrete surface, namely the underlying graph X_1 of $\boldsymbol{X}_1$ is also a trivalent graph.
2. $\boldsymbol{X}_1$ is also a surface graph, and $\boldsymbol{X}_1$ and $\boldsymbol{X}_0$ have the same topological type, namely $\chi(\boldsymbol{X}_1) = \chi(\boldsymbol{X}_0)$.

H. Naito, *Trivalent Discrete Surfaces and Carbon Structures*,
SpringerBriefs in the Mathematics of Materials 5,
https://doi.org/10.1007/978-981-99-5769-9_6

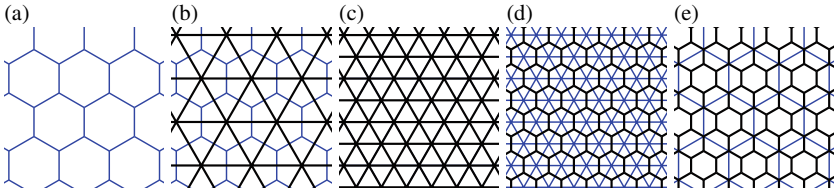

Fig. 6.1 Procedure of the subdivision $\mathrm{GC}_{2,0}(X)$ of a regular hexagonal lattice, **a** regular hexagonal lattice, **b** dual graph of **a**, **c** subdivision of **b**, **d** dual graph of **c**, and **e** a regular hexagonal lattice and its subdivision (Kotani–Naito–Omori [24] (CC BY-NC-ND 4.0))

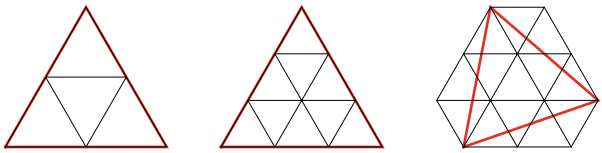

Fig. 6.2 Procedure of subdivision for (k, ℓ)-Goldberg–Coxeter constructions

Definition 6.1 (*Dutour–Deza* [9, 10]) Let X be a trivalent plane graph. The $(2, 0)$-*Goldberg–Coxeter subdivision* (or *Goldberg–Coxeter construction* of X is defined by the following procedure (see Fig. 6.1):

1. Take the dual graph $\widehat{X}$ of X. The dual graph is a triangulation, since X is trivalent.
2. On each triangle of $\widehat{X}$, make the sub-triangulation by taking the midpoints of the three edges and connecting each midpoint to the others. This procedure makes the subdivision of $\widehat{X}$, say $\widehat{X}_1$ (see Fig. 6.2).
3. Take the dual graph $X_1 = \widehat{\widehat{X}_1}$,

finally, we define the $(2, 0)$-Goldberg–Coxeter subdivision $\mathrm{GC}_{2,0}(X) = X_1$.

Definition 6.2 (*Dutour–Deza* [9, 10]) Let X be a trivalent plane graph and $(k, \ell) \in \mathbb{Z}_{>0} \times \mathbb{Z}_{\geq 0}$. The (k, ℓ)-*Goldberg–Coxeter subdivision* of X is defined by the following procedure (see Fig. 6.2):

1. Take the dual graph $\widehat{X}$ of X. The dual graph is triangulation, since X is trivalent.
2. Considering a simple closed path of $\widehat{X}$ as a regular triangle with coordinates 0, $z = k + \ell\omega$ and $z\omega$, where $\omega = (1 + \sqrt{-3})/2$, we set $\widehat{X}_1$ as a regular triangular graph with edge length 1.
3. Take the dual graph $X_1 = \widehat{\widehat{X}_1}$.

Finally, we define the (k, ℓ)-Goldberg–Coxeter subdivision $\mathrm{GC}_{k,\ell}(X) = X_1$.

Example 6.1 A truncated icosahedral graph (graph of C_{60}) is a $(1, 1)$-subdivision of a dodecahedral graph (Fig. 6.3).

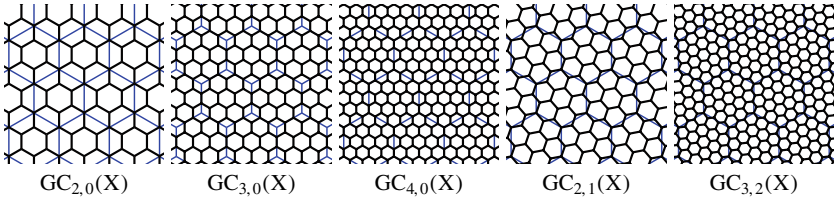

Fig. 6.3 Examples of subdivisions of a regular hexagonal lattice (Kotani–Naito–Omori [24] (CC BY-NC-ND 4.0))

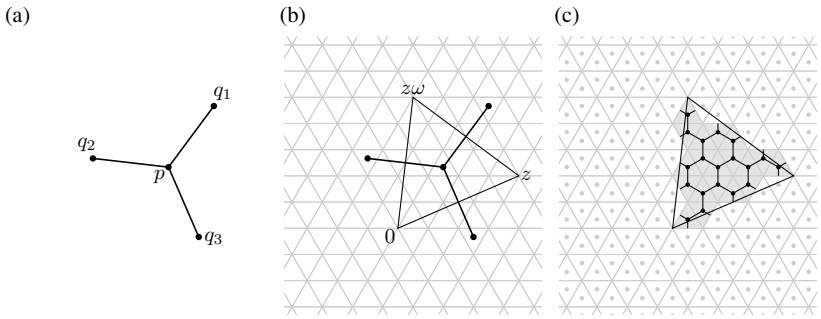

Fig. 6.4 The Goldberg–Coxeter construction around each vertex. In the case of a surface graph, we construct the "local subdivisions" as in **c**, and then patch them according to the local coordinates patch of the surface (Omori–Naito–Tate [41])

Remark 6.1 The original definition of the Goldberg–Coxeter construction is defined for plane graphs; however, the definition is given by procedures around each vertex of the graphs. Hence we can easily extend the definition for surface graphs (see Fig. 6.4). We note that a plane graph is also a surface graph by using the inverse of the stereographic projection $\mathbb{R}^2 \to S^2$.

Theorem 6.1 (Dutour–Deza [9, 10]) *The Goldberg–Coxeter subdivision satisfies*

$$\mathrm{GC}_{k,\ell}(X) = \mathrm{GC}_{k_1,\ell_1}\left(\mathrm{GC}_{k_2,\ell_2}(X)\right),$$

where $k + \ell\omega = (k_1 + \ell_1\omega)(k_2 + \ell_2\omega)$.

Remark 6.2 Goldberg–Coxeter construction for trivalent graph preserves the number of n-gons except for $n = 6$. Hence, it satisfies $\chi(X) = \chi(\mathrm{GC}_{k,\ell}(X))$.

In general, (k, ℓ)-subdivision for a trivalent graph is slightly complicated; however, $(2, 0)$-subdivision is easily described as follows (see also Fig. 6.5):

1. Draw an n-gon $(v_1, \ldots, v_n)$ in each n-gon $(u_1, \ldots, u_n)$ of the original graph X.
2. Connect u_i and v_i as an edge of $\mathrm{GC}_{2,0}(X)$.
3. Delete original edges in X.

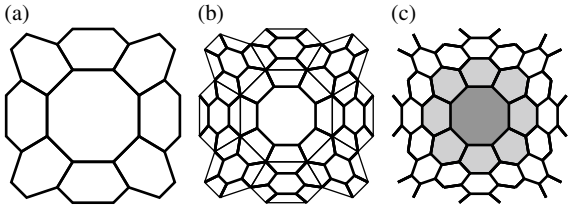

Fig. 6.5 (2, 0)-Goldberg–Coxeter subdivision near an octagon. **a** Original discrete surface (near an octagon), **b** take the (2, 0)-subdivision, **c** (2, 0)-subdivided discrete surface, the process generates eight new hexagons near the octagon (Kotani–Naito–Tao [25])

As a result,

$$\begin{aligned} V(\mathrm{GC}_{2,0}(X)) &= V(X) \cup \{\text{vertices } \{v_i\} \text{ of new } n\text{-gons for all } n\text{-gons in } X\}, \\ E(\mathrm{GC}_{2,0}(X)) &= \{(u_i, v_i), (v_i, v_{i+1}) \text{ for all } n\text{-gons in } X\}. \end{aligned} \tag{6.1}$$

6.2 Subdivisions of Trivalent Discrete Surfaces

Let $\{\boldsymbol{X}_j\}_{j=0}$ be a sequence of trivalent discrete surfaces. We need to consider: (1) Does the sequence converge to a smooth surface or not, and also can we detect underlying continuous objects of the trivalent discrete surface? (2) Do the curvatures converge to that of the smooth surface? If the above questions are true, it may be sufficient to compute a continuous model for study physical properties of materials with a huge number of atoms.

By using the Goldberg–Coxeter construction, we can construct a sequence $\{X_j\}_{j=0}$ of "topological subdivisions" with $X_0 = X$. However, to define a sequence of trivalent discrete surfaces, we should define realizations (embeddings) $\Phi_j : X_j \longrightarrow \mathbb{R}^3$.

Example 6.2 For a dodecahedron or a truncated icosahedron $\boldsymbol{X}$, define $X_k = \mathrm{GC}_{k,0}(X)$, then X_k can be realized as a polyhedron in $\mathbb{R}^3$. Such polyhedra are called *Goldberg polyhedra* (see Fig. 6.6). Note that, in the previous section, we only define the Goldberg–Coxeter construction for trivalent graphs, but it can be defined for tetravalent graphs. Fujita–Ueda–Sato–Mizuno–Kumasaka–Fujita [12] synthesized polyhedral molecule structures, whose forms are GC-constructions (for tetravalent graphs) of regular polyhedra, by using self-organization processes.

First, we consider subdivisions of an SWNT. Since cylinders are underlying continuous objects of SWNTs, the realization of a subdivided graph of an SWNT is a map from X into a cylinder.

Theorem 6.2 (Kotani–Naito–Omori [24]) *Let* $\{\mathrm{CNT}(\lambda_n, c_n)\}$ *be the sequence of subdivisions of* $\mathrm{CNT}(\lambda, c)$ *satisfying*

$$\mathrm{CNT}(\lambda_n, c_n) = \mathrm{GC}_{k_n,\ell_n}(\mathrm{CNT}(\lambda, c)), \quad k_n \geq 2, \ \ \ell_n \geq 0,$$

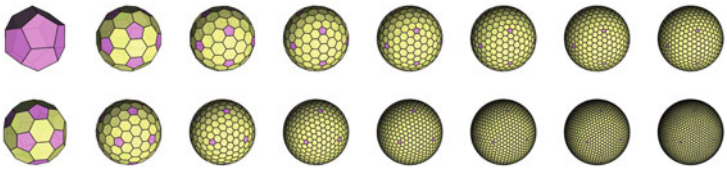

Fig. 6.6 Examples of Goldberg polyhedra. The upper row is $\mathrm{GC}_{k,0}(X)$ for a dodecahedron, and the lower row is $\mathrm{GC}_{k,0}(X)$ for a truncated icosahedron, $k = 1, \ldots, 8$

where $\lambda_n = \dfrac{\lambda}{|k_n + \overline{\omega}\ell_n|}$, $(c_n)_1\omega + (c_n)_2 = (\omega c_1 + c_2)(k_n + \overline{\omega}\ell_n)$, *then we obtain* $K_n \to 0$ *and* $H_n \to -1/2r(\lambda, c)$. *That is,* K_n *and* H_n *converge to the curvature of the underlying surface* (*a cylinder*).

In general, we may prove the following.

Theorem 6.3 (Kotani–Naito–Omori [24]) *Let* X *be a trivalent discrete surface, and* $\{X_k\}$ *a sequence of subdivisions of* X. *Moreover, we assume;*

1. *there exists a smooth surface* $M \subset \mathbb{R}^3$ *such that* $\boldsymbol{X}_k$ *converges to* M *in Hausdorff topology;*
2. *for any* $p \in M$, *there exists a sequence* $\{v_k\}$ ($v_k \in V(X_k)$) *with* $v_k \to p$ *such that the sequence of unit normal vectors* $\{\boldsymbol{n}_k(x_k)\}$ *converges to the unit normal vector* $\boldsymbol{n}(p)$ *at* $p \in M$;
3. *the Weingarten map* $S_k \colon T_{v_k} \to T_{v_k}$ *of embedding* $\boldsymbol{X}_k$ *converges to the Weingarten map* $S \colon T_pM \to T_pM$.

Then the Gauss curvatures and the mean curvatures of $\boldsymbol{X}_k$ *converge to those of* M. *That is to say,* $K(X_k)(v_k) \to K(M)(p)$ *and* $H(X_k)(v_k) \to H(M)(p)$ *hold.*

Theorem 6.3 assumes very strong properties. The first and the second assumptions may be natural to prove convergence; however, the last assumption is difficult to confirm for concrete examples.

To construct a sequence of subdivisions for a crystal structure, we may use a standard realization of the underlying graph structure. It is easy to show that symmetries of standard realizations are invariant with respect to the Goldberg–Coxeter constructions. Namely, we obtain the following.

Proposition 6.1 *Let* X *be a* d*-dimensional trivalent topological crystal and* $\{\boldsymbol{e}_i\}_{i=1}^d$ *be a basis of parallel transformations of a standard realization of* X. *Moreover, we assume that* X *is a surface graph. Then* $\mathrm{GC}_{k,\ell}(X)$ *is also a* d*-dimensional trivalent topological crystal and* $\{\boldsymbol{e}_i\}_{i=1}^d$ *is a basis of parallel transformations of a standard realization of* $\mathrm{GC}_{k,0}(X)$.

Proof First we have to show $\mathrm{Aut}(X) \subset \mathrm{Aut}(\mathrm{GC}_{k,\ell}(X))$. For any $x \in V(X)$, we define a cluster $\triangle(x) \subset \mathrm{GC}_{k,\ell}(X)$ to be Fig. 6.4c, and define $[x] \in V(\mathrm{GC}_{k,\ell}(X))$ to be a vertex in $\triangle(x)$. For any $\sigma \in \mathrm{Aut}(X)$, we define a $\tilde{\sigma} \in \mathrm{Aut}(\mathrm{GC}_{k,\ell}(X))$ by

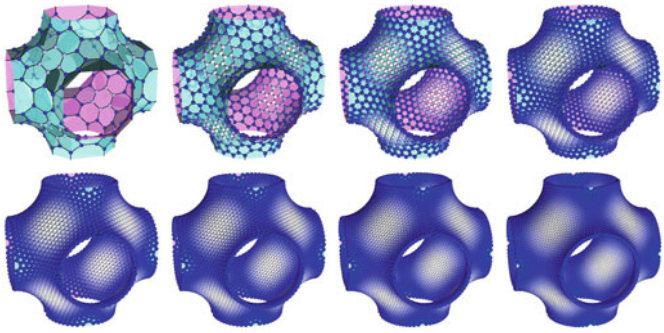

Fig. 6.7 Gauss curvatures of $\mathrm{GC}_{k,0}(X)$ $(k = 2, \ldots, 9)$ of the Mackay–Terrones structure (Kotani–Naito–Omori [24] (CC BY-NC-ND 4.0))

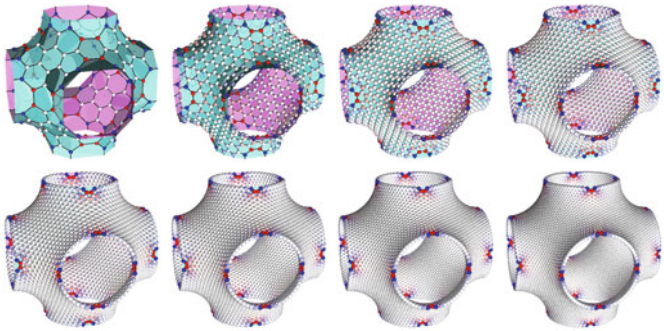

Fig. 6.8 Mean curvatures of $\mathrm{GC}_{k,0}(X)$ $(k = 2, \ldots, 9)$ of the Mackay–Terrones structure (Kotani–Naito–Omori [24] (CC BY-NC-ND 4.0))

$\tilde{\sigma}([x]) = [y]$, if $\sigma(x) = y \in V(X)$. By using this definition, we may extend $\tilde{\sigma}$ to the set of edges of $\mathrm{GC}_{k,\ell}(X)$, and we obtain $\tilde{\sigma} \in \mathrm{Aut}(\mathrm{GC}_{k,\ell}(X))$.

Since a standard realization satisfies Theorem 3.3, if $\{\boldsymbol{e}_i\}$ is a basis of parallel transformations of the standard realization of X, then it is also a basis of parallel transformations of the standard realization of $\mathrm{GC}_{k,\ell}(X)$ to preserve the symmetry. □

By using the above proposition, we may construct a sequence of subdivisions of a standard realized crystal by using the Goldberg–Coxeter construction and standard realizations. For the Mackay–Terrones structure we construct a standard realization for embedding into $\mathbb{R}^3$, and calculate subdivisions numerically. Figures 6.7 and 6.8 are results of numerical calculations. In the case of the Mackay–Terrones structure, curvatures of subdivided discrete surfaces are very similar to curvatures of their dual triangular surfaces (see Figs. 6.9 and 6.10). This fact supports that our definition of curvatures for trivalent discrete surfaces is reasonable.

By these numerical calculations, we may confirm the Hausdorff convergence of the sequence of subdivisions of the Mackay–Terrones structure, but we cannot check

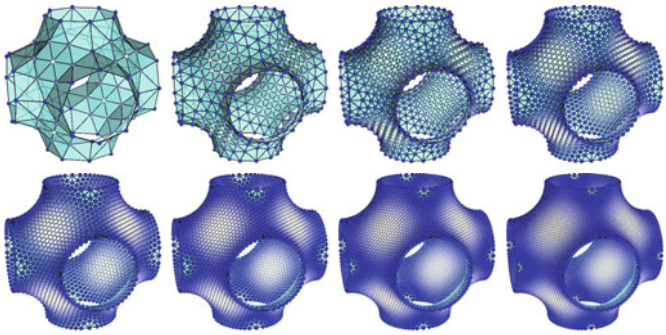

Fig. 6.9 Gauss curvatures of triangular duals of $\mathrm{GC}_{k,0}(X)$ of the Mackay–Terrones structure (Kotani–Naito–Omori [24] (CC BY-NC-ND 4.0))

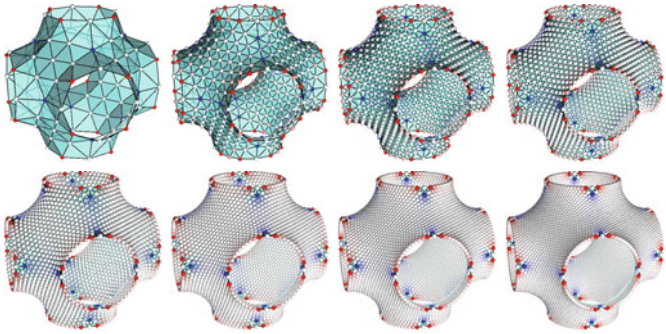

Fig. 6.10 Mean curvatures of triangular duals of $\mathrm{GC}_{k,0}(X)$ of the Mackay–Terrones structure (Kotani–Naito–Omori [24] (CC BY-NC-ND 4.0))

the convergence of normal vectors (see near octagons of Fig. 6.8), and the rate of Hausdorff convergence near octagons is slower than near hexagons.

6.3 Another Method of Subdivision of Trivalent Discrete Surfaces

In the previous section, we constructed two types of sequences of subdivisions for trivalent discrete surfaces. One is applicable for a trivalent discrete surface with an underlying smooth surface, which an SWNT satisfies. The other is for a standard realized trivalent discrete surface. But, these methods cannot be used to construct a subdivision of a truncated icosahedron (C_{60}). In this section, we use the other method to construct a subdivision of trivalent discrete surfaces; however, it can only construct the $(2, 0)$-Goldberg–Coxeter subdivision [25].

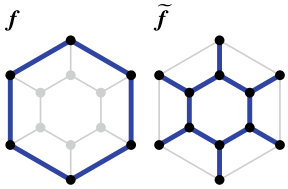

Fig. 6.11 An n-gonal face f and a graph $\widetilde{f}$ consist of the edges marked in blue, respectively

Let $\boldsymbol{X}$ be a trivalent discrete surface with an underlying graph X, namely, $\boldsymbol{X} = \Phi(X)$, $\Phi\colon X \longrightarrow \mathbb{R}^3$, and $X_1 = \mathrm{GC}_{2,0}(X)$ be the $(2,0)$-Goldberg–Coxeter subdivision of X. By using (6.1), for an n-gonal face $f = (u_1, \ldots, u_n)$ of X, there exists an n-gonal face $f' = (v_1, \ldots, v_n)$ of X_1 such that $(u_i, v_i) \in E(X_1)$.

Definition 6.3 (*Kotani–Naito–Tao* [25]) For an n-gonal face $f = (u_1, \ldots, u_n)$ of X, we define a subgraph $\widetilde{f}$ of X_1 by

$$V(\widetilde{f}) = \{u_i,\ v_i \mid i = 1, \ldots, n\},$$
$$E(\widetilde{f}) = \{(v_i, v_{i+1}),\ (u_i, v_i) \mid i = 1, \ldots, n,\ v_{n+1} = v_1\},$$

(see Fig. 6.11). Moreover, we define *local energy* $E_D(\boldsymbol{f})$ and $E_D(\widetilde{\boldsymbol{f}})$ by

$$E_D(\boldsymbol{f}) = \sum_{i=1}^{n} |\boldsymbol{u}_{i+1} - \boldsymbol{u}_i|^2,$$
$$E_D(\widetilde{\boldsymbol{f}}) = \sum_{i=1}^{n} |\boldsymbol{v}_{i+1} - \boldsymbol{v}_i|^2 + \sum_{i=1}^{n} |\boldsymbol{u}_i - \boldsymbol{v}_i|^2.$$

Definition 6.4 (*Kotani–Naito–Tao* [25]) Let $\boldsymbol{X}$ be a finite or periodic trivalent discrete surface with an underlying graph X, and $X_1 = \mathrm{GC}_{2,0}(X)$ be the $(2,0)$-Goldberg–Coxeter subdivision of X. The subdivision $\boldsymbol{X}_1$ of $\boldsymbol{X}$ is defined by the following steps (see Fig. 6.12):

1. For each n-gonal face $f = (u_1, \ldots, u_n)$ in X, define the position $\boldsymbol{v}_i$ of a vertex of f' by $\min E_D(\widetilde{\boldsymbol{f}})$ with respect to fixed vertices $\boldsymbol{u}_i$.
2. We change the position $\boldsymbol{u}_i$ to the barycenter of its three adjacent points, whose position is defined by step 1.

Note that this procedure applies to any trivalent discrete surfaces, even C_{60} and the K_4 lattice.

Theorem 6.4 (Kotani–Naito–Tao [25]) *Let $\boldsymbol{X}$ be a trivalent discrete surface and $\{\boldsymbol{X}_i\}_{i=1}$ be the sequence of iteratively subdivisions of $\boldsymbol{X}$. Namely, $\boldsymbol{X}_{i+1}$ is the subdivision of $\boldsymbol{V}_i$ defined by the process in Definition 6.4. Then,*

1. *The sequence $\{\boldsymbol{X}_i\}$ consists of a Cauchy sequence with respect to the Hausdorff topology.*

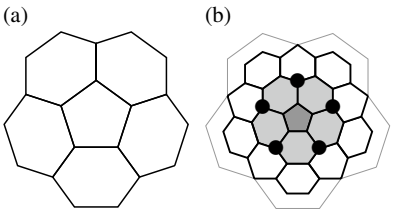

Fig. 6.12 **a** an example of a face in $\boldsymbol{X}$, **b** vertices of the inner (dark gray) face are defined by minimization of the local energy, black vertices, which are also vertices of X defined by the balancing condition

2. *The limit set* $\boldsymbol{X}_\infty = \overline{\bigcup \boldsymbol{X}_i}$ *satisfies*

$$\begin{aligned}
\boldsymbol{X}_\infty &= \boldsymbol{X}_F \cup \boldsymbol{X}_V \cup \boldsymbol{X}_S, \\
\boldsymbol{X}_F &= \bigcup \{b(\boldsymbol{f}^{(i)});\ \textit{the barycenter of a face } f^{(i)} \textit{ of } X_i\}, \\
\boldsymbol{X}_V &= \cup \boldsymbol{X}_i, \\
\boldsymbol{X}_S &= \ \textit{otherwise},
\end{aligned}$$

   where if $\boldsymbol{X}$ *is "unbranched", then* $\boldsymbol{X}_S = \emptyset$.
3. *The total energy* $E(\boldsymbol{X}_i)$ *is bounded.*
4. *If* X *contains no* $n(>6)$*-gonal faces, and contains at least one* $n(<6)$*-gonal face, then* $\{E(\boldsymbol{X}_i)\}$ *is monotone decreasing.*

The key lemma to prove Theorem 6.4 is an eigenvalue problem of a linear equation:

Lemma 6.1 (Kotani–Naito–Tao [25]) *Let* f *be an* n*-gonal face of* $\boldsymbol{X}$*, then the inequality*

$$E_D(\widetilde{\boldsymbol{f}}) \le \lambda(n) E_D(\boldsymbol{f}), \quad \lambda(n) = (1 + 4\sin^2(\pi/n))^{-1} \tag{6.2}$$

holds.

Proof *(Outline of Proof)* Let $\boldsymbol{x} = \left[\boldsymbol{x}_i\right]$ and $\boldsymbol{x}' = \left[\boldsymbol{x}'_i\right]$ be coordinates of vertices of $\boldsymbol{f}$ and $\boldsymbol{f}'$, then $\boldsymbol{x}$ and $\boldsymbol{x}'$ satisfy

$$A_n \boldsymbol{x}' = \boldsymbol{x}, \quad A_n = \begin{bmatrix} 3 & -1 & & & -1 \\ -1 & 3 & -1 & & \\ & \ddots & \ddots & \ddots & \\ & & -1 & 3 & -1 \\ -1 & & & -1 & 3 \end{bmatrix}, \tag{6.3}$$

since $\boldsymbol{x}'$ is determined as a minimizer of $E_D(\widetilde{\boldsymbol{f}})$. The first eigenvalue of A_n is $\lambda(n) = \lambda_1(n) = 1 + 4\sin^2(\pi/n)$, and $\lambda(n)$ satisfies $\lambda(n) < \lambda(6) = 1/2 < \lambda(m) < 1$, for $n < 6 < m$. □

For a proof of the Hausdorff convergence of $\{\boldsymbol{X}_i\}$, we may show that

$$\begin{aligned} d_H(\boldsymbol{X}_i, \widetilde{\boldsymbol{X}}_{i+1}) &\le E\sqrt{\lambda^{i+1}}, \\ d_H(\boldsymbol{x}, \pi(\boldsymbol{x})) &\le E\sqrt{\lambda^{i+1}}, \quad \boldsymbol{x} \in V(\widetilde{\boldsymbol{X}_{i+1}}), \\ d_H(\boldsymbol{X}_i, \boldsymbol{X}_{i+1}) &\le E\sqrt{\lambda^{i+1}}, \end{aligned} \tag{6.4}$$

where d_H is the Hausdorff distance, $E = E(\boldsymbol{X}_0)$, $\lambda = \lambda(N) < 1$, and $\widetilde{\boldsymbol{X}_{i+1}}$ is the discrete surface constructed by only step 1 in Definition 6.4:

$$\boldsymbol{X}_i \xrightarrow{\text{solve minimizing problem}} \widetilde{\boldsymbol{X}}_{i+1} \xrightarrow{\pi\text{: projection to barycenter}} \boldsymbol{X}_{i+1}.$$

Since we assume $\boldsymbol{X}$ is periodic or finite, $N = \max\{n \mid n\text{-gonal face in } \boldsymbol{X}\}$ is finite, there exists a finite $\lambda = \lambda(N) < 1$. The last inequality of (6.4) implies the Hausdorff convergence of $\{\boldsymbol{X}_i\}$.

For a proof of the boundedness and the monotonicity of energies, we may show that

$$E_D(\boldsymbol{X}_{i+1}) \le E_D(\tilde{\boldsymbol{X}}_{i+1}) = \sum_{\text{all faces}} E_D(\widetilde{\boldsymbol{f}}) \le \sum_{\text{all faces}} \lambda(n) E_D(\boldsymbol{f}). \tag{6.5}$$

Therefore by (6.5), we obtain

$$\begin{aligned} E(\boldsymbol{X}_{i+1}) &\le \sum_{\text{all}} \lambda(n) E_D(\boldsymbol{f}) = \frac{1}{2} \sum_{n=6} E_D(\boldsymbol{f}) + \sum_{n\neq 6} \lambda(n) E_D(\boldsymbol{f}) \\ &= \frac{1}{2} \sum_{\text{all}} E_D(\boldsymbol{f}) + \sum_{n\neq 6} \left(\lambda(n) - \frac{1}{2}\right) E_D(\boldsymbol{f}) \\ &= E(\boldsymbol{X}_i) + \sum_{n\le 5} \left(\lambda(n) - \frac{1}{2}\right) E_D(\boldsymbol{f}) + \sum_{n\ge 7} \left(\lambda(n) - \frac{1}{2}\right) E_D(\boldsymbol{f}). \end{aligned} \tag{6.6}$$

Since the number of $n(\neq 6)$-gonal faces is finite $\lambda(n) - 1/2 < 0$ for $n < 6$, $0 < \lambda(n) - 1/2 < 1/2$ for $n > 6$, by (6.6), we obtain

$$E(\boldsymbol{X}_{i+1}) \le E(\boldsymbol{X}_i) + \frac{1}{2} \sum_{n>6} E_D(\boldsymbol{f}) \le E(\boldsymbol{X}) + M E_D(\boldsymbol{f}^0), \tag{6.7}$$

where M is the number of $n(> 6)$-gonal faces in $\boldsymbol{X}$. Therefore, the energy $\{E(\boldsymbol{X}_i)\}$ is bounded. If $\boldsymbol{X}$ contains no $n(> 6)$-gonal faces and contains at least $n(< 6)$-gonal face, then we also obtain the monotone decreasing of $\{\boldsymbol{X}_i\}$ as

$$E(\boldsymbol{X}_{i+1}) \le E(\boldsymbol{X}_i) + \sum_{n\le 5} \left(\lambda(n) - \frac{1}{2}\right) E_D(\boldsymbol{f}) < E(\boldsymbol{X}_i). \tag{6.8}$$

Example 6.3 We show numerical results of subdivisions of the Mackay–Terrones structure and a truncated icosahedron (C_{60}) in Figs. 6.13 and 6.14. Both sequences

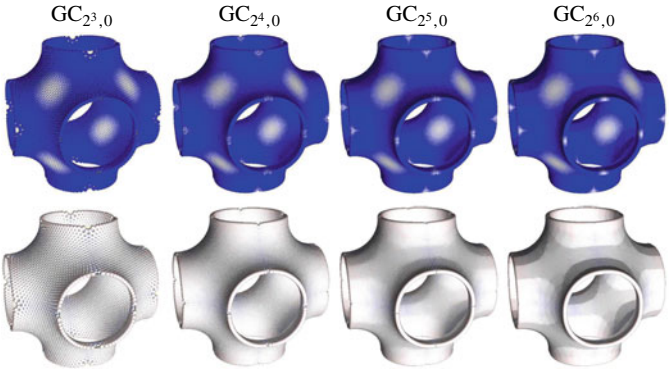

Fig. 6.13 Numerical results of subdivisions of the Mackay–Terrones structure by the method of Definition 6.4 (compare with Figs. 6.7 and 6.8). Upper row: the Gauss curvature, lower row: the mean curvature (Kotani–Naito–Tao [25])

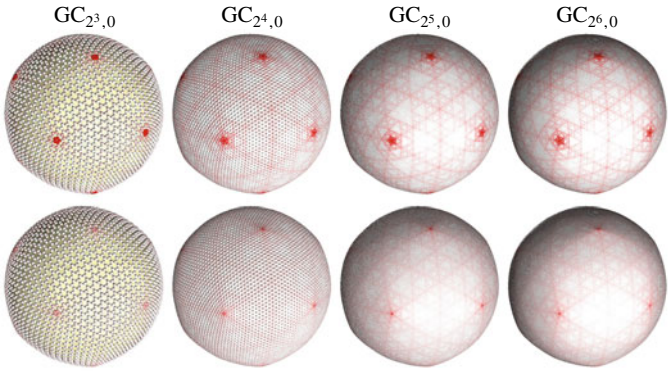

Fig. 6.14 Numerical results of subdivisions of a truncated icosahedron (C_{60}) by the method of Definition 6.4. Upper row: the Gauss curvature, lower row: the mean curvature (Kotani–Naito–Tao [25])

converge in the Hausdorff topology; however, at least the limit set of the sequence of C_{60} is not smooth.

Remark 6.3 A trivalent discrete surface $\boldsymbol{X}$ is called *unbranched* if and only if $\boldsymbol{X}$ satisfies that each edge shares at most two faces. If $\boldsymbol{X}$ is not unbranched, it is called *branched*. For example, the K_4 lattice is a trivalent discrete surface by the definition and is branched (see Fig. 3.9). Even if $\boldsymbol{X}$ is branched, we may construct subdivisions of it, and Theorem 6.4 also holds.

Chapter 7
Miscellaneous Topics

7.1 Carbon Nanotubes from Geometric Viewpoints

Carbon nanotubes are carbon allotropes, whose carbon atoms chemically bind with three other atoms with sp^2-orbitals, and they are graphenes rolled up in cylinders. There are many types of carbon nanotubes. However, in this section, we only consider *single wall nanotubes* (*SWNT*). SWNTs have a parameter (chiral index) $\boldsymbol{c} = (c_1, c_2)$, which is defined as follows.

Choose a vertex of a regular hexagonal lattice (a graphene) as an origin $(0, 0)$, then select the fundamental piece, whose vertices are $\{\boldsymbol{v}_i\}_{i=0}^3$ of a regular hexagonal lattice (7.1), and translation vectors as in (7.2):

$$\boldsymbol{v}_0 = [0, 0]\,, \quad \boldsymbol{v}_1 = [0, -1]\,, \quad \boldsymbol{v}_2 = \left[1/2, \sqrt{3}/2\right], \quad \boldsymbol{v}_3 = \left[-1/2, \sqrt{3}/2\right], \tag{7.1}$$

$$\boldsymbol{a}_1 = \left[\sqrt{3}, 0\right], \quad \boldsymbol{a}_2 = \left[1/2, -\sqrt{3}/2\right]. \tag{7.2}$$

Select (c_1, c_2) with $c_1 \in \mathbb{N}_{>0}$ and $c_2 \in \mathbb{N}_{\geq 0}$, and set $\boldsymbol{c} = c_1\boldsymbol{a}_1 + c_2\boldsymbol{a}_2$, we call $\boldsymbol{c}$ a *chiral vector* (or a *chiral index*) of an SWNT. On the other hand,

$$\boldsymbol{t} = (1/\gcd(c_1, c_2))((c_1 + 2c_2)\boldsymbol{a}_1 - (2c_1 + c_2)\boldsymbol{a}_2),$$

which is called a lattice vector, satisfies $\langle \boldsymbol{c}, \boldsymbol{t} \rangle = 0$ (see Fig. 7.1).

An SWNT with the chiral index $\boldsymbol{c}$ is the structure identifying $\boldsymbol{0}$ and $\boldsymbol{c}$, i.e., identifing the line between from $\boldsymbol{0}$ to $\boldsymbol{t}$ and from $\boldsymbol{c}$ to $\boldsymbol{c} + \boldsymbol{t}$. Note that the fundamental region of the SWNT with the chiral index $\boldsymbol{c}$ is the rectangle with vertices $\boldsymbol{0}, \boldsymbol{t}, \boldsymbol{t} + \boldsymbol{c}$, and $\boldsymbol{c}$. The diameter of an SWNT with chiral index $\boldsymbol{c} = (c_1, c_2)$ is $L = \sqrt{c_1^2 + c_1c_2 + c_2^2}$.

SWNTs with $c_1 = c_2$ are called *zigzag type*, $c_2 = 0$ are called the *armchair type*, and otherwise are called *chiral type*. These names come from the shape of the edges of SWNTs (see Fig. 7.2).

H. Naito, *Trivalent Discrete Surfaces and Carbon Structures*,
SpringerBriefs in the Mathematics of Materials 5,
https://doi.org/10.1007/978-981-99-5769-9_7

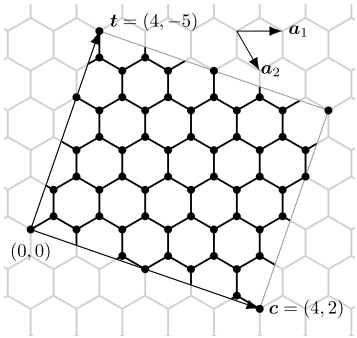

Fig. 7.1 Construction of an SWNT from a regular hexagonal lattice. The chiral index of this example is $\boldsymbol{c} = (4, 2)$

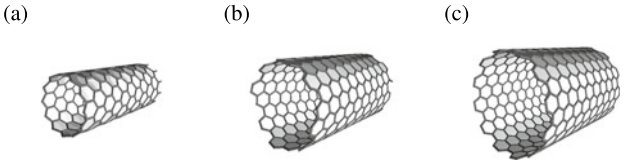

Fig. 7.2 **a** A zigzag type ($\boldsymbol{c} = (12, 0)$), **b** a chiral type ($\boldsymbol{c} = (12, 8)$), **c** an armchair type ($\boldsymbol{c} = (12, 12)$)

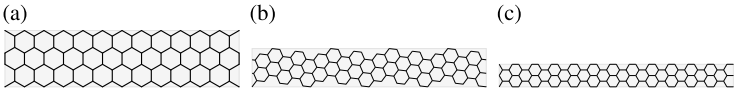

Fig. 7.3 Examples of SWNTs with short length index. **a** $\boldsymbol{c} = (12.0)$, length index ~ 2.89, **b** $\boldsymbol{c} = (12.8)$, length index ~ 2.85, **c** $\boldsymbol{c} = (12.12)$, length index $= 2$

Electronic properties of SWNTs are also geometric. The following result is well-known, and is obtained by tight binding approximations. If $c_1 \equiv c_2 \pmod 3$, then SWNTs with $\boldsymbol{c} = (c_1, c_2)$ are metallic; if not, then such SWNTs are semiconductors.

Recently, several researchers have synthesized SWNTs of short length using organic chemistry (see [18, 34]), and hence an index measuring the length of SWNTs is needed. Matsuno–Naito–Hitosugi–Sato–Kotani–Isobe proposed such an index, which is called the *length index* of SWNTs [34]:

$$\frac{\sqrt{3}|c_1(a_1 - b_1) - c_2(a_2 - b_1)|}{2\sqrt{c_1^2 + c_1c_2 + c_2^2}}, \tag{7.3}$$

for edge atom coordinates (a_1, b_1) and (a_2, b_1).

The index (7.3) measures how many benzene rings (hexagons) are in the length direction (see Fig. 7.3).

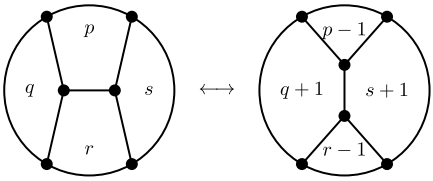

Fig. 7.4 The *Stone–Wales transformation*. In the case of graphenes, we flip an edge yielding two pentagons and two heptagons

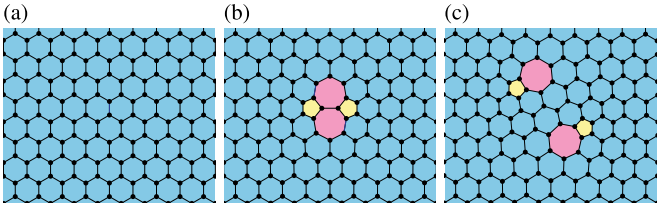

Fig. 7.5 Flipping an edge (colored in blue) in **a**, we obtain pentagon/heptagon pairs **b**. **c** By flipping two edges in **b**, pentagon/heptagon pairs separate

7.2 Material Properties and Discrete Geometry

In [7], we study the relationship between geometric properties (curvatures) of crystal/molecule and material properties for 5–7 graphenes.

In graphene structures, $n(\neq 6)$-member-rings are called *defects*; here, an $n(\neq 6)$-member-ring geometrically means a simple closed path with length $n \neq 6$. A typical defect is called a *Stone–Wales defect*, which is a pentagon/heptagon-pair (see Fig 7.4), and a graphene including this type of defect is called a *5–7 graphene* (see Fig 7.5).

The curved structure of it cannot be reproduced by computing a standard realization of 5–7 graphenes. Meanwhile, 5–7 graphenes are curved near defects by calculations using density functional theory (DFT). Introducing an additional term as in (7.4) for the energy (3.1), we may reproduce profiles of 5–7 graphenes:

$$E = \sum_{(i,j)\in \mathrm{NN}} |\boldsymbol{x}_i - \boldsymbol{x}_j|^2 + \frac{d^3\sqrt{3}}{2} \sum_{(k,\ell)\in \mathrm{NNN}} |\boldsymbol{x}_k - \boldsymbol{x}_\ell|^{-1}, \tag{7.4}$$

where d is a length scale, "NN" and "NNN" mean nearest neighbours and next-nearest neighbours. In other words, an edge $e = (i, j)$ in "NN" is equivalent to an edge e of the underlying graph of the structure, and $(k, \ell) \in$ NNN is equivalent to a the graph distance between x_k and x_ℓ of 2 (see Fig. 7.6). We call (7.4) the *energy with replusive interactions*, and critical points *SRRI* (*standard realizations with replusive interaction*). The first term of (7.4) expresses the attractive force of covalent bonds between adjacent atoms, and the second term expresses the Coulomb repulsive force. The structure which minimizes the energy with replusive interactions (7.4) for graph structures of a 5–7 graphene reproduces profiles of it (see Fig. 7.7), and

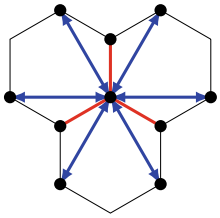

Fig. 7.6 Red lines: nearest neighbour (covalent bonds in graphenes), Blue lines: next-nearest neighbour

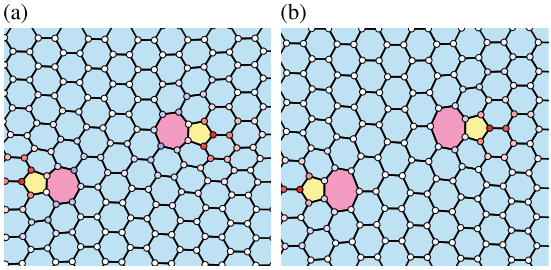

Fig. 7.7 Profiles of a 5–7 graphene computed by **a** SRRI and **b** DFT. Colors of vertices express the Gauss curvature (scaled by maximum as 1). Both profiles are not completely matched; however, profiles of the Gauss curvature are sufficiently matched to consider physical properties of 5–7 graphenes

the calculation speed to get an SRRI (minimizer of (7.4)) is several times faster than to get optimized structure by DFT and/or MD (molecular dynamics). We note that mathematical properties of the functional (7.4) have not been studied yet, however, numerical calculations for it are work well.

On the other hand, in classical surface theory, for surfaces completely determined by the Gauss and the mean curvatures (the fundamental theorem of surface theory), the Gauss curvature is intrinsic but the mean curvature is not [58]. For trivalent discrete surfaces, the same property is also expected. Hence, we consider the relationship between the Gauss curvature and physical properties. In fact, doping energies for replacing a carbon atom in 5–7 graphene by a nitrogen atom relate to the Gauss curvature, but there is no significant relationship to the mean curvature (see Figs. 7.8 and 7.9).

In the case of these problem sizes (number of atoms), DFT/MD calculations work; however, in the case of very large number of systems, such calculations cannot be done in realistic time. As discussed in Chap. 6, if we find the underlying surface of such a system, we may predict some physical properties by using geometric properties of the underlying surface.

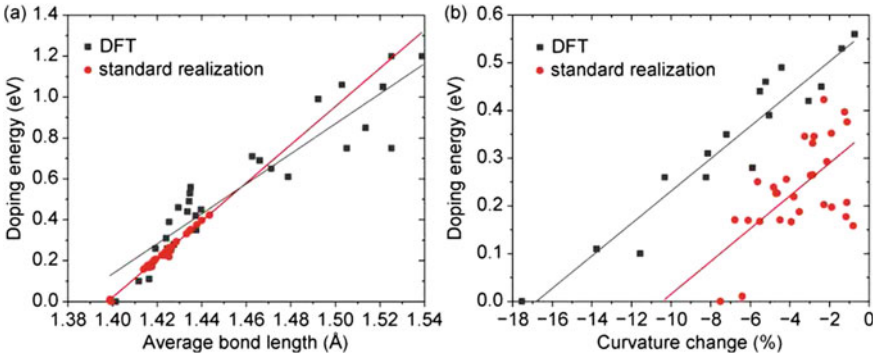

Fig. 7.8 Relationship between doping energy and changing total Gauss curvature before and after doping (Dechant–Ohto–Ito–Makarova–Kawabe–Agari–Kumai–Takahashi–Naito– Kotani [7], (CC BY-NC-ND 4.0))

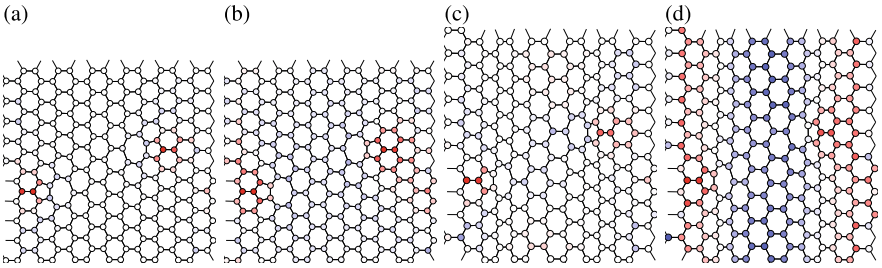

Fig. 7.9 Curvature distributions of a 5–7 graphene and a 30-degree bending 5–7 graphene. **a** The Gauss curvature, **b** the mean curvature of a 5–7 graphene, **c** the Gauss curvature, **d** the mean curvature of a 30-degree bending 5–7 graphene (Dechant–Ohto–Ito–Makarova–Kawabe–Agari–Kumai–Takahashi–Naito– Kotani [7], (CC BY-NC-ND 4.0))

7.3 Graph Spectra and Electronic Properties of Carbon Structures

States of electrons of atoms, molecules, and solids follow the Schrödinger equation

$$-\Delta\psi + V\psi = E\psi, \quad \text{in } \mathbb{R}^3, \tag{7.5}$$

where V is a potential, E is the energy of an electron and $\psi : \mathbb{R}^3 \longrightarrow \mathbb{C}$ is called a *wave function*.

7.3.1 The Hückel Method

In the case of molecular structures, wave functions are also called *molecular orbitals*. It is very difficult (or impossible) to rigorously calculate molecular orbitals in general

cases. The *Hückel method* provides an approximate method to calculate molecular orbitals of conjugated hydrocarbons. Hydrocarbons consisted only of hydrogen (H) and carbon (C). We assume that each carbon atom has three σ-electrons and binds with other carbons or hydrogens covalently bonds using σ-electrons. Since a carbon atom has four outermost electrons, each carbon atom has one π-electron. We call such molecules conjugated hydrocarbons. A molecular orbital ψ, which is normalized as $\|\psi\|_{L^2(\mathbb{R}^3)} = 1$, satisfies (7.5); then ψ expresses the probability distributions in the hydrocarbon. The Hückel method assumes that molecular orbitals for hydrocarbons are determined only by the carbon skeleton of the molecule.

Definition 7.1 For a conjugated hydrocarbon molecule, the graph $X = (V, E)$ defined as follows is called the *carbon skeleton* or the *Hückel graph* of the molecule: n be the number of carbon atoms in the molecule, and $V = \{v_1, \ldots, v_n\}$, and $(v_i, v_j) \in E$ if and only if the i-th and j-th carbon atoms bind with each other covalently.

In the Hückel method, we assume that molecular orbitals (wave functions) ψ consist of superpositions

$$\psi = \sum_{i=1}^{n} \alpha_i \phi_i, \quad \alpha_i \in \mathbb{C} \tag{7.6}$$

of wave functions ϕ_i (distribution probability of a π-electron belonging in the i-th carbon atom), and assume that

$$\int_{\mathbb{R}^3} \langle \phi_i, \phi_j \rangle \, dV = \delta_{ij}, \quad \int_{\mathbb{R}^3} \langle \widehat{H}\phi_i, \phi_j \rangle \, dV = H_{ij} = \begin{cases} \alpha & i = j, \\ -\beta & (v_i, v_j) \in E, \\ 0 & (v_i, v_j) \notin E, \end{cases} \tag{7.7}$$

where α, $\beta > 0$, $\langle \bullet, \bullet \rangle$ is the Hermitian inner product on $\mathbb{C}$ and $\widehat{H} = -\Delta_{\mathbb{R}^3}$ (i.e., $V = 0$). To find a molecular orbital (steady state of (7.5)), we should calculate critical points of the functional

$$\mathcal{H}[\psi] = \int_{\mathbb{R}^3} \langle \widehat{H}\psi, \psi \rangle \, dv - E \int_{\mathbb{R}^3} \langle \psi, \psi \rangle \, dV, \tag{7.8}$$

where E is a Lagrange multiplier in mathematics, an energy of the orbital in physics/chemistry. By using (7.6) and (7.7), ψ is a critical point of the functional (7.8) if and only if $\boldsymbol{c} = [c_i] \in \mathbb{C}^n$ is a non-zero solution of

$$\mathcal{H}[\boldsymbol{c}] = \boldsymbol{c}^\dagger H \boldsymbol{c} - E|\boldsymbol{c}|^2. \tag{7.9}$$

Namely, $\boldsymbol{c}$ is an eigenvector of H with the eigenvalue E. On the other hand, by (7.7),

$$H = \alpha I - \beta A, \tag{7.10}$$

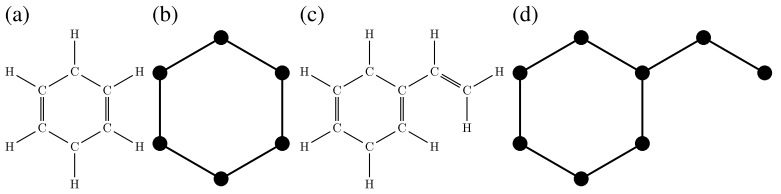

Fig. 7.10 Conjugated hydrocarbons and their carbon skeleton graphs. **a** Benzene, **b** its carbon skeleton, **c** styrene, **d** its carbon skeleton

where A is the adjacency matrix of the graph of the carbon skeleton, and I is the identity matrix. Therefore, we may consider the Hückel method as an eigenvalue problem in graph theory.

Example 7.1 Let X be the graph of benzene skeleton (see Fig. 7.10a, b). Then,

$$H = \alpha \begin{bmatrix} 1&0&0&0&0&0\\ 0&1&0&0&0&0\\ 0&0&1&0&0&0\\ 0&0&0&1&0&0\\ 0&0&0&0&1&0\\ 0&0&0&0&0&1 \end{bmatrix} - \beta \begin{bmatrix} 0&1&0&0&0&1\\ 1&0&1&0&0&0\\ 0&1&0&1&0&0\\ 0&0&1&0&1&0\\ 0&0&0&1&0&1\\ 1&0&0&0&1&0 \end{bmatrix},$$

and its eigenvalues and eigenvectors are

$$\begin{aligned} \lambda_1 = \alpha - 2\beta,\ \ \phi_1 &= \frac{1}{6}\left[+1\ +1\ +1\ +1\ +1\ +1\right]^T,\\ \lambda_2,\ \lambda_3 = \alpha - \beta,\ \ \phi_2 &= \frac{1}{\sqrt{12}}\left[+1\ +2\ +1\ -1\ -2\ -1\right]^T,\\ \phi_3 &= \frac{1}{2}\left[+1\ 0\ -1\ -1\ 0\ +1\right]^T,\\ \lambda_4,\ \lambda_5 = \alpha + \beta,\ \ \phi_5 &= \frac{1}{\sqrt{12}}\left[+1\ -2\ +1\ +1\ -2\ +1\right]^T,\\ \phi_4 &= \frac{1}{2}\left[+1\ 0\ -1\ -1\ 0\ +1\right]^T,\\ \lambda_6 = \alpha + 2\beta,\ \ \phi_6 &= \frac{1}{\sqrt{6}}\left[-1\ +1\ -1\ +1\ -1\ +1\right]^T, \end{aligned}$$

and we have $\lambda_1 < \lambda_2 = \lambda_3 < \lambda_4 = \lambda_5 < \lambda_6$. A benzene molecule has six π-electrons. On the other hand, each molecular orbital contains at most two electrons by the Pauli exclusion principle, hence orbitals in the ground state are expressed by superposition of ϕ_1, ϕ_2 and ϕ_3. Molecular orbitals with highest energy in the ground state are called *highest occupied molecular orbitals* (*HOMO*), and the next large energy orbitals are called *lowest unoccupied molecular orbitals* (*LUMO*). In this case, HOMO are ϕ_2 and ϕ_3, and LUMO are ϕ_4 and ϕ_5.

As is explained in Example 7.1, a conjugated hydrocarbon contains an even number of carbon atoms, molecular orbitals in the ground state are superpositions of $\phi_1, \ldots, \phi_{n/2}$.

Proposition 7.1 *For a conjugated hydrocarbon with n carbon atoms, we assume that the graph X of its carbon skeleton is bipartite and n is even, so that the density of states of π-electrons in the ground state is equally distributed in each carbon atom.*

Proof Let $\{\mu_j\}_{j=1}^n$ be eigenvalues of the adjacency matrix A_X of X in descending order, and $\phi_j = \left[x_{jk}\right]^T$ $(j = 1, \ldots, n)$ be orthonormal eigenvectors of A_X. Then,

$$c_q = \sum_{j=1}^{n} g_j x_{jq}^2, \quad q = 1, \ldots, n \tag{7.11}$$

expresses the π-electron charge of the q-th carbon, where g_j is the number of π-electrons ascribed in the j-th orbital.

Now we assume that X is bipartite and n is even, $\mu_j = \mu_i$ and $x_{jq}^2 = x_{iq}^2$ if $i + j = n + 1$ by Theorem 2.5. Since the number of π-elections of the molecule is n, by Pauli's law, π-electrons occupy the lower $n/2$ orbitals in the ground state. Therefore we have $g_j = 2$ $(j \leq n/2)$ and $g_j = 0$ $(j > n/2)$. Hence, by (7.11) and $\left[\phi_1 \ \ldots \ \phi_n\right] \in O(n)$, we obtain

$$c_q = \sum_{j=1}^{n} g_j x_{jq}^2 = 2 \sum_{j=1}^{n/2} x_{jq}^2 = \sum_{j=1}^{n} x_{jq}^2 = 1. \tag{7.12}$$

Example 7.2 Benzene molecules (C_6H_6, Fig. 7.10a, b) satisfy Proposition 7.1. Hence the chemical structure formula of benzenes is often draw as Fig. 7.11b.

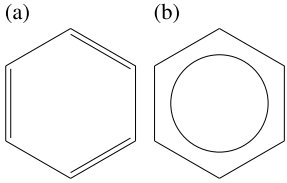

Fig. 7.11 Chemical structure formulas of benzenes. **a** The carbon atom of benzene is bound to other carbon atoms by three covalent bonds, so that double bonds and single bonds appear alternately. **b** However, there is no distinction between a double bond and a single bond in the bond between carbons

7.3.2 Tight-Binding Approximations

In the case of a d-dimensional crystal structure, wave functions ψ should be $\psi \in L^2(\mathbb{R}^d)$; however, the potential V is a periodic function on $\mathbb{R}^d$. For the sake of simplicity, we only consider wave functions satisfying (7.5) for 1-dimensional crystals and $V = 0$.

The 1-dimensional Euclidean space $\mathbb{R}$ is the universal covering group of S^1, and its covering transformation group is $\mathbb{Z}$, i.e., $S^1 = \mathbb{R}/(2\pi\mathbb{Z})$. Here, for each $k \in \mathbb{R}/(2\pi\mathbb{Z})$, we define Hilbert spaces L^2_k as follows: First we set

$$C_k = \{\phi \in C(\mathbb{R}, \mathbb{C}) \mid \phi(x + 2\pi) = e^{ik}\phi(x)\},$$

where $C(\mathbb{R}, \mathbb{C})$ is the space of complex-valued continuous functions on $\mathbb{R}$. The Hilbert space L^2_k is the completion by the norm

$$\|\phi\|^2 = \int_0^{2\pi} |\phi(x)|^2 \, dx.$$

Then, L^2_k is isomorphic to $L^2(S^1)$ by $L^2_k \ni \psi(x) \mapsto e^{-ikx/2\pi}\psi(x) \in L^2(S^1)$. The Laplacian Δ_k is densely defined on L^2_k and satisfies $\Delta_k : L^2_k \to L^2_k$, which is called a *twisted Laplacian* (see for example [51]). Since for $k \in \mathbb{R}/(2\pi\mathbb{Z})$ and $n \in \mathbb{Z}$, $\phi_{k,n}(x) = e^{(n+k)ix/2\pi} \in L^2_k$ satisfies $-\Delta_k\phi_{k,n} = (4\pi^2)^{-1}(2\pi n + k)^2\phi_{k,n}$, eigenvalues of Δ_k are $(4\pi^2)^{-1}(2\pi n + k)^2$. The function $E_n(k) = (4\pi^2)^{-1}(2\pi n + k)^2$ is called the *band structure* of the 1-dimensional crystal with $V = 0$, which is well-known as a result according to Bloch's theorem (Fig. 7.12).

A method approximating wave functions here only binding between atoms in a crystal is considered is called a *tight-binding approximation*, which is a discretization of the above arguments. First we consider a 1-dimensional crystal, whose discretization is a 1-dimensional lattice $X = (V, E)$. The maximal abelian covering of a cycle graph $C_N = (V_0, E_0)$ is X, therefore, we may consider C_N instead of a periodic structure of X.

Let $\phi : \mathbb{Z} \longrightarrow \mathbb{C}$ be a wave function on $\mathbb{Z}$ that satisfies

$$-\Delta_{\mathbb{Z}}\phi = E\phi, \quad \text{i.e., } 2\phi(n) - \phi(n+1) - \phi(n-1) = E\phi(n), \quad n \in \mathbb{Z}, \tag{7.13}$$

which is a discretization of (7.5). Instead of (7.13), the equation

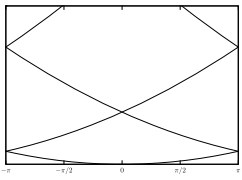

Fig. 7.12 The band structure of $\mathbb{R}$ with $V = 0$

$$t(\phi(n+1)+\phi(n-1))-\varepsilon\phi(n)=E\phi(n),\quad t,\ \varepsilon\in\mathbb{R}$$

is usually considered in physics books, similarly to α and β in the Hückel method; however, we consider (7.13) in this monograph.

For an integer $N>0$ and $k\in\mathbb{R}$, we set

$$\ell^2_k=\{\phi\in C(\mathbb{Z},\mathbb{C})\mid \phi(n+N)=e^{2\pi ik}\phi(n),\ \text{for any } n\in\mathbb{Z}\},$$

and define a function $\widetilde{\phi}$ on a cycle graph C_N by $\widetilde{\phi}(n)=e^{-2\pi ikn/N}\phi(n)$. Then we obtain

$$\begin{aligned}-\Delta_{\mathbb{Z}}\phi(n)&=\phi(n+1)+\phi(n-1)-2\phi(n)\\&=e^{2\pi ik(n+1)/N}\widetilde{\phi}(n+1)+e^{2\pi ik(n-1)/N}\widetilde{\phi}(n-1)-2e^{2\pi ikn/N}\widetilde{\phi}(n)\\&=e^{2\pi ikn/N}\left(e^{2\pi ik/N}\widetilde{\phi}(n+1)+e^{-2\pi ik/N}\widetilde{\phi}(n-1)-2\widetilde{\phi}(n)\right).\end{aligned}\tag{7.14}$$

Namely, we define

$$-\Delta_{k,N}=\begin{bmatrix}-2 & e^{2\pi ik/N} & & & e^{-2\pi ik/N}\\ e^{-2\pi ik/N} & -2 & e^{2\pi ik/N} & & \\ & \ddots & \ddots & \ddots & \\ & & e^{-2\pi ik/N} & -2 & e^{2\pi ik/N}\\ e^{2\pi ik/N} & & & e^{-2\pi ik/N} & -2\end{bmatrix},$$

and if ϕ satisfies (7.13), then $\widetilde{\phi}$ satisfies

$$-\Delta_{k,N}\widetilde{\phi}=E\widetilde{\phi}.\tag{7.15}$$

Define a function $\widetilde{\phi}$ on C_N by $\widetilde{\phi}=\left[(e^{2\pi ia/N})^{j\ell}\right]_j=\left[e^{2\pi iaj\ell/N}\right]_j$ for $\ell=0,\dots,N-1$, then we obtain

$$\begin{aligned}-\Delta_{k,N}\widetilde{\phi}&=\left[e^{2\pi ik/N}e^{2\pi ia(j+1)\ell/N}+e^{-2\pi ik/N}e^{2\pi ia(j-1)\ell/N}-2e^{2\pi iaj\ell/N}\right]\\&=\left[e^{2\pi i(a(j+1)\ell+k)/N}+e^{2\pi i(a(j-1)\ell-k)/N}-2e^{2\pi iaj\ell/N}\right]\\&=\left[e^{2\pi iaj\ell/N}(e^{2\pi i(a\ell+k)/N}+e^{-2\pi i(a\ell+k)/N}-2)\right]\\&=(e^{2\pi i(a\ell+k)/N)}+e^{-2\pi i(a\ell+k)/N)}-2)\left[e^{2\pi iaj\ell/N}\right]\\&=(e^{2\pi i(a\ell+k)/N}+e^{-2\pi i(a\ell+k)/N}-2)\widetilde{\phi}.\end{aligned}$$

Therefore, $2\cos(2\pi((a\ell+k)/N))-2=-4\sin^2(\pi(a\ell+k)/N)$ $(\ell=0,\dots,N-1)$ are eigenvalues of $-\Delta_{k,N}$. Hence $E(k)=\sin^2(\pi(a+k)/N)$ for $a\in\mathbb{R}$. Since $N^2\sin^2(\pi(a+k)/N)\to(\pi(a+k))^2$ $(N\to\infty)$, the $E(k)$ of C_N approximates the $E(k)$ of $\mathbb{R}$.

Next we consider electronic states of graphenes by a tight-binding approximation. Let $X=(V,E)$ be a graph structure of a graphene (a hexagonal graph, see Fig. 7.13), and let ϕ be a wave function on the graph. Instead of the Laplacian, we consider the adjacency matrix A_X, then we obtain

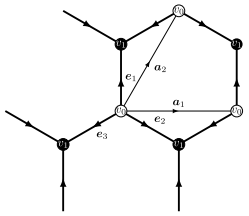

Fig. 7.13 Vertices and edges of a graphene; $\{\boldsymbol{a}_j\}_{j=1}^2$ is a basis of parallel transformations

$$
\begin{aligned}
A_X\phi(v_0) &= \phi(v_0+e_1)+\phi(v_0+e_2)+\phi(v_0+e_3)\\
A_X^2\phi(v_0) &= \phi(v_0+e_1-e_1)+\phi(v_0+e_1-e_2)+\phi(v_0+e_1-e_3)\\
&\quad+\phi(v_0+e_2-e_1)+\phi(v_0+e_2-e_2)+\phi(v_0+e_2-e_3)\\
&\quad+\phi(v_0+e_3-e_1)+\phi(v_0+e_3-e_2)+\phi(v_0+e_3-e_3)\\
&= 3\phi(v_0)+\phi(v_0+a_1)+\phi(v_0-a_1)+\phi(v_0+a_2)+\phi(v_0-a_2)\\
&\quad+\phi(v_0+a_1-a_2)+\phi(v_0-a_1+a_2).
\end{aligned}
\tag{7.16}
$$

Here, we define $\ell_{\boldsymbol{k}}$ and $\widetilde{\phi}\in\ell_{\boldsymbol{k}}$ ($\boldsymbol{k}=(k_1,k_2)\in\mathbb{R}^2$) by

$$
\begin{aligned}
&\ell_{\boldsymbol{k}}=\{\phi\in C(X,\mathbb{C})\mid \phi(x+a_1)=e^{ik_1}\phi(x),\ \phi(x+a_2)=e^{ik_2}\phi(x)\},\\
&\widetilde{\phi}(\alpha_1a_1+\alpha_2a_2+v_j)=e^{-i(\alpha_1k_1+\alpha_2k_2)}\phi(v_j),
\end{aligned}
$$

then, by (7.16), we obtain

$$
A_X^2\widetilde{\phi}(v_i)=(3+e^{ik_1}+e^{-ik_1}+e^{ik_2}+e^{-ik_2}+e^{i(k_1-k_2)}+e^{-i(k_1-k_2)})\widetilde{\phi}(v_i),
\tag{7.17}
$$

and we may define a twisted operator $A_{\boldsymbol{k}}\colon \ell_{\boldsymbol{k}}\to\ell_{\boldsymbol{k}}$ by

$$
A_{\boldsymbol{k}}=\begin{bmatrix}0 & D(\boldsymbol{k})\\ \overline{D(\boldsymbol{k})} & \end{bmatrix},\quad A_{\boldsymbol{k}}^2=\begin{bmatrix}D_2(\boldsymbol{k}) & 0\\ 0 & D_2(\boldsymbol{k})\end{bmatrix},
\tag{7.18}
$$

where

$$
\begin{aligned}
D(\boldsymbol{k}) &= e^{ik_1}+e^{ik_2}+1,\\
D_2(\boldsymbol{k}) &= |D(\boldsymbol{k})|^2=3+e^{ik_1}+e^{-ik_1}+e^{ik_2}+e^{-ik_2}+e^{i(k_1-k_2)}+e^{-i(k_1-k_2)}\\
&= 3+2\cos(k_1)+2\cos(k_2)+2\cos(k_1-k_2).
\end{aligned}
\tag{7.19}
$$

Hence, by (7.18), the dispersive relation $\boldsymbol{k}$ to eigenvalues $\mu(\boldsymbol{k})$ of $A_{\boldsymbol{k}}$ is obtained as

$$
\boldsymbol{k}\mapsto E(\boldsymbol{k})=\pm\sqrt{D_2(\boldsymbol{k})}=\pm\sqrt{3+2\cos(k_1)+2\cos(k_2)+2\cos(k_1-k_2)}.
\tag{7.20}
$$

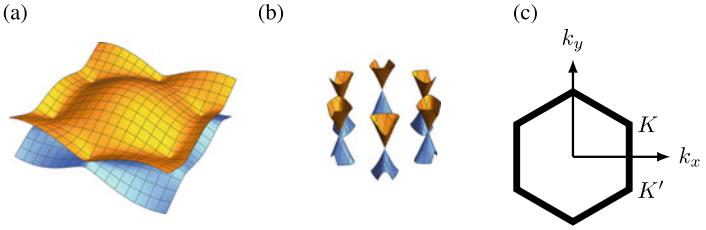

Fig. 7.14 **a** $E(\xi)$ of graphenes (band structure), **b** closed up $E(\xi)$ near K and K' points. **c** highly-symmetric points in the Fourier space

It is easy to show that $E(\boldsymbol{K}_\pm) = 0$, where $K_\pm = \pm(2\pi/3, -2\pi/3)$, and D_2 satisfies

$$E(\boldsymbol{k}) \sim \pm\sqrt{k_1^2 + k_2^2 - k_1 k_2}, \quad \boldsymbol{k} \sim \boldsymbol{K}_\pm. \tag{7.21}$$

Now, we apply data of a standard realization of a graphene. The angle between a basis of parallel transformations $\boldsymbol{a}_1$, $\boldsymbol{a}_2$ of a regular hexagonal lattice is $\pi/3$. We take $\{\boldsymbol{k}_j\}_{j=1}^2$ as the dual basis of $\{\boldsymbol{a}_j\}_{j=1}^2$, and we express $\boldsymbol{k} = k_x\boldsymbol{k}_1 + k_y\boldsymbol{k}_2$, for an example, $k_x = (-k_1 + \sqrt{3}k_2)/3$, $k_y = (k_1 + \sqrt{3}k_2)/3$. By (7.20), we obtain the band structure $E(\boldsymbol{k})$ as in Fig. 7.14a. By (7.21), we also obtain

$$E(\boldsymbol{k}) \sim \pm\sqrt{k_x^2 + k_y^2}, \quad \boldsymbol{k} \sim \boldsymbol{K}_\pm. \tag{7.22}$$

Note that the lower band (valence band) and the upper band (conductor band) attach at $K = K_+$ and $K' = K_-$ points on $E = 0$, and as in shown in (7.22), the band structure has cone-like points at K and K' (see Fig. 7.14b and for example [3]). A cone-like point of a band is called a *Dirac point*. Roughly speaking, if a band has a Dirac point at ξ_0, the effective mass of electrons with the wave number ξ_0 is zero. Diamonds and K_4-carbons, which are also strongly isotropic, have Dirac points, as well as graphenes, but such Dirac points are in valence bands (Tsuchiizu [57]).

From a graph-theoretic viewpoint, we may write $D(\boldsymbol{k})$ as

$$D(\boldsymbol{k}) = e^{i\langle \boldsymbol{k}, \boldsymbol{e}_1\rangle} + e^{i\langle \boldsymbol{k}, \boldsymbol{e}_2\rangle} + e^{i\langle \boldsymbol{k}, \boldsymbol{e}_3\rangle} = e^{i\langle \boldsymbol{k}, \boldsymbol{e}_3\rangle}(e^{i\langle \boldsymbol{k}, \boldsymbol{a}_1\rangle} + e^{i\langle \boldsymbol{k}, \boldsymbol{a}_2\rangle} + 1),$$

which is considered as "waves" that run over edges on the base graph X_0 (see Fig. 7.13b), and by ignoring the phase-factor, we may easily obtain (7.18) and (7.19). This recipe depends only on data of the covering maps of the base graph of graphenes.

For a kagome lattice, taking $\{\boldsymbol{e}_i\}_{i=1}^6$ as in Fig. 3.13a, and using the above recipe, we obtain a twisted operator

$$A_{\boldsymbol{k}} = \begin{bmatrix} 0 & e^{i\langle \boldsymbol{k}, \boldsymbol{e}_1\rangle} + e^{i\langle \boldsymbol{k}, \boldsymbol{e}_4\rangle} & e^{-i\langle \boldsymbol{k}, \boldsymbol{e}_3\rangle} + e^{-i\langle \boldsymbol{k}, \boldsymbol{e}_6\rangle} \\ e^{-i\langle \boldsymbol{k}, \boldsymbol{e}_1\rangle} + e^{-i\langle \boldsymbol{k}, \boldsymbol{e}_4\rangle} & 0 & e^{i\langle \boldsymbol{k}, \boldsymbol{e}_2\rangle} + e^{i\langle \boldsymbol{k}, \boldsymbol{e}_5\rangle} \\ e^{i\langle \boldsymbol{k}, \boldsymbol{e}_3\rangle} + e^{i\langle \boldsymbol{k}, \boldsymbol{e}_6\rangle} & e^{-i\langle \boldsymbol{k}, \boldsymbol{e}_2\rangle} + e^{-i\langle \boldsymbol{k}, \boldsymbol{e}_5\rangle} & 0 \end{bmatrix}. \tag{7.23}$$

For a maximal abelian covering lattice of the base graph X_0, as shown as in (3.35), a basis $\{\widetilde{a}_j\}_{j=1}^4$ of parallel transformations satisfies

$$\begin{aligned} \widetilde{\boldsymbol{e}}_1 &= (1/6)(3\widetilde{\boldsymbol{a}}_1 + \widetilde{\boldsymbol{a}}_3 + \widetilde{\boldsymbol{a}}_4), \\ \widetilde{\boldsymbol{e}}_2 &= (1/6)(3\widetilde{\boldsymbol{a}}_2 + \widetilde{\boldsymbol{a}}_3 + \widetilde{\boldsymbol{a}}_4), \\ \widetilde{\boldsymbol{e}}_3 &= (1/6)(-3\widetilde{\boldsymbol{a}}_1 - 3\widetilde{\boldsymbol{a}}_2 + 4\widetilde{\boldsymbol{a}}_3 - 2\widetilde{\boldsymbol{a}}_4), \\ \widetilde{\boldsymbol{e}}_4 &= (1/6)(-3\widetilde{\boldsymbol{a}}_1 + \widetilde{\boldsymbol{a}}_3 + \widetilde{\boldsymbol{a}}_4), \\ \widetilde{\boldsymbol{e}}_5 &= (1/6)(-3\widetilde{\boldsymbol{a}}_2 + \widetilde{\boldsymbol{a}}_3 + \widetilde{\boldsymbol{a}}_4), \\ \widetilde{\boldsymbol{e}}_6 &= (1/6)(3\widetilde{\boldsymbol{a}}_1 + 3\widetilde{\boldsymbol{a}}_2 - 2\widetilde{\boldsymbol{a}}_3 + 4\widetilde{\boldsymbol{a}}_4). \end{aligned} \tag{7.24}$$

A kagome lattice is the projection of the maximal abelian covering lattice onto the subspace $H = \mathrm{span}\{\widetilde{\boldsymbol{e}}_1 + \widetilde{\boldsymbol{e}}_2 + \widetilde{\boldsymbol{e}}_3, \widetilde{\boldsymbol{e}}_4 + \widetilde{\boldsymbol{e}}_5 + \widetilde{\boldsymbol{e}}_6\} \subset H_1(X_0, \mathbb{R})$. Therefore combining (7.24) and

$$\widetilde{\boldsymbol{e}}_1 + \widetilde{\boldsymbol{e}}_2 + \widetilde{\boldsymbol{e}}_3 = \widetilde{\boldsymbol{e}}_4 + \widetilde{\boldsymbol{e}}_5 + \widetilde{\boldsymbol{e}}_6 = \boldsymbol{0},$$

we obtain that a basis $\{\boldsymbol{a}_j\}_{j=1}^2$ of parallel transformations of a kagome lattice satisfies

$$\begin{aligned} &\boldsymbol{e}_1 = (1/2)\boldsymbol{a}_1, \quad \boldsymbol{e}_2 = (1/2)\boldsymbol{a}_2, \quad \boldsymbol{e}_3 = -(1/2)(\boldsymbol{a}_1 + \boldsymbol{a}_2), \\ &\boldsymbol{e}_4 = -(1/2)\boldsymbol{a}_1, \ \boldsymbol{e}_5 = -(1/2)\boldsymbol{a}_2, \quad \boldsymbol{e}_6 = (1/2)(\boldsymbol{a}_1 + \boldsymbol{a}_2). \end{aligned} \tag{7.25}$$

By using (7.23) and (7.25), we obtain

$$\begin{aligned} A_{\boldsymbol{k}} &= \begin{bmatrix} 0 & e^{(i/2)k_1} + e^{-(i/2)k_1} & e^{(i/2)(k_1+k_2)} + e^{-(i/2)(k_1+k_2)} \\ e^{-(i/2)k_1} + e^{(i/2)k_1} & 0 & e^{-(i/2)k_2} + e^{(i/2)k_2} \\ e^{(i/2)(k_1+k_2)} + e^{-(i/2)(k_1+k_2)} & e^{(i/2)k_2} + e^{-(i/2)k_2} & 0 \end{bmatrix} \\ &= \begin{bmatrix} 0 & 2\cos(k_1/2) & 2\cos((k_1+k_2)/2) \\ 2\cos(k_1/2) & 0 & \cos(k_2/2) \\ 2\cos((k_1+k_2)/2) & 2\cos(k_2/2) & 0 \end{bmatrix}, \end{aligned}$$

and

$$E(\boldsymbol{k}) = \{-2, 1 \pm \sqrt{3 + 2\cos(k_1) + 2\cos(k_2) + 2\cos(k_1 - k_2)}\}. \tag{7.26}$$

A band with $E(\xi_0) \equiv$ const. is called a *flat band*, which means that there exists an electron with infinite effective mass with energy $E(\xi_0)$. Hence we confirm that kagome lattices have a flat band and Dirac points (see Fig. 7.15).

A kagome lattice is the line graph of a hexagonal lattice (see Fig. 7.16). In general, Shirai shows that there exists a flat band in the line graph of an infinite d-regular graph (Shirai [49], see also [35]). Katsura–Maruyama [21] also explain the existence of flat bands in the abelian covering of a line graph. In their paper, the band structure of a decorated hexagonal lattice is considered (see Fig. 7.17a). Let $X_0 = (V, E)$ be

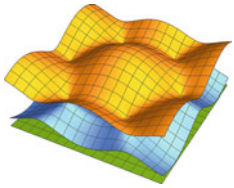

Fig. 7.15 $E(\xi)$ of a kagome lattice (band structure), compare Fig. 7.14a

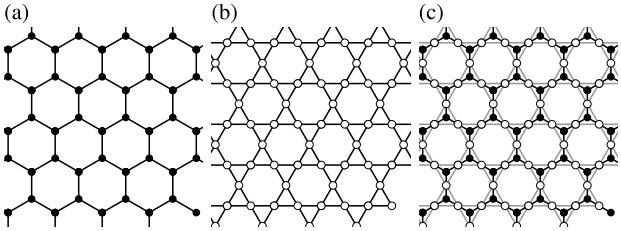

Fig. 7.16 **a** a hexagonal lattice, **b** a kagome lattice, **c** merged lattices

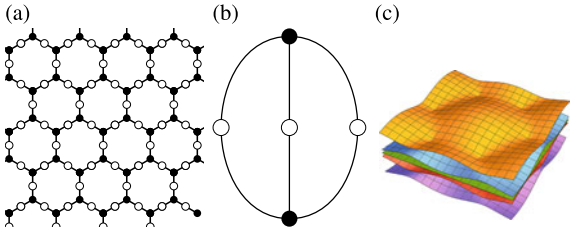

Fig. 7.17 **a** A decorated hexagonal lattice, **b** its base graph, **c** $E(\xi)$ of a decorated hexagonal lattice, compare Figs. 7.14a and 7.15

a base graph of a decorated hexagonal lattice, and V_B be black vertices V_W be white vertices (see Fig. 7.17b). Then X_0 and a decorated hexagonal lattice are bipartite. The twisted Laplacian of X_0 is written as

$$-\Delta_{\boldsymbol{k}} = \begin{bmatrix} O & -\Delta_{BW,\boldsymbol{k}} \\ -\Delta_{WB,\boldsymbol{k}} & O \end{bmatrix},$$

and $-\Delta_{BW}$, $-\Delta_{WB}$ are 3×3, 2×2-Hermite matrices, respectively. By Theorem 2.5, if λ is an eigenvalue of $-\Delta_{\boldsymbol{k}}$, then $-\lambda$ is also an eigenvalue. On the other hand, the size of $-\Delta_{\boldsymbol{k}}$ is odd, therefore $-\Delta_{\boldsymbol{k}}$ has at least one zero-eigenvalue. Hence a flat band exists in the band structure of a decorated hexagonal lattice (see Fig. 7.17c).

Here, we note several terminologies in solid-state physics. The *Wigner–Seitz cell* of a crystal structure is the fundamental region of parallel transformations. In the case of a graphene, a basis of the Wigner–Seitz cell is $\{\boldsymbol{e}_2 - \boldsymbol{e}_1, \boldsymbol{e}_3 - \boldsymbol{e}_1\}$, which is a

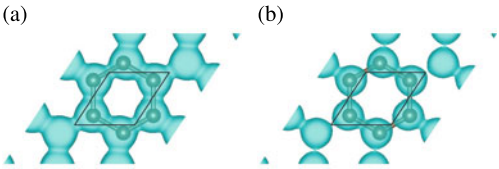

Fig. 7.18 Iso-surfaces of the density of electrons in graphenes by DFT. **a** Probability 0.18, **b** probability 0.30

region in $H_1(X_0, \mathbb{R})$. The *first Brillouin zone* of a crystal structure is the dual region of the Wigner–Seitz cell, which is in $H^1(X_0, \mathbb{R})$.

As explained in the Hückel method and tight-binding approximations of a graphene, each orbital or band contains at most two electrons by the Pauli exclusion principle. If a crystal model contains $2n$ electrons, then in the ground state, n bands from below are occupied by electrons, and such bands are called *valence bands*. Other bands, which have higher energy than valence bands, are called *conductor bands*. A crystal is called *metallic* when the valence band with the highest energy and the conductor band with the lowest energy have shared points. A crystal is called a *semiconductor* when the gap between the valence band with the highest energy and the conductor band with the lowest energy is small (less than about 1eV in solid state physics).

7.3.3 The Density Function Theory

Finally, we briefly describe the *density functional theory* (*DFT*) fist proposed by Kohn–Hohenberg [16] and Kohn–Sham [23]. It is very difficult to numerically solve the Schrödinger equation (7.5) by direct methods, if the number of electrons $N \gg 1$. In stead of solving (7.5), we consider the density of electrons

$$\rho(x) = \sum_{j=1}^{N} |\phi_j(x)|^2,$$

where ϕ_j is a wave function for an electron. Kohn–Hohenberg show that the energy E_G of the ground state is uniquely determined by ρ, and the density ρ_0 of the ground state is the minimizer of the energy functional, namely, $E_G = E[\rho_0] \leq E[\rho]$. For each given potential V, the cost of calculations of energy by this method is $O(N^3)$ by using a suitable approximation.

As in Figs. 7.18, 7.19 and 7.20, numerical calculations using DFT give us the density of electrons of molecule/crystal structures. Figs. 7.18, 7.19 and 7.20 are generated by Dr. Tomoya Naito and calculated using OpenMX [31, 42–44] with the LDA-PZ81 functional [45] and drawn using VESTA [36].

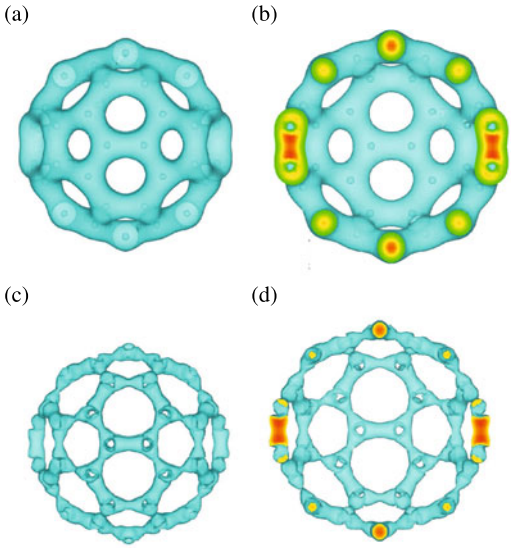

Fig. 7.19 Iso-surface of distributions of electrons of C_{60} by DFT. **a** Probability 0.15, **b** its cut-model, **c** probability 0.25, **d** its cut-model

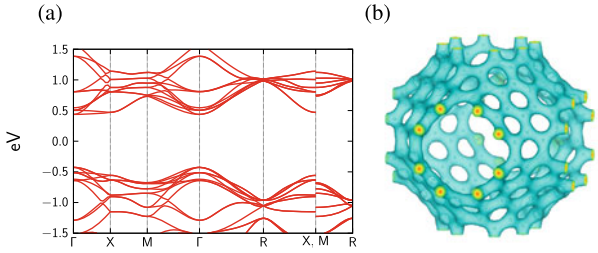

Fig. 7.20 DFT calculation result for the Mackay–Terrones structure. **a** Electronic state, band gap is about 1 eV, and hence the Mackay–Terrones structure is a semiconductor. **b** Iso-surface of the density of electrons ($p = 0.15$)

7.4 Eigenvalues of Subdivisions of Trivalent Discrete Surfaces

As described in Sect. 7.3, eigenvalues of the Laplacian are an important property of graphs, and also one of the main objects in discrete geometric analysis (see for example [5, 15, 30]). On the other hand, we define subdivisions of trivalent graphs in Sect. 6.1. Therefore, relationships between eigenvalues of Laplacian and subdivisions of trivalent graphs are of interest.

Theorem 7.1 (Omori–Naito–Tate [41]) *Let $X = (V(X), E(X))$ be a connected, finite and simple trivalent graph equipped with an orientation at each vertex,*

$X' = \mathrm{GC}_{k,l}(X)$ be the Goldberg–Coxeter construction of X, where $k \geq l \geq 0$ and $k \neq 0$ and

$$0 = \lambda_1(X) < \lambda_2(X) \leq \cdots \leq \lambda_{|V(X)|}(X),$$
$$0 = \lambda_1(X') < \lambda_2(X') \leq \cdots \leq \lambda_{|V(X')|}(X')$$

be the eigenvalues of their Laplacians Δ_X, $\Delta_{X'}$, respectively. Then for $i = 1, 2, \ldots, |V(X)|$,

$$\lambda_i(\mathrm{GC}_{k,l}(X)) \leq \frac{3k}{k^2 + kl + l^2}\lambda_i(X). \tag{7.27}$$

If X is a bipartite, then for $i = 1, 2, \ldots, |V(X)|$,

$$\lambda_{|V(\mathrm{GC}_{k,l}(X))|-i+1}(\mathrm{GC}_{k,l}(X)) \geq 6 - \frac{3k}{k^2 + kl + l^2}\lambda_i(X). \tag{7.28}$$

In the case that $l = 0$, the last $|V(X)|$ eigenvalues of $\mathrm{GC}_{k,0}(X)$ satisfy

$$\lambda_{|V(\mathrm{GC}_{k,0}(X))|-i+1}(\mathrm{GC}_{k,0}(X)) \geq 3 + \sqrt{5 + 4\cos\frac{2\pi}{k}}, \tag{7.29}$$

for $i = 1, 2, \ldots, |V(X)|$.

Theorem 7.2 (Omori–Naito–Tate [41]) *Let $X = (V(X), E(X))$ be a connected, finite and simple trivalent graph equipped with an orientation at each vertex, and $\mathrm{GC}_{k,0}(X)$ be the Goldberg–Coxeter construction of X for $k \geq 1$. Then, for any number $o(k^2)$ satisfying $o(k^2)/k^2 \to 0$ as $k \to \infty$, the first (resp. the last) $o(k^2)$ eigenvalues of the Laplacian of $\mathrm{GC}_{k,0}(X)$ tend to 0 (resp. tend to 6 as k goes to infinity).*

Theorem 7.3 (Omori–Naito–Tate [41]) *By the same assumption as Theorem 7.2, $\mathrm{GC}_{2k,0}(X)$ has eigenvalues 2 and 4, whose multiplicities are $\lfloor k/2 \rfloor$ and $\lceil k/2 \rceil$, respectively. Moreover, under the assumption that the number of edges surrounding each face is divided by 3, $\mathrm{GC}_{k,0}(X)$ has eigenvalues 2 and 4, whose multiplicities are $\lfloor k/2 \rfloor$ and $\lceil k/2 \rceil$, respectively.*

Here, we note that eigenvalues λ of the Laplacian $-\Delta$ satisfy $\lambda \in [0, 6]$ since X is trivalent (see Theorem 2.3).

The above results are obtained by analysis of eigenvalues of cluster $\triangle_{k,\ell}(p)$ (see Fig. 7.21).

Proposition 7.2 (Omori–Naito–Tate [41]) *There exists an eigenvector χ (eigenvalue λ) of $\mathrm{GC}_{k,0}(X)$ such that the restriction $\chi|_{\triangle_{k,0}(p)}$ is an eigenvector (eigenvalue λ) under the Neumann boundary condition. Eigenvalues of a $(k, 0)$-cluster $\triangle_{k,0}(p)$ under the Neumann boundary condition are*

$$\lambda^{\pm}_{s,t} = \lambda^{\pm}_{s,t}(k) = 3 \pm \sqrt{3 + 2\cos\frac{2\pi s}{k} + 2\cos\frac{2\pi t}{k} + 2\cos\frac{2\pi(s-t)}{k}}, \tag{7.30}$$

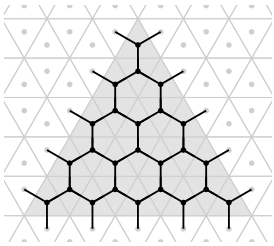

Fig. 7.21 Cluster $\triangle_{k,\ell}(p)$, where p is a vertex of the original graph X and the cluster is a subgraph of X'. This figure expresses $\triangle_{5,0}(p)$. The Neumann boundary condition means that an eigenvector takes the same value at both ends of an edge stood over the gray and white regions

$0 \leq s, t \leq k-1$.

By using Proposition 7.2 and gluing eigenvectors of clusters, we may construct eigenvectors of $\mathrm{GC}_{k,0}(X)$, which shows results. We note that the condition "the number of edges surrounding each face is divided by 3" produces an edge coloring on X, and guarantees a D_3-invariant eigenvector (eigenvalue 4) on a cluster with constant boundary values (for precise arguments, see [41]).

7.5 Graph Algorithms and Miscellaneous Computation Methods

In the final section, we explain graph algorithms and numerical methods that appeared in calculations of standard realizations.

7.5.1 Graph Algorithms

To calculate standard realizations, we need to obtain a spanning tree of base graphs (Kruskal's algorithm) and to find one of the shortest paths between the given two vertices of base graphs (Dijkstra's algorithm). Other algorithms are also available for them (see for example [1]).

Algorithm 7.1 (Kruskal's algorithm [1]) Let $X = (V, E)$ be a connected weighted graph. An algorithm to find a minimum spanning tree of X is as follows:

1. $F = V$ and $S = E$, where F is called a forest (a set of trees),
2. while $S \neq \emptyset$ and F is not spanning tree yet, repeat:
   a. remove an edge e with minimum weight from S,
   b. if e connects $t_1, t_2 \in F$ $(t_1 \neq t_2)$, then add $t = t_1 \cup e \cup t_2$ to F (and remove t_1, t_2 from F).

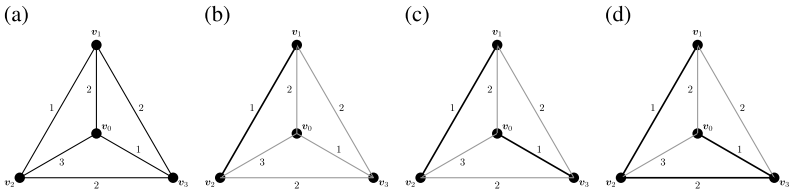

Fig. 7.22 Calculation of a minimum spanning tree of K_4 graph by using Kruskal's algorithm. Numbers in the above figures denote the weights of edges

Since the number of edges contained in the minimum spanning tree is $|V| - 1$, the loop in step 2 repeats at most $|V| - 1$ times. On other hand, the cost to sort S by weights is $O(|E| \log |E|)$. Therefore, the cost to find a minimum spanning tree by this algorithm is $O(|E| \log |E|) = O(|E| \log |V|)$.

Example 7.3 Let $X = (V, E)$ be the graph in Fig. 7.22a, Kruskal's algorithm works as:

1. there exists two edges (v_1, v_2) and (v_0, v_3) with weight 1; choose the edge (v_1, v_2), then F is the graph in Fig. 7.22b.
2. There exists only one edge (v_0, v_3) with weight 1; choose the edge (v_0, v_3), then F is the graph in Fig. 7.22c.
3. There exists three edges (v_0, v_1), (v_1, v_3), and (v_2, v_3) with weight 2; choose the edge (v_2, v_3), then F is the graph in Fig. 7.22d, and F is a spanning tree, since F contains all vertices of X.

Note that F is also a spanning tree even if we select another edge with weight 2 in the step 1.

Algorithm 7.2 (Dijksta's algorithm [1]) Let $X = (V, E)$ be a connected weighted graph. An algorithm to find the shortest path from a given vertex $s \in V$ to other vertices is as follows:

1. set $d(s) = 0$, $d(x) = \infty$ $(V \ni x \neq s)$, $p(v) =$ NONE, and $Q = V$,
2. while $Q \neq \emptyset$ repeat:
   a. select and remove a vertex $x \in Q$ such that $d(x)$ is minimum among vertices in Q,
   b. for each vertex $y \in V$ such that $(x, y) \in E$:
   if $d(x) > d(y) + w(x, y)$, then set $d(x) = d(y) + w(x, y)$ and $p(x) = y$.

Here d expresses the distance from s and p expresses the previous vertex of the shortest path founded. After the algorithm finishes, the path $(x, p(x)) \ldots (p(\cdots(p(x))), s)$ is a shortest path from x to s, and $d(x)$ is the distance from s to x.

The highest-cost procedure of this algorithm is the step to select one of the nearest vertices. By using a priority queue, for example, a binary heap, the total cost of this algorithm is $O((|V| + |E|) \log |V|)$.

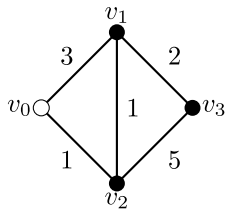

Fig. 7.23 An example to test Dijkstra's algorithm

Example 7.4 Let $X = (V, E)$ be the graph in Fig. 7.23 and let us find the shortest paths from v_0 to other vertices. Dijkstra's algorithm works as:

0. $Q = \{v_0, v_1, v_2, v_3\}$: $d(v_0) = 0$,
1. set $x := v_0$, $Q = \{v_1, v_2, v_3\}$: set $d(v_1) = 3$, $p(v_1) = v_0$, $d(v_2) = 1$ and $d(v_2) = v_0$,
2. set $x := v_2$, $Q = \{v_1, v_3\}$: since $d(v_1) > d(v_2) + d(v_2, v_1)$, set $d(v_1) = 2$ and $p(v_1) = v_2$: set $d(v_3) = d(v_2) + 5 = 6$, $p(v_3) = v_2$,
3. set $x := v_1$, $Q = \{v_3\}$: since $d(v_3) > d(v_1) + d(v_1, v_3)$, set $d(v_3) = 5$ and $p(v_3) = v_1$: d and p do not change,
4. set $x := v_3$, $Q = \emptyset$: d and p do not change.

At the end of this procedure,

$$\begin{aligned} &p(v_0) = \text{NONE}, \quad &&p(v_1) = v_2, \quad &&p(v_2) = v_0, \quad &&p(v_3) = v_1, \\ &d(v_0) = 0, &&p(v_1) = 3, &&p(v_2) = 1, &&p(v_3) = 5, \end{aligned}$$

hence a shortest path from v_0 to v_3 is $(v_0, v_2)(v_2, v_1)(v_1, v_3)$, and its length is 5.

7.5.2 Numerical Methods for Matrices

To obtain standard realizations, we also need numerical schemes for matrix calculations.

For an $n \times n$ real symmetric matrix A, if there exists an upper triangular matrix X such that $A = X^T X$, then the decomposition is called a *Cholesky decomposition* of A. If $A = [a_{ij}]$ and $X = [x_{ij}]$ satisfy $A = X^T X$, then we obtain

$$\begin{aligned} a_{ii} &= \sum_{k=1}^{i} x_{ki}^2, \\ a_{ij} &= \sum_{k=1}^{j} x_{ki} x_{kj}, \quad (i < j). \end{aligned} \tag{7.31}$$

Hence we may calculate x_{ij} as

$$
\begin{aligned}
a_{11} &= x_{11}^2, & x_{11} &= \sqrt{a_{11}}, \\
a_{1j} &= x_{11}x_{1j}, & x_{1j} &= a_{1j}/x_{11}, \ j = 2, \ldots, n, \\
a_{ii} &= x_{ii}^2 + \sum_{k=1}^{i-1} x_{ki}^2, & x_{ii} &= \sqrt{a_{ii} - \sum_{k=1}^{i-1} x_{ki}^2}, \\
a_{ij} &= x_{ji}x_{jj} + \sum_{k=1}^{j-1} x_{ki}x_{kj} & x_{ji} &= \frac{1}{x_{jj}} \left(a_{ij} - \sum_{k=1}^{j-1} x_{ki}x_{kj} \right), \ j = i+1, \ldots, n,
\end{aligned}
\tag{7.32}
$$

inductively. The following theorem gives the well-known necessary and sufficient conditions to proceed with the Cholesky decomposition.

Theorem 7.4 *An $n \times n$ real symmetric matrix A has a Cholesky decomposition if A is positive definite. The cost of calculation in a Cholesky decomposition is $O(n^3)$.*

Proof It is obvious that if A has a Cholesky decomposition then A is semi-positive.

Let $A_k = [a_{ij}]_{1 \le i,j \le k}$ and $X_k = [x_{ij}]_{1 \le i,j \le k}$ be the leading principal minor matrix of order k. Since X is upper triangular, we obtain

$$
\det(A_{k-1}) = \det(X_{k-1})^2 = \prod_{i=1}^{k-1} x_{kk}^2,
$$

and

$$
x_{kk}^2 \det(A_{k-1}) = \det(A_k). \tag{7.33}
$$

Obviously $x_{11}^2 = a_{11} = \det(A_1)$ holds. On the other hand, if A is positive definite, $\det(A_k) > 0$ for all $k = 1, \ldots, n$ (Sylvester's criterion). Therefore, we may determine x_{ij} by using (7.32), namely a Cholesky decomposition of A exists.

We need $O(i)$ times multiplication to calculate x_{ij} in (7.32), hence the cost of calculation is $O(n^3)$.

Remark 7.1 For an $n \times n$ matrix A, if there exists a lower triangular matrix L and an upper triangular matrix U such that $A = LU$, then the decomposition is called an *LU decomposition* of A. We may show that an $n \times n$ matrix A has an LU decomposition if and only if all leading principal minors of A are non-zero by using arguments similar to those in the proof of Theorem 7.4.

Calculating a standard realization of the Mackay–Terrones structure, we solve the Poisson equation $\Delta_X \boldsymbol{v} = \boldsymbol{f}$, where Δ_X is the Laplacian of the graph expressing the structure and $\boldsymbol{f}$ is the vector expressing the periodic condition. Since the Laplacian Δ_X is non-singular, we could not directly solve the Poisson equation. However, considering the pseudo-inverse Δ_X^+ of Δ_X, we may solve the equation as $\boldsymbol{u} = \Delta_X^+ \boldsymbol{f}$.

Definition 7.2 For an $n \times n$ matrix A, the matrix A^+ satisfying

$$
AA^+A = A^+, \quad A^+AA^+ = A \tag{7.34}
$$

is called *pseudo-inverse* (*Moore–Penrose inverse*).

Assume that $A = P\Lambda P^{-1}$, where P is a non-singular matrix and $\Lambda = \mathrm{diag}(\lambda_i)$, then

$$A^+ = P\Lambda^+ P^{-1}, \quad \Lambda^+ = \mathrm{diag}(\lambda_i^+), \quad \lambda_i^+ = \begin{cases} 0 & \text{if } \lambda_i = 0, \\ 1/\lambda_i & \text{otherwise.} \end{cases}$$

In particular, if A is non-singular, $A^+ = A^{-1}$.

Proposition 7.3 ([47]) *A linear equation $A\boldsymbol{u} = \boldsymbol{f}$ admits a solution, then $\boldsymbol{v} = A^+\boldsymbol{f}$ is the solution with least norm among all solutions of the equation.*

Remark 7.2 The pseudo-inverse Δ_X^+ of the Laplacian Δ_X gives us a harmonic/standard realization; however, the cost of calculation is expensive since the cost of eigenvalue decompositions of Δ_X is expensive even though the Laplacian is real-symmetric. Hence this method is not practical if the number of vertices n is huge. The Gaussian elimination (the cost $O(n^3)$) is one practical method to obtain a solution of $\Delta_X \boldsymbol{u} = \boldsymbol{f}$, even if Δ_X is singular.

References

1. A.V. Aho, J.E. Hopcroft, J.D. Ullman, *The Design and Analysis of Computer Algorithms* (Pearson, 1974)
2. The Australian National University, The EPINET Project. http://epinet.anu.edu.au/
3. C. Barreteau, F. Ducastelle, T. Mallah, A bird's eye view on the flat and conic band world of the honeycomb and Kagome lattices: towards an understanding of 2D Metal-Organic Frameworks electronic structure. J. Phys. Cond. Mat. **29**, 465302 (2017)
4. J.A. Bondy, U.S.R. Murty, *Graph Theory*, Graduate Texts in Mathematics, vol. 244 (Springer, 2008)
5. D. Cvetković, P. Rowlinson, S. Simić, *An Introduction to the Theory of Graph Spectra*, London Mathematical Society, Student Texts, vol. 75 (2010)
6. G. Davidoff, P. Sarnack, A. Valette, *Elementary Number Theory, Group Theory, and Ramanujan Graphs*, London Mathematical Society, Student Texts, vol. 55 (2003)
7. A. Dechant, T. Ohto, Y. Ito, M.V. Makarova, Y. Kawabe, T. Agari, H. Kumai, Y. Takahashi, H. Naito, M. Kotani, Geometric model of 3D curved graphene with chemical dopants. Carbon **182**, 223–232 (2021)
8. O. Delgado-Friedrichs, M. O'Keeffe, Identification of and symmetry computation for crystal nets. Acta Crystallogr. A **59**, 351–360 (2003)
9. M. Deza, M. Dutour Sikirić, *Geometry of Chemical Graphs: Polycycles and Two-faced Maps*, Encyclopedia of Mathematics and its Applications, vol. 119 (Cambridge University Press, Cambridge, 2008)
10. M. Dutour, M. Deza, Goldberg-Coxeter construction for 3- and 4-valent plane graphs. Electron. J. Combin. **11**, ♯R20 (2004)
11. J. Eells, J.H. Sampson, Harmonic mappings of Riemannian manifolds. Am. J. Math. **86**, 109–160 (1964)
12. D. Fujita, Y. Ueda, S. Sato, N. Mizuno, T. Kumasaka, M. Fujita, Self-assembly of tetravalent Goldberg polyhedra from 144 small components. Nature **540**, 563 (2016)
13. M. Goldberg, A class of multi-symmetric polyhedra. Tohoku Math. J., First Series, **43**, 104–108 (1937)
14. G.H. Golub, C.E. van Loan, *Matrix Computations*, 3rd edn. (The John Hopkins University Press, 1996)

H. Naito, *Trivalent Discrete Surfaces and Carbon Structures*,
SpringerBriefs in the Mathematics of Materials 5,
https://doi.org/10.1007/978-981-99-5769-9

15. Yu. Higuchi, T. Shirai, Some spectral and geometric properties for infinite graphs. Contemp. Math. **347**, 29–56 (2004)
16. P. Hohenberg, W. Kohn, Inhomogeneous electron gas. Phys. Rev. **136**, B864–B871 (1964)
17. G. Huisken, Flow by mean curvature of convex surfaces into spheres. J. Differ. Geom. **20**, 237–266 (1984)
18. K. Ikemoto, S. Yang, H. Naito, M. Kotani, S. Sato, H. Isobe, A nitrogen-doped nanotube molecule with atom vacancy defects. Nat. Commun. **11**, 1807 (2020)
19. M. Itoh, M. Kotani, H. Naito, T. Sunada, Y. Kawazoe, T. Adschiri, New metallic carbon crystal. Phys. Rev. Lett. **102**, 055703 (2009)
20. T. Kajigaya, R. Tanaka, Uniformizing surfaces via discrete harmonic maps. Ann. H. Lebesgue **4**, 1767–1807 (2021)
21. H. Katsura, I. Maruyama, Construction method of flat bands. Kotai Butsuri **50**, 257–270 (2015). (in Japanese)
22. K. Kawasumi, Q. Zhang, Y. Segawa, L.T. Scott, K. Itami, A grossly warped nanographene and the consequences of multiple odd-membered-ring defects. Nat. Chem. **5**, 739–744 (2013)
23. W. Kohn, L.J. Sham, Self-consistent equations including exchange and correlation effects. Phys. Rev. **140**, A1133-1138 (1965)
24. M. Kotani, H. Naito, T. Omori, A discrete surface theory. Comput. Aided Geom. Design **58**, 24–54 (2017)
25. M. Kotani, H. Naito, C. Tao, Construction of continuum from a discrete surface by its iterated subdivisions. Tohoku Math. J. **74**, 229–252 (2022)
26. M. Kotani, T. Sunada, Albanese maps and off diagonal long time asymptotics for the heat kernel. Comm. Math. Phys. **209**, 633–670 (2000)
27. M. Kotani, T. Sunada, A central limit theorem for the simple random walk on a crystal lattice, in *Proceedings of the Second ISAAC Newton Congress*, vol. 1 (Springer, 2000), pp. 1–6
28. M. Kotani, T. Sunada, Jacobian tori associated with a finite graph and its abelian covering graphs. Adv. Appl. Math. **24**, 89–110 (2000)
29. M. Kotani, T. Sunada, Standard realizations of crystal lattices via harmonic maps. Trans. Am. Math. Soc. **353**, 1–20 (2001)
30. M. Kotani, T. Sunada, Spectral geometry of crystal lattices. Contemp. Math. **338**, 271–305 (2003)
31. K. Lejaeghere et al., Reproducibility in density functional theory calculations of solids. Science **351**, aad3000 (2016)
32. T. Lenosky, X. Gonze, M. Teter, V. Elser, Energetics of negatively curved graphitic carbon. Nature **355**, 333–335 (1992)
33. A. Mackay, H. Terrones, Diamond from graphite. Nature **352**, 762 (1991)
34. T. Matsuno, H. Naito, S. Hitosugi, S. Sato, M. Kotani, H. Isobe, Geometric measures of finite carbon nanotube molecules: a proposal for length index and filling indexes. Pure Appl. Chem. **86**, 489–495 (2014)
35. A. Mizuno, Y. Shuku, M.M. Matsushita, M. Tsuchiizu, Y. Hara, N. Wada, Y. Shimizu, K. Awaga, 3D spin-liquid state in an organic hyperkagome lattice of mott dimers. Phys. Rev. Lett. **119**, 057201 (2017)
36. K. Momma, F. Izumi, VESTA 3 for three-dimensional visualization of crystal, volumetric and morphology data. J. Appl. Crystallogr. **44**, 1272–1276 (2011)
37. H. Naito, Visualization of standard realized crystal lattices. Contemp. Math. **484**, 153–164 (2009)
38. H. Naito, Construction of negatively curved carbon crystals via standard realizations. Springer Proc. Math. Stat. **166**, 83–100 (2016)
39. H. Naito, A short lecture on topological crystallography and a discrete surface theory, in *Anam Lecture Notes in Mathematics, An Introduction to Discrete Differential Geometry*, vol. 2, pp. 83–147 (2020), arXiv:2002.09562
40. M. O'Keeffe, B.G. Hyde, Plane nets in crystal chemistry. Philos. Trans. R. Soc. A **295**, 553–618 (1980)

41. T. Omori, H. Naito, T. Tate, Eigenvalues of the Laplacian on the Goldberg-Coxeter constructions for 3- and 4-valent graphs. Electron. J. Combin. **26**, P3.7 (2019)
42. T. Ozaki, Variationally optimized atomic orbitals for large-scale electronic structures. Phys. Rev. B **67**, 155108 (2003)
43. T. Ozaki, H. Kino, Numerical atomic basis orbitals from H to Kr. Phys. Rev. B **69**, 195113 (2004)
44. T. Ozaki, H. Kino, Efficient projector expansion for the ab initio LCAO method. Phys. Rev. B **72**, 045121 (2005)
45. J.P. Perdew, A. Zunger, Self-interaction correction to density-functional approximations for many-electron systems. Phys. Rev. B **23**, 5048 (1981)
46. U. Pinkall, K. Polthier, Computing discrete minimal surfaces and their conjugates. Experim. Math. **2**, 15–36 (1993)
47. M. Planitz, Inconsistent systems of linear equations. Math. Gazette **63**, 181–185 (1979)
48. M. Ross, Schwarz' *P* and *D* surfaces are stable. Differ. Geom. Appl. **2**, 179–195 (1992)
49. T. Shirai, The spectrum of infinite regular line graphs. Trans. Am. Math. Soc. **352**, 115–132 (2000)
50. L.M. Singer, J.A. Thorpe, *Lecture Notes on Elementary Topology and Geometry* (Springer, 1967)
51. T. Sunada, Laplacian and Fundamental Groups (Kinokuniya, 1988) (in Japanese)
52. T. Sunada, Crystals that nature might miss creating. Notices Am. Math. Soc. **55**, 208–215 (2008). Correction: "Crystals that nature might miss creating", Notices Am. Math. Soc. **55**, 343 (2008)
53. T. Sunada, Lecture on topological crystallography. Jpn. J. Math. **7**, 1–39 (2012)
54. T. Sunada, *Topological Crystallography, Surveys and Tutorials in the Applied Mathematical Sciences*, vol. 6 (Springer, Tokyo, 2013)
55. M. Tagami, Y. Liang, H. Naito, Y. Kawazoe, M. Kotani, Negatively curved cubic carbon crystals with octahedral symmetry. Carbon **76**, 266–274 (2014)
56. C. Tao, A construction of converging Goldberg-Coxeter subdivisions of a discrete surface. Kobe J. Math. **38**, 35–51 (2021)
57. M. Tsuchiizu, Three dimensional higher-spin Dirac and Weyl dispersions in strongly isotropic K_4 crystal. Phys. Rev B **94**, 195426 (2016)
58. M. Umehara, K. Yamada, *Differential Geometry of Curves and Surfaces* (World Scientific, 2017)
59. S. Zhang, J. Zhou, Q. Wang, X. Chen, Y. Kawazoe, P. Jena, Penta-graphene: a new carbon allotrope. Proc. Nat. Acad. Sci. **112**, 2372–2377 (2015)

Index

H. Naito, *Trivalent Discrete Surfaces and Carbon Structures*,
SpringerBriefs in the Mathematics of Materials 5,
https://doi.org/10.1007/978-981-99-5769-9